Multi-species planktonic foraminiferal Mg/Ca and δ^{18}O as recorders of surface ocean paleoclimatic processes: 2 case studies from diverse oceanographic regions and timescales

Tesis doctoral realizada por:

LAURA RODRÍGUEZ SANZ

Bajo la dirección del Doctor P. Graham Mortyn en el Instituto de Ciencia y Tecnología Ambiental (ICTA), de acuerdo con los requerimientos del programa de doctorado en Ciencia y Tecnología Ambientales de la Universidad Autónoma de Barcelona (UAB) para la obtención del título de **Doctor en Ciencia y Tecnología Ambientales**.

Bellaterra (Barcelona), 2012

_____   _____

El doctorando   El director de la tesis

INDEX

CHAPTER 1

Introduction

CHAPTER 2

Analytical Methodologies

CHAPTER 3

Glacial Southern Ocean freshening at the onset of the Middle Pleistocene Climate Transition

CHAPTER 4

Subantarctic Zone thermocline shoaling at the onset of the Middle Pleistocene Transition: improving conditions for glacial marine productivity in the region?

CHAPTER 5

Salinity increases in the southern California Current in tandem with Northern Hemisphere cold events

CHAPTER 6

Acknowledgements/Agradecimientos

RESUMEN

Durante procesos de calcificación los foraminíferos planctónicos incorporan Mg/Ca y fraccionan los isótopos de oxígeno ($\delta^{18}O$) en sus cáscaras dependiendo de la temperatura, y de la temperatura-$\delta^{18}O$ de la masa de agua ($\delta^{18}O_{SW}$) donde calcifican, respectivamente. Medidas de Mg/Ca-$\delta^{18}O$ en foraminíferos planctónicos han sido ampliamente utilizadas para reconstruir cambios de temperatura y derivar $\delta^{18}O_{SW}$ (corregido por el volumen de hielo; $\delta^{18}O_{SW-IVC}$) como proxy de salinidad. Esta tesis utiliza nuevas reconstrucciones de Mg/Ca-temperatura y $\delta^{18}O_{SW-IVC}$ para entender cambios en la estructura de la columna de agua durante la Transición del Pleistoceno Medio (MPT; 1250-700 ka) y la Terminación 1 (T1)-Holoceno temprano (20-3 ka) en el Océano Austral y Océano Pacífico, respectivamente. Aunque escalas de tiempos diferentes, ambos fueron períodos de cambios climáticos importantes y entender sus causas es importante para establecer factores que originan la variabilidad natural del clima.

La combinación de procesos físicos y biogeoquímicos en el Océano Austral regulan el intercambio de CO_2 entre el océano y la atmósfera durante ciclos glaciales-interglaciales. Reconstrucciones de Mg/Ca-temperatura y $\delta^{18}O_{SW-IVC}$ basados en *Neogloquadrina pachyderma* (sinistral) en la Zona Subantártica (ODP Site 1090) muestran que al comienzo del MPT (~1250 ka), la expansión de los frentes polares Antárcticos originó el enfriamiento glacial y reducción de salinidad de la superficie del Océano Austral. Se propone que estos cambios conllevaron a la estratificación de la superficie de este océano durante glaciaciones, evitando el intercambio de CO_2 con la atmósfera y por lo tanto incrementando el almacenamiento de carbono (C) en profundidad en las glaciaciones siguientes. Adicionalmente se estudió la influencia de la expansión de los frentes polares en la estructura de la columna de agua de la Zona Subantártica mediante la comparación de registros de Mg/Ca-temperatura y $\delta^{18}O_{SW-IVC}$ de foraminíferas planctónicos con profundidades de hábitat distintos; *Globigerina bulloides* (superficie), *N. pachyderma* (subsuperficie), and *Globorotalii crassaformis* (thermoclina). Estos resultados sugieren que la termoclina/haloclina de esa zona se hizo más somera entre 1500-1300 ka probablemente incrementando la disponibilidad de

Resumen

macro-nutrientes en la superficie de la zona. Esto, aunado a la fertilización por Fe durante las glaciaciones del MPT, eventualmente permitió el aumento de productividad observado en la zona, lo cual junto con la estratificación del Océano Austral posiblemente, pudo ocasionar la reducción glacial de pCO$_2$ (~30 ppm) a ~1250 ka. Las condiciones hidrográficas de la parte superficial de la columna de agua fueron también estudiadas Corriente de California (CC, MD02-2505) durante la T1. Se ha sugerido que la formación de aguas profundas en el Atlántico Norte durante el Younger Dryas (YD) y stadial-H1 menguó, incrementando el transporte de calor y salinidad al Océano Austral. Sin embargo sus consecuencias en el Océano Pacífico aún no están bien establecidas. Aquí, reconstrucciones de Mg/Ca-temperatura y $\delta^{18}O_{SW\text{-}IVC}$ utilizando los morfotipos de *Globigerinoides ruber* white en el MD02-2505 muestran el calentamiento relativo de la zona debido al debilitamiento de la CC durante la T1 concordando el perfil de $\delta^{18}O_{SW\text{-}IVC}$ que sugiere condiciones menos salinas hacia el Holoceno. Incrementos pronunciados de $\delta^{18}O_{SW\text{-}IVC}$ (~0.7‰) durante YD y stadial-H1 aparentemente son consecuencia de un efecto combinado del debilitamiento de la CC y la advección de aguas relativamente más salinas en el Pacífico durante YD y stadial-H1 en respuesta a los cambios en el Atlántico Norte.

Este trabajo enfatiza la respuesta e importancia de las condiciones superficiales de la columna de agua en el sistema climático. En base a reconstrucciones de temperatura y salinidad superficiales se han sugerido mecanismos plausibles de la influencia de las condiciones hidrográficas del Océano Austral en el intercambio de C con la atmósfera durante el MPT y en la respuesta del Océano Pacífico a cambios en el Atlántico Norte durante la T1.

ABSTRACT

During the calcification process planktonic foraminifera incorporate Mg/Ca and fractionate oxygen isotopes (δ^{18}O) in their shells depending on the water mass' temperature and temperature-seawater δ^{18}O composition ($\delta^{18}O_{SW}$), respectively, where they calcified. Paired Mg/Ca-δ^{18}O measurements in planktonic foraminifera have been widely used as a powerful tool to reconstruct ocean temperature and salinity changes, the latter by deconvolving ice volume corrected $\delta^{18}O_{SW}$ ($\delta^{18}O_{SW\text{-}IVC}$). This thesis builds on new planktonic foraminiferal Mg/Ca-temperature and $\delta^{18}O_{SW\text{-}IVC}$ records as proxies to understand past changes in the structure of the water column during the Middle Pleistocene Transition (MPT; 1250-700 ka) and Termination 1 (T1)-early Holocene (20 to 3 ka) focusing on two regions, the Southern Ocean and North-East Pacific Ocean respectively. Although very different timescales, the MPT and T1 were two periods of important climatic changes, the causes and internal feedbacks surrounding's which are of special interest to assess the drivers of the natural climate variability.

A combination of physical and biogeochemical processes in the Southern Ocean regulates the partitioning of CO_2 between the ocean and the atmosphere on glacial-interglacial timescales. *Neogloquadrina pachyderma* (sinistral) Mg/Ca-temperature and $\delta^{18}O_{SW\text{-}IVC}$ records from a core located in the Subantarctic Zone (ODP Site 1090) have shown that at ~1250 ka, the onset of the MPT, the seaward expansion of the Antarctic ice sheets promoted glacial cooling and freshening of the surface Southern Ocean. We suggest that the glacial freshening could have induced Southern Ocean upper water column stratification and hence hindered the outgassing of respired CO_2 to the atmosphere, increasing the storage of C at depth during glacial periods. We further explored changes in the water column structure induced by the expansion of the Antarctic polar fronts by exploiting the different depth habitat preferences of *Globigerina bulloides* (surface), *N. pachyderma* (subsurface), and *Globorotalii crassaformis* (thermocline). Their Mg/Ca-temperature and $\delta^{18}O_{SW\text{-}IVC}$ reconstructions suggested that the thermocline and halocline of the Subantarctic Zone shoaled from 1500-1300 ka, and persisted as such across the MPT, likely improving macro-nutrient

availability in the surface waters. This, in combination with glacial Fe-fertilization, probably allowed the spike in productivity observed during glacial stages in and after the transition. This together with Southern Ocean stratification contributed to the glacial 30 ppm MPT drop in $p\mathrm{CO_2}$. The influence of past upper ocean hydrographical changes in the climate system was further studied in a core located in the southern California Current (CC, MD02-2505) across T1. Declining deep water formation in the North Atlantic during Younger Dryas (YD) and stadial-H1 resulted in an increase of heat and salinity transport to the Southern Ocean; however the response of the Pacific Ocean to those changes remains elusive. Mg/Ca-temperature reconstructions inferred from *Globigerinoides ruber* white morphotypes suggest that the CC weakened across T1, allowing a relative warming of the CC at ~25ºN compared to northern positions. This is further supported by $\delta^{18}\mathrm{O_{SW\text{-}IVC}}$ changes toward fresher conditions into the Holocene. Increases of $\delta^{18}\mathrm{O_{SW\text{-}IVC}}$ (~0.7‰) in tandem with YD and stadial-H1 are suggested to reflect the combined effect of the weakening of the fresh CC and advection of relatively salty water masses to the core in response to the North Atlantic freshening and oceanic reorganization.

Overall, this work highlights the role of the upper ocean's physical properties in the Earth's climate. Based on temperature and salinity proxy reconstructions we provide plausible mechanisms to explain the role of the Southern Ocean hydrographical conditions in the storage/release of carbon at/from depth during the MPT as well as new insights on the response of the Pacific Ocean to decreases of heat and salinity transport to the North Atlantic within the last period of natural global warming.

CHAPTER 1

Introduction

1.1. <u>What is the driver of climate change on glacial-interglacial timescales?</u>

The seminal work of Hays *et al.*, 1976 highlighted the occurrence of the 100, 41, and 23 ky cyclicities in the ice volume changes of the past 450 ky, thereby supporting the Milankovitch theory *(Milankovitch, 1930)* of the ice ages. Accordingly, variations in the eccentricity of the orbit (100 and 400 ky), obliquity (41 ky), and precession (23 ky) of the Earth acted as pacemaker of the climate variability on glacial-interglacial timescales by controlling the amount of incoming solar radiation (insolation) at the top of the atmosphere *(Paillard, 1998)*.

* Eccentricity of the Earth's orbit: It refers to the change in the shape of the orbit of the Earth as result of the interaction with other planets. It varies with a periodicity of ~100 ky and ~400 ky, and it also shows a weak cycle of ~2100 ky (Fig. 1.1a)

* Obliquity of the Earth's axis: It refers to the variations in the angle tilt of the Earth, i.e., the angle between the rotational axis and the equatorial plane. This angle varies between 22.2º to 24.5º with a periodicity of ~41 ky (Fig. 1.1b).

* Precession of the equinoxes: It can be divided into two movements, which together vary with a periodicity of ~23 ky and ~19 ky (weaker signal). *The axial precession* it is related to a change in the position of the rotational earth axis around the pole elliptic in which the resultant movements form a cone (Fig. 1.1c). The other movement called the *precession of the ellipse* is the rotation of the earth around its orbit, which makes it closer (perihelion) or further (aphelion) from the sun.

According to the orbital theory of the ice ages, the Earth enters into a glacial stage when summer insolation is weak in the northern hemisphere (highly controlled by precession)*,* that is high precession and low obliquity; such that the snow and ice are able to persist and accumulate in the ice sheets (*Raymo and Huybers*, 2008). Although

Milankovitch's hypothesis explains fairly well the glacial-interglacial oscillations of the Earth climate system it is insufficient to provide a sensible explanation for the origin of the saw-tooth glacial-interglacial 100 ky cycles of the late Quaternary (e.g. *Paillard*, 1998; *Gildor and Tziperman*, 2000; *Tziperman et al.*, 2006).
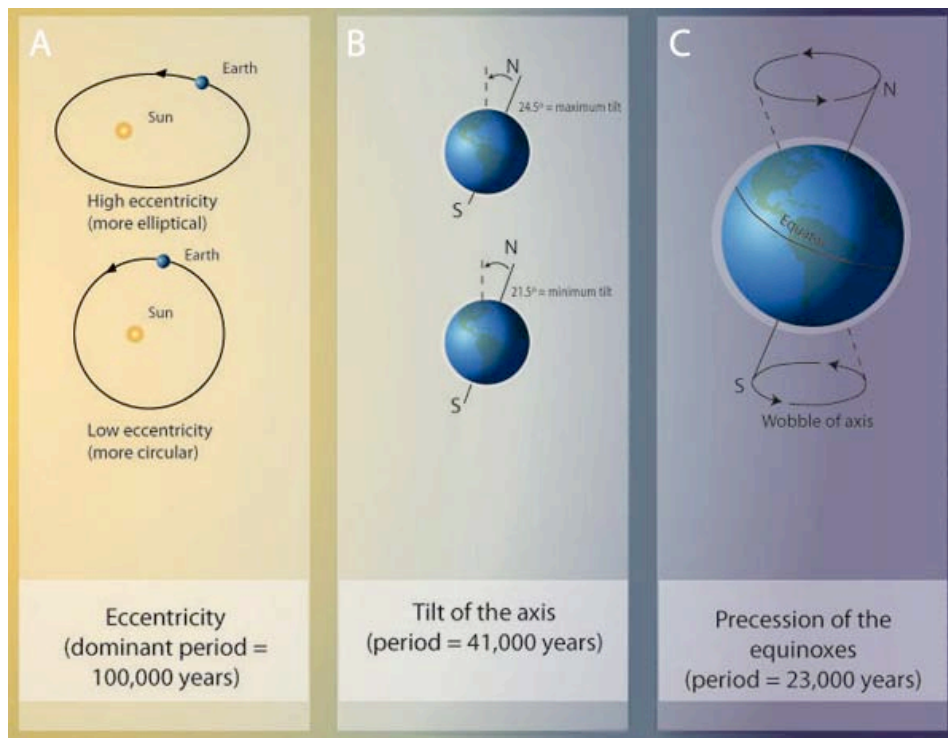
Figure 1.1. Schematic representation of the Milankovitch cycles: (a) eccentricity of the orbit, (d) obliquity or tilt of the axis, (c) precession of the equinoxes. Copyright: 2011 Nature Education, All rights reserved (http://www.nature.com/scitable/knowledge/library/factors-affecting-global-climate-17079163).

Therefore, it was brought into play the role of the internal climatic processes as important feedbacks that modulated the glacial-interglacial cycles (*Broecker and Denton*, 1989; Sigman et al., 2000, 2010 and references therein). Changes in oceanic processes, that in the modern ocean are the responsible of redistributing heat and moisture around the globe, and in the atmospheric composition have probably play a key role in the climate system. Many paleoceanographic studies have indeed provided evidence changes in the strength of Atlantic meridional overturning circulation (AMOC) and atmospheric carbon dioxide concentrations (pCO$_2$) as an important factor in the glacial-interglacial changes *(Lea et al., 2000; McManus et al., 2004; Anderson et al., 2009; Barker et al., 2009, 2010, 2011; Toggweiler and Lea, 2010)*. Remarkably,

despite its large size and oceanic-atmospheric teleconnections with remote areas of the globe (e.g. *Alexander et al., 2002; Chiang and Vimot 2004; Chiang and Lanter, 2005*), the Pacific Ocean changes and role during glacial-interglacial timescales are not as well constrained as in the Atlantic Ocean.

The chemical composition of the atmosphere, especially the greenhouse gas (GHG) concentration, is considered another important feedback of the climate system. GHGs have the ability of absorbing and emitting infrared radiation hence affecting the temperature of the earth depending on their concentration in the atmosphere. Measurements of atmospheric carbon dioxide concentration (pCO$_2$; *Luthi et al.*, 2008; *Petit et al.*, 1999; *Siegenthaler et al.*, 2005), methane (CH$_4$; *Loulergue et al.*, 2008; *Petit et al.*, 1999; *Spahni et al.*, 2005), and nitrous oxyde (N$_2$O) in the European Project for Ice Coring in Antarctica (EPICA) have shown that the concentrations of these gases in the atmosphere were tightly linked to glacial-interglacial temperature and ice volume changes over the past 800 ky (Fig. 1.2). However the role of the GHGs on glacial-interglacial oscillations is yet not well understood and it is a matter of current special interest due to the continuous release of anthropogenic CO$_2$ to the atmosphere (IPCC2007).

The ocean is thought to have been key in regulating pCO$_2$ variations in glacial-interglacial timescales since it holds 50 times more inorganic carbon than the atmosphere (*Jaccard et al.*, 2005). Because of this, most of the paleoceanographic studies that attempt to shed light on understanding the response of the climate system to pCO$_2$ increases have focused on understanding changes in ocean circulation and atmospheric-oceanic dynamics across glacial-interglacial timescales. In this sense, this research exploits well-established inorganic geochemical proxies from planktonic foraminifera to reconstruct upper water column temperature and salinity changes from key oceanic regions at 2 separate and important timescales: The Middle Pleistocene Transition (MPT) and the Termination 1 (T1)-early Holocene, in the Southern Ocean and Pacific Ocean, respectively.
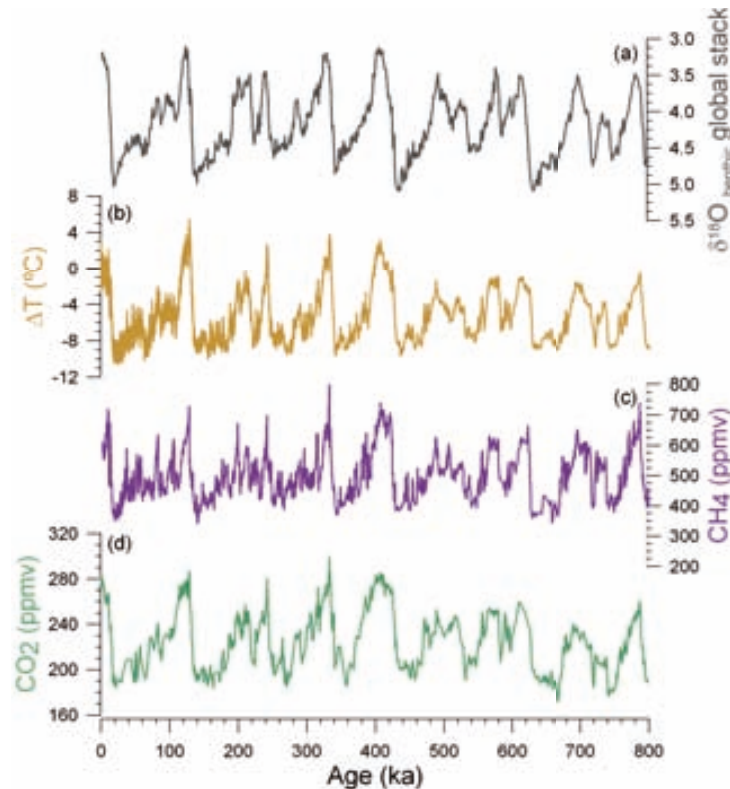
Figure 1.2. Comparison between the $\delta^{18}O$ global benthic stack (LR04; (Lisiecki and Raymo. 2005), which represents a mixed signal between ice volume changes and deep ocean temperatures, (b) Antarctic temperature gradient with respect to present temperatures (Jouzel et al., 2007) and variations in the atmospheric (c) CH_4 (*Loulergue et al.*, 2008; *Petit et al.*, 1999; *Spahni et al.*, 2005) and (d) CO_2 (*Luthi et al.*, 2008; *Petit et al.*, 1999; *Siegenthaler et al.*, 2005) concentrations measured in the EPICA Dome C core over the last 800 ky.

1.2. The MPT (1250-700 ka) in the Southern Ocean

1.2.1. The MPT and earth's climate changes across the transition

The MPT was a major reorganization of Earth's climate that occurred between 1250 and 700 ka (Clark, et al. 2006). The dominant periodicity of the glacial-interglacial cycles changed from a 41 ky rhythm, possibly triggered by insolation changes coupled with obliquity variations *(Huybers and Wunsch, 2005)* to a less frequent, more intense, and asymmetric 100 ky rhythm, for which causal mechanisms remain debated *(Clark et al., 2006; Park and Maasch, 1993; Mudelsee and Schulz, 1997; Schmieder et al., 2000)*. The emergence of the 100-kyr cycle was paralleled by an increase in the severity of glaciations starting at 1250 ka, with maximum glaciations being established at 700 ka (*Clark et al. 2006*; Fig. 1.3).

Most of our knowledge of the environmental changes occurred during the MPT predominantly derives from long and continuous marine records retrieved from the main basins of the world's ocean. In the following some of the main contributions from these paleoceanographic studies are summarized.
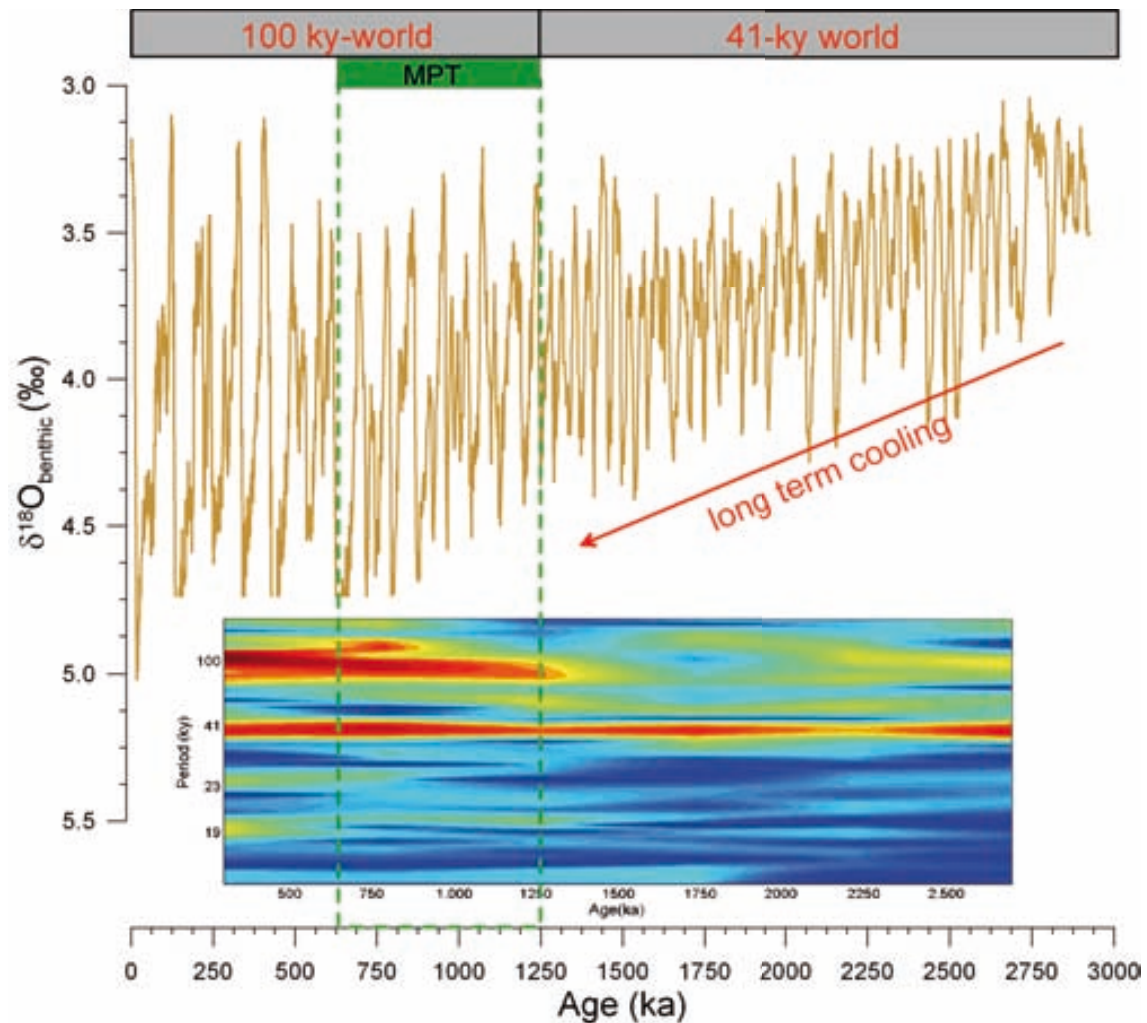
Figure 1.3. LR04 benthic δ^{18}O stack *(Lisiecki and Raymo, 2005)* and its evolutionary spectral analyses are shown to highlight major deep ocean temperature and δ^{18}O (ice volume) changes across the MPT. The evolutionary spectrum displays the emergence of the 100 ky band at 1250 ka and its further intensification at 900 ka, in parallel to the onset of heavier δ^{18}O in the LR04 stack during glacials. The MPT interval is indicated by the green box area. The evolutionary spectral analysis was performed with MATLAB (Annex II) package using a 600 ky Hamming window with an 80% overlap. The LR04 series was resampled to a 2 ky time step resolution, detrended and prewhitened using Analyseries 1.1.1 before performing the spectral analysis.

In the **Pacific Ocean**, the MPT featured increases of the west to east sea surface temperature (SST) gradients *(de Garidel-Thoron et al., 2005)* and intensification of the

Walker atmospheric circulation *(McClymont and Rosell-Mele, 2005; Li et al., 2011)*. These changes in the ocean-atmosphere system are thought to have played also a role in the onset to the major Northern Hemisphere glaciations (NHG) by enhancing the poleward transport of moisture *(McClymont and Rosell-Mele, 2005)*. The Pacific cold tongue also developed during the MPT *(Martínez-Garcia et al., 2010)*, leading to a westward restriction of the Pacific warm pool, which during the Pliocene was covering the entire tropical Pacific Ocean *(Brierley et al., 2009)*. This promoted a profound hydrographic reorganization in the upper water column (by shoaling the thermocline) of the eastern sector of the basin, enhancing primary productivity in the west coasts of the American continents *(Lawrence et al., 2006; Liu et al., 2005)*. In the west Pacific warm pool, the shift from 41 to 100 ky cyclicity of the glacial-interglacial SST changes were likely modulated by variations in the periodicity of the radiative forcing by CO_2 *(Medina-Elizalde and Lea, 2005; Russon et al., 2011)*. The winter Asian Monsoon intensified during the MPT *(Sun et al., 2006)*.

In the **Southern Ocean**, reconstructions based on organic biomarkers suggest that the establishment of a sea ice configuration comparable to the Last Glacial Maximum (LGM) took place at ~1250 ka and coincided with the enhanced northward advection of polar waters to the Subantarctic Atlantic Ocean *(Martínez-Garcia et al., 2010)*. At the same time, the West Antarctic ice sheet expanded seaward and ice shelves developed *(Naish et al., 2009)*. These changes at the high southern latitudes were paralleled by a shift from precession dominated cyclicity (Subtropical-like conditions) to a progressive intensification of the obliquity signal (Subantarctic-like conditions) in the alkenone-based SST reconstructions from ~42°S in the Atlantic Ocean *(Martínez-Garcia et al., 2010)*. Studies based on coccolithofore and diatom assemblages point to meridional variations in the position of the Antarctic polar frontal system across the MPT *(Martínez-Garcia, et al., 2010; Becquey and Gersonde, 2002; Flores and Sierro, 2007; Kemp et al., 2010)*. Glacial increases in eolian supply of iron (Fe) to the Southern Ocean took place at the onset of the MPT and it has been shown as a recurrent factor that operated for all the glaciations of the late Quaternary *(Martinez-Garcia et al., 2011)*.

Regarding the **Atlantic Ocean**, it has been suggested that changes in the upwelling activity along the coast of Africa *(Marlow et al., 2000; Etourneau et al., 2009)* and variations in the surface ocean hydrology of the Caribbean Sea (likely) stem from a shift of the mean position of the Intertropical Convergence Zone (ITCZ) during the MPT

(Sepulcre et al., 2010). The first appearance of ice rafted detritus (IRD) in the subpolar North Atlantic occurred by the end of the MPT (~640 ka), suggestive of increasing size and/or instability of the Laurentide Ice Sheet *(Hodell et al., 2008)*.

The evolution across the MPT of **deep ocean temperature and global ice volume** recorded in the benthic $\delta^{18}O$ records remains debated. A study from the deep North Atlantic shows deep ocean cooling by ~1.3°C at ~900 ka marked the internsification of the Northern Hemisphere glaciations *(Sosdian and Rosenthal, 2009)*. Another record from the deep Pacific instead shows no change in the glacial deep ocean temperatures throughout the last 1500 ka, implying that the benthic foraminiferal $\delta^{18}O$ increase during the MPT was primarily controlled by sea level fall *(Elderfield et al., 2012)* due an abrupt expansion of the West Antarctic ice sheet *(Pollard and DeConto, 2009)*. Major changes in the **deep ocean ventilation** were documented in North Atlantic $\delta^{13}C$ and other sedimentary proxies from the Southwest Pacific, alluding to the suppression of the North Atlantic Deep Water (NADW) formation during glacial stages after 1500 ka *(Hall et al., 2001; Raymo et al., 1990)*. Furthermore, based on benthic foraminiferal $\delta^{13}C$ some authors *(Schmieder et al., 2000; Venz and Hodell, 2002)* have inferred a decrease in Southern Ocean deep water ventilation across the MPT. Inter-ocean benthic $\delta^{13}C$ gradients suggest that deep water masses in the Southern Ocean during the MPT were considerably depleted in ^{13}C, reaching isotopic values lighter than the in the Pacific *(Hodell and Venz-Curtis, 2006)*. This implies that the deep Southern Ocean was well isolated from the ocean surface system. A major reorganization of the **global carbon cycle** coincided with the abrupt increase in glacial ice volume at 900 ka, likely in response to the transfer of 300 Pg of isotopically depleted marine organic carbon to the deep ocean *(Elderfield et al., 2012)*. An alternative mechanism for this change involves an enhanced in the input of terrestrial carbon to the ocean as consequence of a shift to more arid conditions globally during the MPT *(Raymo et al., 1997)*.

1.2.2. Causes of the MPT

The pattern of profound climate change that featured the MPT occurred without any variation in orbital forcing *(Clark et al., 2006; Park and Maasch, 1993; Mudelsee and Schulz, 1997; Schmieder et al., 2000)*. Thus, most of the theories that attempt to explain the MPT suggest a major reorganization of feedback processes internal to the climate system that amplified the response of the Earth's climate to orbital parameters *(Paillard*

et al., 1998; Clark and Pollard, 1998; Berger et al., 1999; Tziperman and Gildor, 2001; Clark et al., 2006). Nevertheless, none theories put forward to date has accounted in full for the changes observed in the paleocenographic record (e.g. *Clark, et al. 2006*).

Clark et al., 1999 proposed that the exposure of Precambrian Shield bedrock during the MPT, in combination with the long-term cooling across the Plio-Pleistocene, allowed the accumulation of a large ice sheets in the Northern Hemisphere, hence amplifying the response of the climate system to the orbital parameters. Other theories that try to explain the emergence of the saw-tooth pattern in the benthic $\delta^{18}O$ point to the stabilizing effect of the long-term cooling deep water temperatures on the water column, which weakened the AMOC (and its associated heat transport) and favored ice sheet growth (*Tziperman and Gildor, 2001)*. The "water column stabilization" helped the climate system to switch into a "glacial mode" that was highly influenced by the sea ice albedo feedback and by the reduced moisture transport to high latitudes *(Gildor and Tziperman, 2001)*. Berger (1999) considered that the long-term cooling across the Plio-Pleistocene (Fig. 1.3; *Lisiecki and Raymo, 2005*), and concomitant pCO$_2$ drawdown, increased the stability of the ice sheets allowing them to persist under moderate Northern Hemisphere summer insolation. Then, only when insolation was maximal, that is at high obliquity, minimum precession (summer northern hemisphere in the perihelion), and high eccentricity, the ice sheets melted (interglacial stages), making the eccentricity cycle an important feature across and after the MPT. Recent pCO$_2$ reconstructions using the planktonic foraminiferal $\delta^{11}B$ proxy across the MPT have shown a decrease of glacial pCO$_2$ after the MPT by 30 ppmv *(Hönisch et al., 2009)*. This evidence lends some support to the theory postulated by *Berger (1999)* and it highlights the role of pCO$_2$ concentrations and enhanced climate sensitivity under glacial boundary conditions as important aspects of the MPT *(van de Wal and Bintanja, 2009)*.

1.2.3. The modern Southern Ocean and feedbacks that potentially contributed to glacial-interglacial pCO$_2$ changes

The Southern Ocean is a critical sector of the global ocean because it involves surface and deep processes that allow the exchange, mixing, and redistribution of water masses from three different ocean basins (e.g. *Schmitz, 1996*). The general overview of the surface circulation patterns of the Southern Ocean is shown in Figure 1.4, with the

Antarctic Circumpolar Current (ACC) connecting the Atlantic, Indian, and Pacific Oceans. The ACC flows eastward around the Antarctic, transporting large volumes of water (~134±34Sv) and largely controlling Southern Ocean circulation (crf. *Rintoul et al., 2001*).
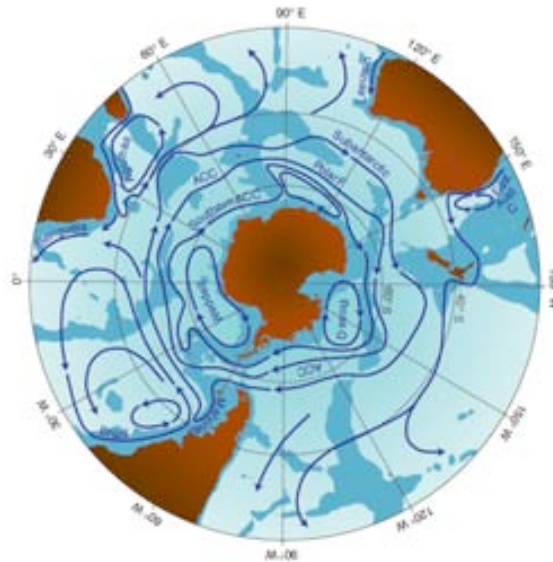
Figure1.4. Schematic view of the main surface circulation patterns in the Southern Ocean: Antarctic Circumpolar Current (ACC), Ross Gyre, Weddell Gyre.

Almost aligned with the ACC is the westerly wind belt. This allows the upwelling of deep waters, laden with nutrients and respired CO_2, south of the ACC. The upwelled water mass, which then sinks at depth in the ocean interior, flows back to the north as the Upper Circumpolar Deep Water (UCDW; Fig. 1.5). South of the ACC the Low Circumpolar Deep Water (LCDW) is mixed with NADW and forms the Antarctic Bottom Water (AABW), which then flows northward to the deep Atlantic Ocean (Fig. 1.5). The formation of the AABW constitutes the major sinking of unused (pre-formed) nutrients in the Southern Ocean, which then ventilates the deep ocean (Marinov et al., 2006) and it is responsible for restricting the efficiency of the biological pump in the modern ocean (crf. *Sigman et al., 2010*).

A distinctive feature of the ACC is its associated polar frontal that features abrupt temperature and salinity gradients at surface that are observed equatorward around the Antarctic (Belkin 2002; Fig. Fig. 1.4). There are three fronts of the ACC, from pole to the equator: Antarctic Polar Front, Subantarctic Polar Front, and Subtropical Polar Front. They define the boundaries of the Polar Zone, Antarctic Zone, and Subtropical

Zone of the ACC. Antarctic Intermediate Waters (AAIW) and Subantarctic Mode Water are formed in the Subantarctic Zone (Fig. 1.5). They flow northward into the Atlantic and Pacific Ocean, and are responsible for supplying pre-formed nutrients to the low latitude thermocline (Sarmiento, et al. 2004); Ribbe 2010).
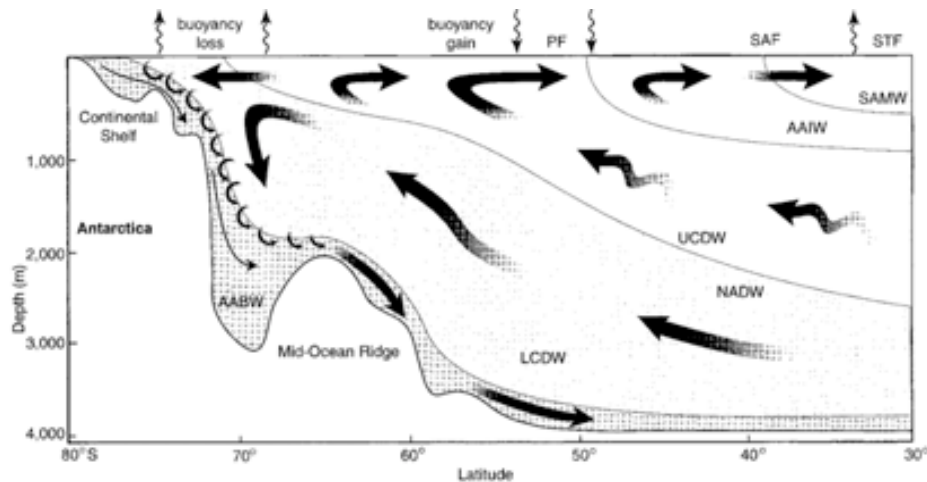
Figure1.5. Schematic view of the overturning circulation in the Southern Ocean in which the main deep, intermediate, and surface currents are shown: Low Circumpolar Deep Water (LCDW), North Atlantic Deep Water (NADW), Upper Circumpolar Deep Water (UCDW), Antarctic Intermediate Water (AAIW), Antartic Bottom Water (AABW), and Subantarctic Mode Water (SAMW). The positions of the Polar Front (PF), Subantarctic Front (SAF), and Subtropical Front (STF) are also shown. Thick arrows indicate the flow direction of the main currents and thin arrows the changes in buoyancy of the water masses. The figure was taken from Speer *et al.,* 2002.

The Southern Ocean has been proposed as the main modulator of $p\text{CO}_2$ concentrations on glacial-interglacial timescales *(Anderson and Carr, 2010; Skinner et al., 2010; Sigman, et al. 2010)*. In general, the role of the Southern Ocean in storing respired CO_2 is twofold: a) biological mechanism and b) physical mechanisms which are linked to different areas of the Southern Ocean *(Marinov et al., 2006)*. They are all summarized in Figure 1.6, which also considers whole ocean circulation changes during glacial-interglacial cycles. That is, the formation of the Glacial North Atlantic Intermediate Water (GNAIW) that further isolated deep water masses from the surface ocean *(Sigman et al., 2010)*.

The **first mechanism** involves the Subantarctic Zone, which is known to be one of the areas of the global ocean areas that featuring high nutrients and low chlorophyll (HNLC) concentrations, with the marine productivity limited by the scarcity of

micronutrients such as Fe (e.g. *Edwards et al., 2004*). Martin (1980) proposed that an increase in the eolian transport of Fe to HNLC regions would increase primary productivity, therefore increasing atmospheric CO_2 uptake and storage in the deep ocean (biological pump) and leading to glacial conditions. Fe-supply increases to the Southern Ocean during glacials were recurrent mechanisms across the last 1100 ky *(Martínez-Garcia et al., 2009)*, possibly contributing to a major utilization of pre-formed Antarctic Ocean nutrients in the Subantarctic Zone *(Sigman et al., 2010; Sigman and Boyle, 2000; Sigman and Haug, 2003)*. However, modeling studies and paleoceanographic data suggest that ocean Fe fertilization can only explain a 40 ppmv of the full glacial-interglacial pCO_2 amplitude change (80-90ppmv; Fig. 1.1.3; *Kohfeld et al. 2005*), suggesting that other mechanisms may have contributed to the glacial pCO_2 drawdown (e.g. *Sigman and Boyle, 2000*). Changes in marine primary productivity in the Subantartic Zone also have important implications in global export production *(Marinov et al., 2006)* due to the impact of newly formed water masses within the Subantartic Zone in supplying nutrients to low latitudes throughout the thermocline *(Sarmiento et al., 2004)*, further affecting the uptake and release of carbon from the ocean.

The **second mechanism** is related to the ability of the ocean to release to the atmosphere the respired CO_2 stored at depth. It is mainly controlled by changes in the efficiency of the biological pump and oceanic and atmospheric circulation in the Antarctic Zone *(Marinov et al., 2006)*. For example, the northward expansion of the Antarctic polar fronts triggered by sea ice expansion during glacial stages would have positioned the westerly wind belt closer to the equator. This could have decreased the upwelling offshore Antarctica of water masses that are enriched in pre-formed nutrients and respired CO_2 *(Toggweiler, 1999; Toggweiler et al., 2006; Toggweiler and Russell, 2008)*. This could have also promoted the build up of a fresh surface water layer in the Southern Ocean (Toggweiler et al., 2006), promoting upper water column stratification during glacial times. A stratified Southern Ocean further enhances the uptake of CO_2 by increasing the residence time of nutrients in surface waters *(Francois, 1998)* and its storage. It also aided the storage by physically inhibiting the outgassing of respired CO_2 *(Keeling and Stephens, 2001; Archer et al., 2003)*.
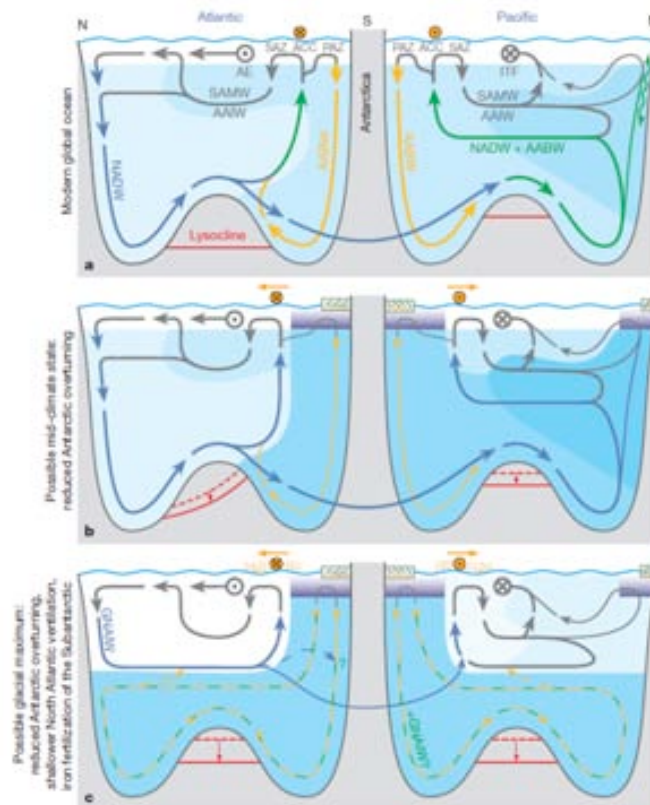
Figure 1.6. (a) Modern Southern Ocean circulation patterns (solid and dashed blue, green and yellow lines) and processes (orange dots in the top of the panels represent the positions of the westerly wind belt; red line shows the steady position of the lysocline while dashed red lines indicate the transient shoaling of the lysocline before reaching the steady state) compared to a proposed Southern Ocean during (b) intermediate-glacial and (c) full glacial state. Modern ocean circulation (a) is more vigorous than it was during cold stages (b and c; indicated by the intensity of blue color). The upwelling in the Antarctic Circumpolar Current (ACC), which in the modern ocean is almost aligned with the westerly wind belt, promotes the release of respired CO_2 back to the atmosphere (a). It also brings pre-formed or unused nutrients to the Southern Ocean surface waters, which are partially transported equatorward and then downwelled in the Antarctic Zone to the ocean interior during the production of Subantarctic Mode Water (SAMW) and Antarctic Intermediate Water (AAIW). The rest of the pre-formed nutrients upwelled in the ACC goes back to the deep ocean when the Antarctic Bottom Water (AABW) is formed (contributing to inefficiency of the biological pump in the modern ocean). SAMW and AAIW transport pre-formed nutrients to low latitudes where they are totally consumed by calcareous organisms (activating the carbonate pump). This reduces the content of pre-formed nutrients in the tropical and north Atlantic waters which are then downwelled in the North Atlantic as North Atlantic Deep Water (NADW) that then flows back to the southern Hemisphere throughout the deep Atlantic Ocean. During cold stages (b and c), the Southern Ocean circulation was reduced because the westerly wind belt migrated equatorward, triggered by sea ice expansion. The Glacial North Atlantic Intermediate Water (GNAIW) was developed, further isolating deep water masses from the surface. The new position of the westerly wind belt promoted the build up of a fresh layer in the surface, increasing ocean stratification and sea ice extension (purple and white boxes in the left side of panel b and c) which collectively inhibited the outgassing of

respired CO_2. Furthermore, an increased of eolian transport of Fe to the Southern Ocean favored primary productivity in the Subantarctic Zone, increasing the uptake of pCO_2 and storage at depth, also modifying deep ocean alkalinity (by increasing it). Consumption of pre-formed micronutrients in this region decreases nutrient availability in low latitudes and therefore primary productivity (decreasing the efficiency of the carbonate pump). Isolation of the deep ocean (by the forming the GNAIW), increases in the biological pump in high latitudes (Fe fertilization and stratification) and decreases of the carbonate pump (decrease in low latitudes nutrients availability) all contribute to increasing the storage of CO_2 in the deep ocean, making deep water masses more corrosive. This transiently increased the dissolution of the $CaCO_3$ in the deep ocean and therefore shoaled the depth of the lysocline, hence increasing the whole ocean alkalinity and further sequestering more pCO_2. The steady lysocline was set when the accumulation of dissolved carbonate at depth deepened the CCD and increased the $CaCO_3$ burial. Figure from Sigman *et al.,* 2010.

Ocean alkalinity changes also have to be taken into account when considering processes that sequestered CO_2 at depth on glacial-interglacial timescales. The biological pump and carbonate pump are the two main processes that controlled the ocean chemistry during glacial-interglacial cycles, with important implications for the pCO_2 variations *(Ridgwell and Zeebe, 2005; Sigman, et al., 2010; Hain et al., 2010)*. The biological pump not only increases the uptake of pCO_2 throughout photosynthesis and storage at depth but also by increasing the export of alkalinity to the deep ocean (Figure 1.2.4.3). Opposite to this, the carbonate pump increases the $CaCO_3$ burial in the deep ocean which is instead decreases alkalinity and in turn decreases the capacity of the ocean to buffer CO_2 (Fig. 1.7).

During glacial stages, increases in the storage of respired CO_2 at depth made deep water masses more corrosive, increasing the dissolution of the $CaCO_3$ and then increasing deep ocean alkalinity. This process shoaled transiently the depth of the carbonate compensation depth (CCD) and lysocline (Fig. 1.2.3.4), resulting in an important dissolution event that further favored the uptake of pCO_2. This transient period then produced high accumulation of dissolved carbonate at depth, therefore deepening the CCD, which in turn increased the area of $CaCO_3$ burial (carbonate pump), decreased alkalinity and the ocean's ability of buffering CO_2 (Toggweiler, 1999; Sigman and Haug 2003; Sigman et al., 2010; Sigman and Boyle 2000; Hain, et al. 2010).
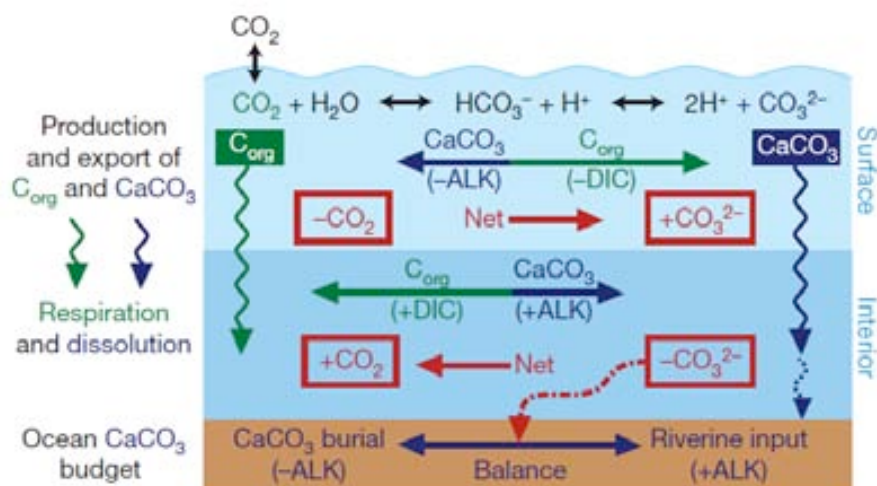
Figure 1.7. Schematic view of the ocean chemistry *(Sigman et al., 2010)*. The biological pump (green arrows and letters) exports dissolve inorganic carbon (DIC) as organic carbon (C_{org}) from the surface to the deep ocean (increasing the uptake pCO$_2$ in the surface). Remineralization of the C_{org} increases CO_2 concentration at depth. This stimulates carbonate dissolution and in turns shoals the carbonate compensation depth (CCD, the depth at which the seawater is undersaturated in carbonate) and lysocline (the transitional depth between calcite preservation and dissolution), enhancing alkalinity and further uptaking pCO$_2$. On the other hand, the carbonate pump decreases the uptake of pCO$_2$ in the surface when the $CaCO_3$ is precipitated. The burial of $CaCO_3$ is the way that the ocean loses alkalinity. So, an increase in the preservation of the $CaCO_3$ would decrease the ability of the ocean to dissolve pCO$_2$.

Hain *et al.,* 2010 have further demonstrated the importance of ocean alkalinity when considering that coupled biological and physical mechanisms may have played a role in the glacial pCO$_2$ drawdown. They suggest that increases in ocean stratification and sea ice extent not only trapped respired CO_2 at depth but also deep ocean alkalinity, therefore decreasing the ability of the ocean to dissolved pCO$_2$ and counteracting the uptake of pCO$_2$ by the biological pump. They have quantified that the biological and physical mechanisms can account for ~58 ppmv and ~36 ppmv of the glacial pCO$_2$ drawdown, respectively, when they are considered separately. However, when these mechanisms work in tandem the uptake of pCO$_2$ is restricted by the physical mechanisms, thereby only accounting for a 36 ppmv pCO$_2$ change.

1.3. <u>North-East Pacific during the glacial Termination I (T1)</u>

1.3.1. Glacial T1 and interhemispheric climate change on a millennial timescale

Although a comprehensive understanding of the actual causes of the "saw-tooth"

structure of the glacial-interglacial variability (e.g. *Broecker and van Dock, 1970*) remains elusive, recent studies highlighted the ubiquitous associations of orbital- and millennial-scale climate changes across glacial terminations *(Barker et al., 2009; 2010; 2011; Cheng et al., 2009; Denton et al., 2010; Toggweiler and Lea, 2010)*. For each of the last 8 glacial cycles Earth's global temperature decreases and ice volume growth lasted ~90-100 ky, while terminations featured rapid global temperature increases and ice sheet melting on timescale of ~10 ky (e.g. *Denton et al., 2010*; arrows in Figure 1.3.1.1b upper panel). Thereby the nature of the Terminations has become one of the most intriguing questions of the glacial-interglacial cycles and has caught the attention of many paleoceanographic studies Anderson 2009 (e.g. *Skinner et al., 2010; Barker et al., 2009; Anderson et al., 2009*).

Termination 1 (T1; Fig. 1.3.1.1b) is the most recent period of sustained global warming and pCO$_2$ rise (Denton et al., 2010) that led to the present Holocene interglacial *(Mayewski et al., 2004; Wanner et al., 2008)*. The millennial scale patterns of the last deglaciation have been expressed differently in each hemisphere (Fig. 1.3.1.1a-b bottom panel), in that any cooling (warming) in the Northern Hemisphere (NH) is accompanied by a warming (cooling) of its Southern Hemisphere (SH) counterpart. These features led to the notion of the "bipolar seesaw" *(Crowly, 1992; Broecker, 1998)*, which can be seen as an earth climate system buffering mechanism that maintains heat distribution around the globe when the system is perturbed (e.g., by circulation, abrupt temperature changes, etc.). In the NH the deglacial warming (Figure 1.3.1.1b bottom panel) began at ~20 ka and finished at ~7 ka (e.g., *Denton et al., 2010*). It is characterized by two cooling stages defined as the Heinrich stadial 1 (H1; *Barker et al., 2009*) or Mystery Interval *(Denton et al., 2006)* and the Younger Dryas (YD), which were separated by a warm interstadial known as the Bølling-Allerød (B-A). In the Southern Hemisphere, however, T1 was shorter; the warming started at ~18 ka and finished at ~11 ka. It was characterized by a gradual warming that stopped (or slightly cooled) during the Antarctic Cold Reversal (ACR), coinciding with the B-A in the Northern Hemisphere (Figure 1.8a bottom panel).
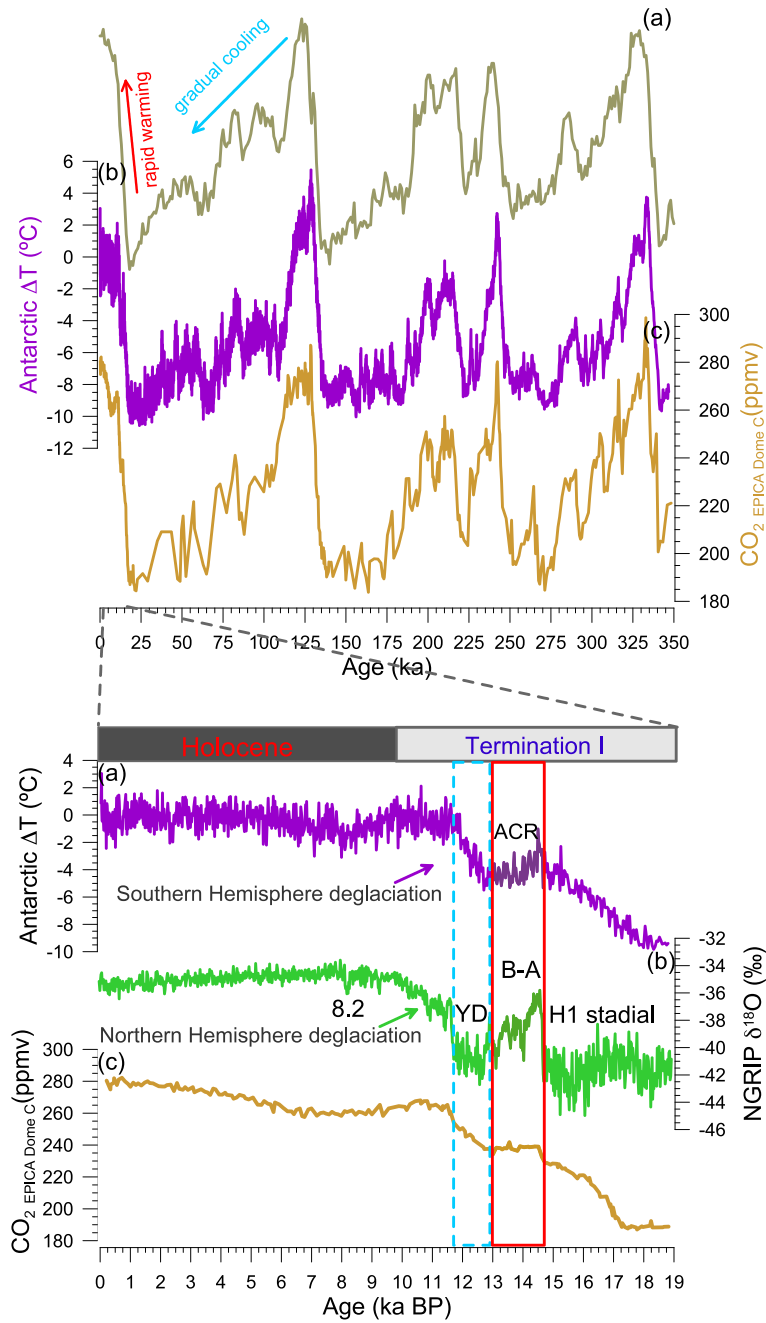
Figure 1.8. Upper panel shows the saw-tooth shape of the glacial-interglacial cycles over the last 350 ky. (a) LR04 $\delta^{18}O$ *(Lisiecki and Raymo, 2005)*, (b) Antarctic temperature gradient with respect to present temperatures *(Jouzel et al., 2007)*, and (c) variations in the atmospheric CO_2 concentrations (*Luthi et al.*, 2008; *Petit et al.*, 1999; *Siegenthaler et al.*, 2005); the last two were measured in the EPICA Dome C ice core over the last 350 ky. Bottom panel displays (a) the Antarctic ΔT, (b) $\delta^{18}O$ measurements from the North Greenland Ice Core Project (NGRIP), and (c) atmospheric CO_2 concentrations. Red and blue box areas define the Heinrich Stadial 1 (H1 stadial), Bølling-Allerød (B-A) and Younger Dryas (YD). The 8.2 ka event is also shown in the figure. Notice that when the Northern Hemisphere (NH) is in the H1 stadial the Southern Hemisphere (SH) is gradually warmed. Then the NH warmed (B-A) and the SH warming was stopped and then resumed when the NH entered into the YD stadial. This is known as the "bipolar seesaw".

16

Given the known sensitivity of the climate system to variations in pCO_2 concentrations (Fig. 1.8), most of the theories that aim to explain the mechanisms that triggered the last deglaciation have focused on understanding the processes that might have modulated the concentrations of this GHG (e.g. *Toggweiler, 2009; Anderson et al., 2010*). Similarities between pCO_2 variations and the pattern of the SH deglacial warming (Figure1.3.1.1, bottom panel) have led to the notion that Southern Ocean processes triggered most of the observed increases in pCO_2 concentrations across T1 *(Barker et al., 2009; Anderson et al., 2009; Skinner et al., 2010)*. However, the proposed mechanisms to explain T1 (based on proxy data and models) are far more complex and not only involve SH processes but also global oceanic-atmospheric teleconnections and/or circulation changes *(Anderson et al., 2010; Denton et al., 2010)*.

Before the last deglaciation began in the NH, i.e. during the LGM, the NH was covered by the Laurentide Ice Sheet (LIS), the demise of which substantially contributed to the ~120 m drop of sea level observed during T1 *(Clark et al., 2002)*. The great size of the LIS at the end the LGM made it unstable *(Raymo et al., 1980)*, such that during some periods it collapsed and discharged icebergs into the North Atlantic. Evidence for the collapse of the LIS is provided by increases in the Ice Rafted Dedritus (IRD) deposition in sediments ~50ºN, known as Heinrich events *(Heinrich 1988)*. These Heinrich events imposed pulses of fresh and cold water discharge to the North Atlantic. During the last stadial H1 increases of cold and fresh water discharge, together with sea ice melting *(Touconne et al., 2009)* and surges *(Liu et al., 2009)*, increased the sea level by 30 m *(Siddall et al., 2003)*, reduced the formation of the North Atlantic Deep Water (NADW; *McManus et al. 2004*), and in turn diminished the heat transport from the tropics to the NH. This allowed the accumulation of warm and salty conditions in the SH and it has been evidenced in some temperature records in the Southern Ocean that also span the Dansgaard–Oeschger oscillations *(Barker et al., 2009)*. This response of the climate system to the weakening of the Atlantic Meridional Overturning Circulation (AMOC) has led to two plausible mechanisms to explained the observed changes in the SH, pCO_2 and hence the T1.

First, it has been suggested that the accumulation of heat in the SH probably triggered the melting of the Antarctic ice sheet during the last deglaciation, increasing the ventilation of the Southern Ocean, and in turn reducing its capacity to store respired

CO_2 at depth (section 1.2.3). The second mechanism involves atmospheric teleconnections, which considers that cold conditions in the NH due to the presence of the great LIS and concomitant discharge of cold and fresh water masses not only weakened the AMOC but also increased the atmospheric temperature gradient between the NH and the tropics. This pushed the Intertropical Convergence Zone (ITCZ) toward the SH and in turn positioned the westerly wind belt closer to the ACC *(Toggweiler et al., 2006; Toggweiler, 2009)* where the upwelling of deep water masses was intensified.
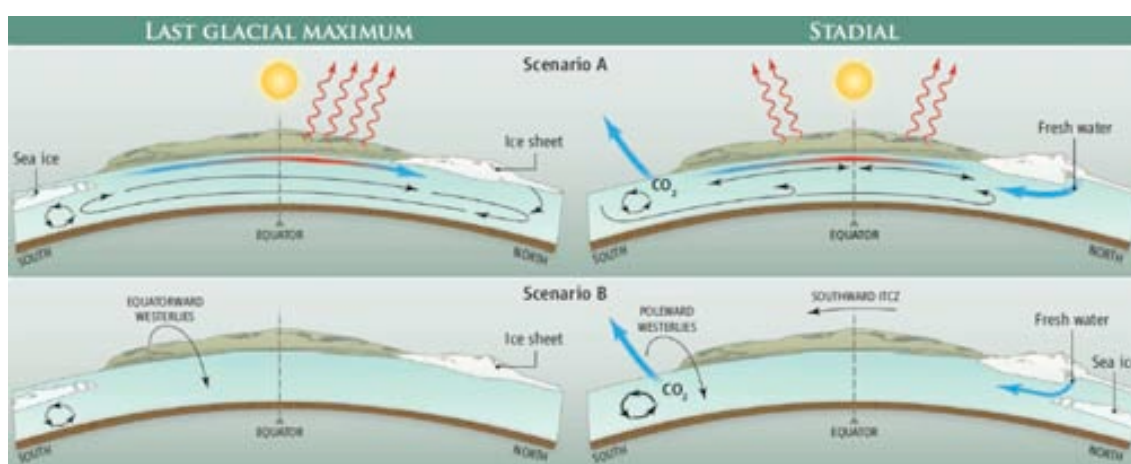
Figure 1.9. Proposed mechanisms for the ocean response to the fresh and cold water pulses in the North Atlantic during the Heinrich stadial, and possibly the Younger Dryas. Scenario A, in the left panel it is schematically represented modern oceanic circulation patterns, in which heat is transported to the Northern Hemisphere (NH) where deep waters are formed and flow southward to the Antarctic Ocean in the ocean interior. In the hypothetical stadial case, the fresh water discharge imposed some stability to the water column avoiding the formation of deep water masses, therefore diminishing the heat transport to the NH. In turn, heat it is accumulated in the SH and allowing the melting of the Antarctic Ice Sheet, strengthening Southern Ocean overturning circulation, the upwelling of deep water masses and then pCO_2 concentrations. In scenario B the cooling in the NH pushed the Intertropical Convergence Zone (ITCZ) southward and then the westerly wind belt also moved poleward, encouraging the upwelling of deep water masses enriched with respired CO_2 to be in contact with the atmosphere. Figure from Anderson and Carr 2009.

Lending support to the two mechanisms described above, Anderson *et al.,* (2009) have shown that opal accumulation rates in the Southern Ocean increased in tandem with the observed pulses of enhanced pCO_2 concentrations in EPICA Dome C (Figure 1.3.1.1c bottom panel), suggestive of an intensification of the upwelling around the Antarctic. Further support to the concept of increasing ventilation in the Southern Ocean in response to the collapse of the AMOC is provided by radiocarbon measurements in

planktonic and benthic foraminifera from the Subantarctic Zone *(Skinner et al., 2010)*. Skinner *et al.,* (2010) have provided evidence that the supply of old water masses (~3000 yr old) from the Southern Ocean to Subantarctic Zone occurred in tandem with increases in the upwelling around Antarctic *(Anderson et al., 2009)*. The presence of very old water masses at intermediate depths of the Eastern Pacific *(Marchitto et al., 2007; Stott et al., 2009)* has been also attributed to the strengthening of the Southern Hemisphere ventilation, which increased the supply of old water masses to the thermocline that are then transported by the SAMW toward the Eastern Pacific *(Sarmiento et al., 2008)*. This interpretation has been highly questioned by other radiocarbon and modelling studies *(Rose et al., 2010, De Pol-Holz et al., 2010; Hain et al., 2011)*, which have not found such old water masses in the Southern Ocean Pacific pathway of the SAMW. On the other hand, planktonic foraminiferal δ^{13}C measurements in a core site located in the Eastern Equatorial Pacific (EEP) suggest the presence of very light δ^{13}C water masses in the subsurface and surface *(Pena et al., 2008)* water column during T1, which has been interpreted as an increased in the Southern Ocean water mass supply to intermediate water masses in the Pacific Ocean *(Spero and Lea, 2000)*. Color reflectance analyses in sediment cores retrieved from the Cariaco Basin offshore Venezuela have been used as a proxy to track past changes in the position of the ITCZ *(Haug et al., 2001; Peterson et al., 2002)*. This record clearly shows evidence of the response of the ITCZ to millennial scale variations in the NH, in that cold (warm) NH events are accompanied by a southward (northward) shift of the ITCZ, providing support to the atmospheric teleconnection mechanism *(Toggweiler, 2009)* to explain upwelling changes around Antarctica during T1 *(Anderson et al., 2009)*.

The ocean circulation response in the Pacific Ocean to the collapse of the AMOC, as well as its role during the deglaciation, is not well understood yet. Modelling studies have suggested that the Pacific Overturning Circulation was strengthened when deep water formation was stopped in the North Atlantic *(Saenko et al., 2004; Timmerman et al., 2005; Okazaki et al., 2010)*, i.e. Pacific Ocean warmed when the North Atlantic cooled ("Atlantic-Pacific seesaw"). On the other hand, other studies suggest that changes in the North Atlantic and North Pacific were rather aligned *(Okumura et al., 2009; Chikamoto et al., 2012; Mix et al., 2012)*. Radiocarbon studies do not provide much help to solve the conundrum since it features the presence of young water masses in the Northwest Pacific *(Sagawa and Ikehara, 2008; Okazaki et al., 2005; Okazaki et*

al., 2010) while very old water masses occur in the eastern counterpart *(Marchitto et al., 2007; Stott et al., 2009)*. Temperature reconstructions in the equatorial and North Pacific are very sparse and depending on the approach they can result misleading. Overall, most of the temperature reconstructions based on the alkenone proxy show deglaciation patterns that resemble the NH warming *(Kienast and McKay, 2001; Pisias et al., 2001; Herbert et al., 2001; Seki et al., 2002; Barron et al., 2003; Yamamoto et al., 2007)*, whereas temperature reconstruction based on the Mg/Ca proxies show more gradual warming development *(Lea et al., 2000; Koutavas et al., 2002; Rosenthal et al., 2003; Benway et al., 2006; Pena et al., 2008; Marchitto et al., 2010)*, although with some exceptions *(McClymont et al., 2012)*. This led to the idea that seasonality differences between signal carriers affect the temperature reconstructions therefore making difficult their comparison *(Kiefer and Kennet et al., 2005; Hendy et al., 2010)* and then restricting the information that they can collectively provide to improve our knowledge on the Pacific hydrological changes across T1. Available reconstructions of $\delta^{18}O_{SW}$ are more consistent in the ocean basin, with oscillation patterns that follow NH deglaciation, i.e. cold (warm) events are characterized by increases in surface salinity in the Pacific Ocean especially in latitudes between 0ºN and 8ºN *(Rosenthal et al., 2003; Benway et al., 2006; Pena et al., 2008; Leduc et al; 2007; Mohatadi et al., 2010)*. These changes have been attributed to variations in the position of the ITCZ and to the reduced transport of moisture from the Atlantic to the Pacific in the eastern part of the basin *(Leduc et al., 2007)*, as well as to changes in the characteristics of the thermocline waters that are outcropping in the EEP *(Pena et al., 2008)*. However, more complex mechanisms that involve the Choco jet atmospheric current have been also proposed *(Prangue et al., 2010)*. El Niño- and La Niña-like conditions have been also called upon as analogs to explain hydrographical changes (temperature and salinity changes) in the Pacific Ocean during the LGM and T1 *(Lea et al., 2000; Koutavas et al., 2002; Pena et al., 2008)*. However, a recent study has argued that the use of El Niño or La Niña as an analogue to explain the changes observed in the Pacific Ocean is insuficient, and that other processes and feedbacks (that are not related to the modern ocean) might have been activated in the Pacific during deglaciation *(McClymont et al., 2012)*. Difficulties in reconciling the observed changes in temperature, salinity and $\delta^{14}C$ during T1 in the Eastern Pacific, and in the North Pacific in general, demand the urgent increase of paleo-temperature and salinity reconstructions in the area.

1.3.2. North-East (NE) Pacific Ocean and its ocean-atmosphere teleconnections

The Pacific Ocean is the largest ocean basin in the earth and it is connected to remote regions of the globe via atmospheric teleconnection (such as ENSO, Altlantic-Pacific moisture bridge, ITCZ position; Alexander *et al.*, 2002; Yuan 2004) and oceanic circulation (e.g. with the Southern Ocean throughout the SAMW formation and advection processes; *Spero and Lea, 2002; Liu and Yang, 2003*) allowing the climatic signal transference between ocean basins. The best-known atmospheric teleconnection of the Pacific Ocean is ENSO (2-7 years oscillation). During El Niño events, the trade winds weaken, allowing warm waters from the Western Equatorial Pacific (WEP) to flow toward the EEP. This Pacific Ocean configuration shifts rainfall patterns from west to east, deepens the thermocline and decreases primary productivity along the western margins of the American continents *(Cane, 2005)*, having important implications for both the local and global climate via ocean-atmosphere teleconnections, as well as human health and economy of the affected areas (e.g. *Grimm,* 2002; *Kovats et al.,* 2003; *Brönnimann,* 2007). Beyond the eastern Pacific, an El Niño event has also implication the Asian (decreases) and American (increases) Monsoon due to its effect in the position of the ITCZ (southward; Deser and Wallace 1990). Overall the ITCZ position highly influences the annual hydrological cycle in the tropical areas of the globe, so its Equatoward/Northward further migration during El Niño/La Niña events clearly modifies the precipitation patterns in those areas (e.g. *Koutavas and Lynch-Stieglitz 2005*). The Pacific Decadal Oscillation has similar characteristics than an El Niño anomaly in the Pacific Ocean, but it is mainly restricted to the North Pacific. In addition El Niño only last 6 to 10 months while the PDO and 20-30 years (Desert et al., 2004).

Surface oceanic circulation patterns of the Pacific Ocean are shown in Figure 1.3.2.1. It features two main tropical gyre circulation patterns that flow clockwise in the NH and anticlockwise in the SH due to the Coriolis Effect. The gyre located north of the equator is formed by the Kuroshio current, Oyashio current, California Current (CC) and North Equatorial Current (NEC), from west to east across the gyre. In the south, the gyre is formed by the Peruvian Current, South Equatorial Current (SEC), East Australian Current and ACC, from east to west in the direction of the gyre. In the Northern Pacific the Alaska Current, Kamchatka Current and Oyashio Current form a third gyre that flows opposite to the North Pacific gyre.
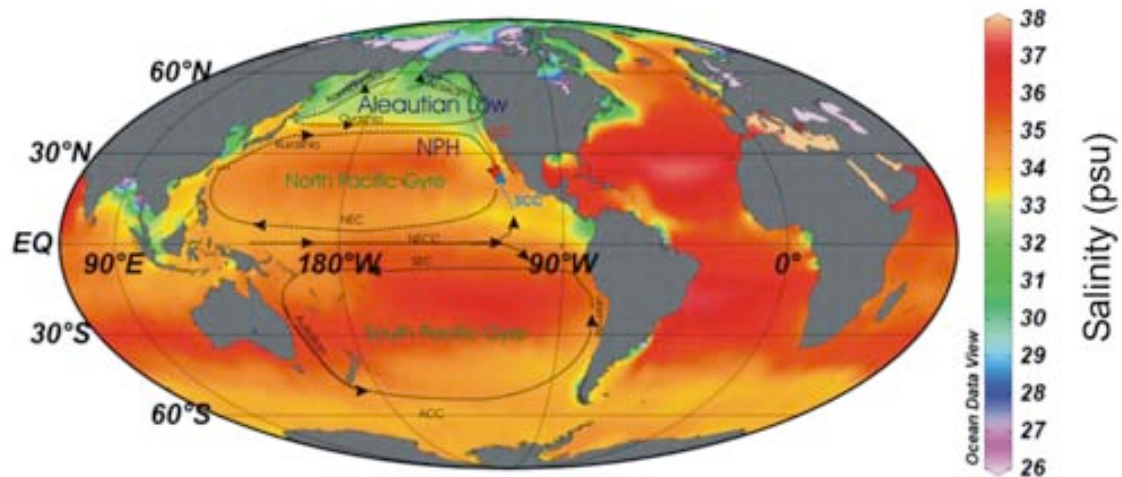
Figure 1.10. Surface salinity and schematic view of the main circulation patterns in the Pacific Ocean. North Equatorial Current (NEC), North Equatorial Countercurrent (NECC), South Equatorial Countercurrent (SEC), Antarctic Circumpolar Current (ACC), South Californian Countercurrent (SCC, in blue) and California Current (CC, in red).

In the vicinity of the equator, the Equatorial Countercurrent (ECC) flows eastward and then northward feeding the Southern California Countercurrent (SCC) that moves poleward and supplies warm and salty waters to the northwest coast of Northern America, especially during winter and fall *(Lynn and Simpson, 1987)*. It is one of the currents that constitute the California Current System (CCS), which is one of the biggest upwelling areas of the ocean. The California Current (CC) is a fresh, cold, high nutrients and oxygen contents water mass, which flows equatorward in the eastern boundary of the North Pacific Gyre *(Lynn et al., 1982)*. It is especially intensified during boreal spring and summer when the North Pacific High (NPH) is also intensified and the Aleutian Low is weakened (Figure1.3.2.1). During winter and fall seasons the opposite situation develops, i.e. NPH weakens and the Aleutian Low intensifies, the SCC is intensified and the CC is relatively weakened. The third component of the CCS is the California Undercurrent (CU). The CU flows beneath the SCC and it transports warm, salty and high nutrients and low content of oxygen (probably fed by the Equatorial Undercurrent (EUC), SAMW and AAIW) water masses to the pole (Figure1.3.2.2).
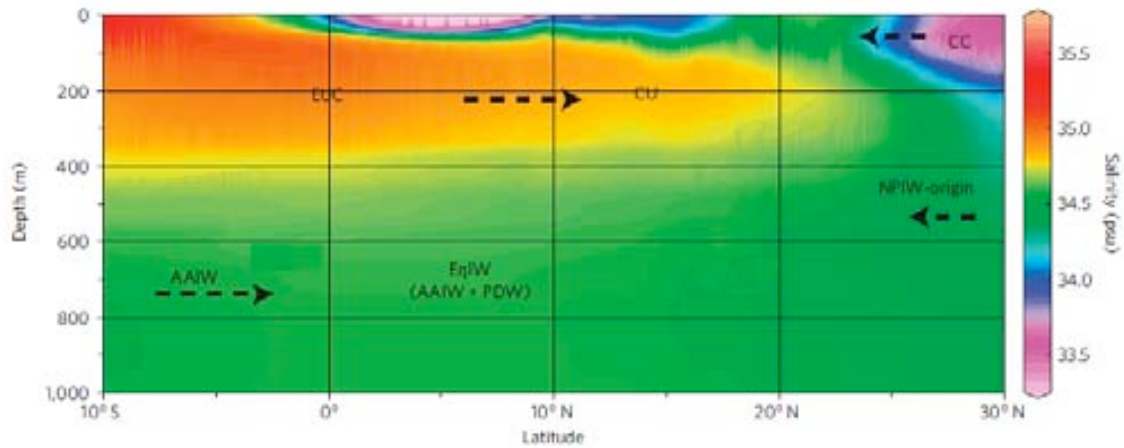
Figure 1.11. Latitudinal salinity transects profile of the North Equatorial Pacific showing deep water masses of the California Current System. Antarctic Intermediate Water (AAIW), Equatorial Intermediate Water (EqIW), North Pacific Intermediate Water (NPIW), Equatorial Undercurrent (EUC), Californian Undercurrent (CU), California Current (CC). Figure modified from Basak et al., 2010.

Besides the interplay between the CC and the SCC during intensification or weakening of the NPH, the CCS is highly susceptible to ENSO variations. El Niño events are characterized by warming, salinity increases, upwelling decreases and thermal expansion in the CCS due to the intensification of the SCC and EUC *(Durazo and Baumgartner 2002)*. The susceptibility of the CCS to different oceanic and atmospheric processes makes it appealing for paleoceanographic studies that on one hand attempt to understand the response of El Niño/La Niña events to changes in the background environment (e.g. global warming during T1). Secondly, they aim to understand the role of the North Pacific Ocean in glacial-interglacial timescale as well as the development and/or intensification of atmospheric-oceanic teleconnections with other ocean basins during key climatic changes.

1.4 <u>Objectives and outlines</u>

Understanding the causes of the natural variability of the climate system, and internal feedbacks involved, is of special interest today due to the well-known sensitivity of the climate to atmospheric CO_2 and the constant release of this gas to the atmosphere. A better knowledge of the long-term trends of the climate can be only achieved through paleoceanographic/paleoclimatic studies. In this sense, the main objective of this thesis is to understand past surface ocean hydrographical changes and their influence on the climate system by means of a set of temperature and salinity change reconstructions

based on the well-established planktonic foraminiferal Mg/Ca and $\delta^{18}O$ proxies, respectively.

The specific objectives are:

- Understanding upper Southern Ocean hydrographical changes across the Middle-Pleistocene Transition (MPT; 1250-700 ka) and their effect on the exchange of carbon (C) between the deep ocean and the atmosphere during this key climatic transition (chapter 3).

- Evaluating changes in the physical structure of the Subantarctic Zone water column as a consequence of the northward expansion of the Antarctic Polar Frontal system at the onset of the MPT, and its effect on the utilization of sharp increases in micro-nutrient availability at 1250 ka (chapter 4).

- Understanding temperature and salinity changes in the North-East Pacific Ocean during periods of enhanced freshwater inputs in the North Atlantic and weakening of the Atlantic Meridional Overturning Circulation between 19 to 3 ka BP, the Termination I-early Holocene (chapter 5).

1.5. <u>References</u>

Anderson, R. F., Ali, S., Bradtmiller, L. I., Nielsen, S. H. H., Fleisher, M. Q., Anderson, B. E., Burckle, L. H., 2009. Wind-Driven Upwelling in the Southern Ocean and the Deglacial Rise in Atmospheric CO2. Science. 323, 1443-1448.

Anderson, R. F. and Carr, M., 2010. Uncorking the Southern Ocean's Vintage CO2. Science. 328, 1117-1118.

Archer, D. E., Eshel, G., Winguth, A., Broecker, W., Pierrehumbert, R., Tobis, M., Jacob, R., 2000. Atmospheric pCO$_2$ sensitivity to the biological pump in the ocean. Global Biogeochem. Cycles. - 1219.

Archer, D. E., Martin, P. A., Milovich, J., Brovkin, V., Plattner, G., Ashendel, C., 2003. Model sensitivity in the effect of Antarctic sea ice and stratification on atmospheric pCO2. Paleoceanography. 18, 1012.

Barker, S., Diz, P., Vautravers, M. J., Pike, J., Knorr, G., Hall, I. R., Broecker, W. S., 2009. Interhemispheric Atlantic seesaw response during the last deglaciation. Nature. 457, 1097-1102.

Becquey, S. and Gersonde, R., 2002. Past hydrographic and climatic changes in the Subantarctic Zone of the South Atlantic – The Pleistocene record from ODP Site 1090. Palaeogeography, Palaeoclimatology, Palaeoecology. 182, 221-239.

Benway, H. M., Mix, A. C., Haley, B. A., Klinkhammer, G. P., 2006. Eastern Pacific Warm Pool paleosalinity and climate variability: 0–30 kyr. Paleoceanography. PA3008.

Berger, A., Li, X. S., Loutre, M. F., 1999. Modelling northern hemisphere ice volume over the last 3 Ma. Quaternary Science Reviews. 18, 1-11.

Brierley, C. M., Fedorov, A. V., Liu, Z., Herbert, T. D., Lawrence, K. T., LaRiviere, J. P., 2009. Greatly Expanded Tropical Warm Pool and Weakened Hadley Circulation in the Early Pliocene. Science. 323, 1714-1718.

Broecker, W. S., and G. H. Denton (1989), The role of ocean-atmosphere reorganizations in glacial cycles, Geochimica Et Cosmochimica Acta, 53(10), 2465-2501, doi: 10.1016/0016-7037(89)90123-3.

Chikamoto, M. O., Menviel, L., Abe-Ouchi, A., Ohgaito, R., Timmermann, A., Okazaki, Y., Harada, N., Oka, A., Mouchet, A., 2012. Variability in North Pacific intermediate and deep water ventilation during Heinrich events in two coupled climate models. Deep Sea Research Part II: Topical Studies in Oceanography. 61–64, 114-126.

Clark, P. U., Archer, D., Pollard, D., Blum, J. D., Rial, J. A., Brovkin, V., Mix, A. C., Pisias, N. G., Roy, M., 2006. The middle Pleistocene transition: characteristics, mechanisms, and implications for long-term changes in atmospheric pCO2. Quaternary Science Reviews. 25, 3150-3184.

Clark, P. U. and Pollard, D., 1998. Origin of the Middle Pleistocene Transition by Ice Sheet Erosion of Regolith. Paleoceanography. 13, 1-9.

de Garidel-Thoron, T., Rosenthal, Y., Bassinot, F., Beaufort, L., 2005. Stable sea surface temperatures in the western Pacific warm pool over the past 1.75[thinsp]million years. Nature. 433, 294-298.

Durazo, R. and Baumgartner, T. R., 2002. Evolution of oceanographic conditions off Baja California: 1997–1999. Progress in Oceanography. 54, 7-31.

Edwards, A. M., Platt, T., Sathyendranath, S., 2004. The high-nutrient, low-chlorophyll regime of the ocean: limits on biomass and nitrate before and after iron enrichment. Ecological Modelling. 171, 103-125.

Elderfield, H., Ferretti, P., Greaves, M., Crowhurst, S., McCave, I. N., Hodell, D., Piotrowski, A. M., 2012. Evolution of Ocean Temperature and Ice Volume Through the Mid-Pleistocene Climate Transition. Science. 337, 704-709.

Etourneau, J., Martinez, P., Blanz, T., Schneider, R., 2009. Pliocene–Pleistocene variability of upwelling activity, productivity, and nutrient cycling in the Benguela region. Geology. 37, 871-874.

Flores, J. and Sierro, F. J., 2007. Pronounced mid-Pleistocene southward shift of the Polar Front in the Atlantic sector of the Southern Ocean. Deep Sea Research Part II: Topical Studies in Oceanography. 54, 2432-2442.

Gildor, H., and E. Tzipermanl, 2000. Sea ice as the glacial cycles' climate switch: Role of seasonal and orbital forcing, *Paleoceanography*, *15*(6), 605-615, doi: 10.1029/1999PA000461

Hain, M. P., Sigman, D. M., Haug, G. H., 2010. Carbon dioxide effects of Antarctic stratification, North Atlantic Intermediate Water formation, and subantarctic nutrient drawdown during the last ice age: Diagnosis and synthesis in a geochemical box model. Global Biogeochemical Cycles. 24, GB4023.

Hain, M. P., Sigman, D. M., and Haug, G. H.: Shortcomings of the isolated abyssal reservoir model for deglacial radiocarbon changes in the mid-depth Indo-Pacific Ocean, Geophys. Res. Lett., 38, L04604, doi:10.1029/2010GL046158, 2011.

Hall, I. R., McCave, I. N., Shackleton, N. J., Weedon, G. P., Harris, S. E., 2001. Intensified deep Pacific inflow and ventilation in Pleistocene glacial times. Nature. 412, 809-812.

Hays, J. D., J. Imbrie, and N. J. Shackleton, 1976. Variations in the Earth's Orbit: Pacemaker of the Ice Ages, *Science*, *194* (4270), 1121-1132, doi: 10.1126/science.194.4270.1121.

Haug GH, Hughen KA, Sigman DM, Peterson LC and Rohl U, 2001. Southward migration of the intertropical convergence zone through the Holocene. Science 293:1304–1308

Herbert, T. D., Schuffert, J. D., Andreasen, D., Heusser, L., Lyle, M., Mix, A., Ravelo, A. C., Stott, L. D., Herguera, J. C., 2001. Collapse of the California Current During Glacial Maxima Linked to Climate Change on Land. Science. 293, 71-76.

Hodell, D. A., Channell, J. E. T., Curtis, J. H., Romero, O. E., Röhl, U., 2008. Onset of "Hudson Strait" Heinrich events in the eastern North Atlantic at the end of the middle Pleistocene transition (~640 ka)? Paleoceanography. 23, PA4218.

Hodell, D. A. and Venz-Curtis, K. A., 2006. Late Neogene history of deepwater ventilation in the Southern Ocean. Geochemistry, Geophysics, Geosystems. 7, Q09001.

Hönisch, B., Hemming, N. G., Archer, D., Siddall, M., McManus, J. F., 2009. Atmospheric Carbon Dioxide Concentration Across the Mid-Pleistocene Transition. Science. 324, 1551-1554.

Huybers, P. and Wunsch, C., 2005. Obliquity pacing of the late Pleistocene glacial terminations. Nature. 434, 491-494.

Jaccard, S. L., G. H. Haug, D. M. Sigman, T. F. Pedersen, H. R. Thierstein, and U. Rohl (2005), Glacial/interglacial changes in subarctic North Pacific stratification, *Science*, *308*(5724).

Keeling, R. F. and Stephens, B. B., 2001. Antarctic sea ice and the control of Pleistocene climate instability. Paleoceanography. 16, 112-131.

Kemp, A. E. S., Grigorov, I., Pearce, R. B., Naveira Garabato, A. C., 2010. Migration of the Antarctic Polar Front through the mid-Pleistocene transition: evidence and climatic implications. Quaternary Science Reviews. 29, 1993-2009.

Kohfeld, K. E., Quere, C. L., Harrison, S. P., Anderson, R. F., 2005. Role of Marine Biology in Glacial-Interglacial CO2 Cycles. Science. 308, 74-78.

Koutavas, A., Lynch-Stieglitz, J., Marchitto, T.M., Sachs, J., 2002. El Niño-like pattern in ice age tropical Pacific sea surface temperature. Science 297, 226–230.

Lawrence, K. T., Liu, Z., Herbert, T. D., 2006. Evolution of the Eastern Tropical Pacific Through Plio-Pleistocene Glaciation. Science. 312, 79-83.

Lea, D.W., Pak, D.K., Spero, H.J., 2000. climate impact of late Quaternary equatorial Pacific sea surface temperature variations. Science 289, 1719–1724.

Leuenberger, M., and U. Siegenthaler (1992), Ice-age atmospheric concentration of nitrous oxide from an Antarctic ice core, *Nature*, *360*(6403), 449-451, doi: 10.1038/360449a0.

Li, L., Li, Q., Tian, J., Wang, P., Wang, H., Liu, Z., 2011. A 4-Ma record of thermal evolution in the tropical western Pacific and its implications on climate change. Earth and Planetary Science Letters. 309, 10-20.

Liu, Z., Altabet, M. A., Herbert, T. D., 2005. Glacial-interglacial modulation of eastern tropical North Pacific denitrification over the last 1.8-Myr. - Geophys. Res. Lett. - L23607.

Lisiecki, L. E. and Raymo, M. E., 2005. A Pliocene-Pleistocene stack of 57 globally distributed benthic δ18O records. Paleoceanography. 20, PA1003.

Loulergue, L., A. Schilt, R. Spahni, V. Masson-Delmotte, T. Blunier, B. Lemieux, J.-M. Barnola, D. Raynaud, T. F. Stocker, and J. Chappellaz, 2008. Orbital and millennial-scale features of atmospheric CH4 over the past 800,000 years, *Nature*, *453*(7193), 383-386, doi: 10.1038/nature06950.

Luthi, D., M. Le Floch, B. Bereiter, T. Blunier, J.-M. Barnola, U. Siegenthaler, D. Raynaud, J. Jouzel, H. Fischer, K. Kawamura, and T. F. Stocker (2008), High-resolution carbon dioxide concentration record 650,000-800,000 years before present, *Nature*, *453*(7193), 379-382, doi: 10.1038/nature06949.

Lynn, R.J., Simpson, J.J., 1987. The California Current System: the seasonal variability f its phyiscal characteristics. Journal of Geophysical Research 92 (C12),2,947–12,966.

Marchitto, T. M., Lehman, S. J., Ortiz, J. D., Flückiger, J., van Geen, A., 2007. Marine Radiocarbon Evidence for the Mechanism of Deglacial Atmospheric CO2 Rise. Science. 316, 1456-1459.

Marlow, J. R., Lange, C. B., Wefer, G., Rosell-Mele, A., 2000. Upwelling Intensification As Part of the Pliocene-Pleistocene Climate Transition. Science. 290, 2288-2291.

Martínez-Garcia, A., A. Rosell-Mele´, W. Geibert, R. Gersonde, P. Masque´, V. Gaspari, and C. Barbante (2009), Links between iron supply, marine productivity, sea surface temperature, and CO2 over the last 1.1 Ma, Paleoceanography, 24, PA1207, doi:10.1029/2008PA001657.

Martinez-Garcia, A., Rosell-Mele, A., Jaccard, S. L., Geibert, W., Sigman, D. M., Haug, G. H., 2011. Southern Ocean dust-climate coupling over the past four million years. Nature. advance online publication, .

Martínez-Garcia, A., Rosell-Melé, A., McClymont, E. L., Gersonde, R., Haug, G. H., 2010. Subpolar Link to the Emergence of the Modern Equatorial Pacific Cold Tongue. Science. 328, 1550-1553.

Mayewski, P. A., Rohling, E. E., Curt Stager, J., Karlén, W., Maasch, K. A., David Meeker, L., Meyerson, E. A., Gasse, F., van Kreveld, S., Holmgren, K., Lee-Thorp, J., Rosqvist, G., Rack, F., Staubwasser, M., Schneider, R. R., Steig, E. J., 2004. Holocene climate variability. Quaternary Research. 62, 243-255.

McClymont, E. L. and Rosell-Mele, A., 2005. Links between the onset of modern Walker circulation and the mid-Pleistocene climate transition. Geology. 33, 389-392.

McClymont, E. L., Ganeshram, R. S., Pichevin, L. E., Talbot, H. M., van Dongen, B. E., Thunell, R. C., Haywood, A. M., Singarayer, J. S., Valdes, P. J., 2012. Sea-surface temperature records of Termination 1 in the Gulf of California: Challenges for seasonal and interannual analogues of tropical Pacific climate change. Paleoceanography. PA2202.

McManus, J.F., Francois, R., Gherardi, J.-M., Keigwin, L.D., Brown-Leger, S., 2004. Collapse and rapid resumption of Atlantic meridional circulation linked to deglacial climate changes. Nature 428, 834–837

Medina-Elizalde, M. and Lea, D. W., 2005. The Mid-Pleistocene Transition in the Tropical Pacific. Science. 310, 1009-1012.

Milankovitch, M. (1930), Mathematische Klimalehre und astronomische Theorie der Klimaschwankungen, *In "Handbuch der Klimatologie, vol. 1*.

Mudelsee, M. and Schulz, M., 1997. The Mid-Pleistocene climate transition: onset of 100 ka cycle lags ice volume build-up by 280 ka. Earth and Planetary Science Letters. 151, 117-123.

Naish, T., Powell, R., Levy, R., Wilson, G., Scherer, R., Talarico, F., Krissek, L., Niessen, F., Pompilio, M., Wilson, T., Carter, L., DeConto, R., Huybers, P., McKay, R., Pollard, D., Ross, J., Winter, D., Barrett, P., Browne, G., Cody, R., Cowan, E., Crampton, J., Dunbar, G., Dunbar, N., Florindo, F., Gebhardt, C., Graham, I., Hannah, M., Hansaraj, D., Harwood, D., Helling, D., Henrys, S., Hinnov, L., Kuhn, G., Kyle, P., Laufer, A., Maffioli, P., Magens, D., Mandernack, K., McIntosh, W., Millan, C., Morin, R., Ohneiser, C., Paulsen, T., Persico, D., Raine, I., Reed, J., Riesselman, C., Sagnotti, L., Schmitt, D., Sjunneskog, C., Strong, P., Taviani, M., Vogel, S., Wilch, T., Williams, T., 2009. Obliquity-paced Pliocene West Antarctic ice sheet oscillations. Nature. 458, 322-328.

Okazaki, Y., Takahashi, K., Asahi, H., Katsuki, K., Hori, J., Yasuda, H., Sagawa, Y., Tokuyama, H., 2005. Productivity changes in the Bering Sea during the late Quaternary. Deep-Sea Res. II 52, 2150–2162.

Okazaki, Y., Timmermann, A., Menviel, L., Harada, N., Abe-Ouchi, A., Chikamoto, M. O., Mouchet, A., Asahi, H., 2010. Deepwater Formation in the North Pacific During the Last Glacial Termination. Science. 329, 200-204.

Okazaki, Y., Sagawa, T., Asahi, H., Horikawa, K., and Onodera, J.: Ventilation changes in the western North Pacific since the last glacial period, Clim. Past Discuss., 7, 2719-2739, doi:10.5194/cpd-7-2719-2011, 2011

Park, J. and Maasch, K. A., 1993. Plio—Pleistocene Time Evolution of the 100-kyr Cycle in Marine Paleoclimate Records. J. Geophys. Res. 98, 447-461.

Paillard, D. (1998), The timing of Pleistocene glaciations from a simple multiple-state climate model, *Nature*, *391*(6665), 378, doi: 10.1038/34891.

Pena, L. D., Cacho, I., Ferretti, P., Hall, M. A., 2008. El Niño–Southern Oscillation–like variability during glacial terminations and interlatitudinal teleconnections. Paleoceanography. PA3101.

Peterson LC, Haug GH, Hughen KA, Rohl U, 2000. Rapid changes in the hydrologic cycle of the tropical Atlantic during the last glacial. Science 290:1947–1951

Pollard, D., and R. M. DeConto, 2009. Modelling West Antarctic ice sheet growth and collapse through the past five million years, *Nature*, *458*(7236), 329-332, doi: 10.1038/nature07809.

Raymo, M. E., Oppo, D. W., Curry, W., 1997. The Mid-Pleistocene Climate Transition: A Deep Sea Carbon Isotopic Perspective. Paleoceanography. 12, 546-559.

Raymo, M. E., Ruddiman, W. F., Shackleton, N. J., Oppo, D. W., 1990. Evolution of Atlantic-Pacific δ13C gradients over the last 2.5 m.y. Earth and Planetary Science Letters. 97, 353-368.

Raymo, M. E., and P. Huybers, 2008. Unlocking the mysteries of the ice ages, *Nature*,*451*(7176), 284-285, doi: 10.1038/nature06589.

Rintoul, S. R., C. Hughes and D. Olbers, 2001. The Antarctic Circumpolar Current System. In:*Ocean Circulation and Climate*, G. Siedler, J. Church, and J. Gould, (Eds.), Academic Press, 271-302.

Rose, K. A., Sikes, E. L., Guilderson, T. P., Shane, P., Hill, T. M., Zahn, R., and Spero, H. J.: Upper-ocean-to-atmosphere radiocarbon offsets imply fast deglacial carbon dioxide release, Nature, 466, 1093–1097, 2010.

Rosenthal, Y., Oppo, D. W., Linsley, B. K., 2003. The amplitude and phasing of climate change during the last deglaciation in the Sulu Sea, western equatorial Pacific. Geophys. Res. Lett. 1428.

Russon, T., Elliot, M., Sadekov, A., Cabioch, G., Corrège, T., De Deckker, P., 2011. The mid-Pleistocene transition in the subtropical southwest Pacific. Paleoceanography. 26, PA1211.

Sarmiento, J. L., Gruber, N., Brzezinski, M. A., Dunne, J. P., 2004. High-latitude controls of thermocline nutrients and low latitude biological productivity. Nature. 427, 56-60.

Sagawa, T. and K. Ikehara, 2008. Intermediate water ventilation change in the subarctic northwest Pacific during the last deglaciation, *Geophys. Res. Lett.*, *35*, L24702, doi:10.1029/2008GL035133.

Schmieder, F., von Dobeneck, T., Bleil, U., 2000. The Mid-Pleistocene climate transition as documented in the deep South Atlantic Ocean: initiation, interim state and terminal event. Earth and Planetary Science Letters. 179, 539-549.

Sepulcre, S. and Vidal, L. and Tachikawa, K. and Rostek, F. and Bard, E., Sea-surface salinity variations in the northern Caribbean Sea across the Mid-Pleistocene Transition.

Seki, O., Ishiwatari, R., Matsumoto, K., 2002. Millennial climate oscillations in NE Pacific surface waters. Geophysical Research Letters 29 (23), 2144.

Sigman, D.M., Haug, G.H., 2003. The Biological Pump in the Past, in: Heinrich D. Holland, Karl K. Turekian (Eds.), Treatise on Geochemistry. Pergamon, Oxford, pp. 491-528.

Sigman, D. M. and Boyle, E. A., 2000. Glacial/interglacial variations in atmospheric carbon dioxide. Nature. 407, 859-869.

Sigman, D. M., Hain, M. P., Haug, G. H., 2010. The polar ocean and glacial cycles in atmospheric CO2 concentration. Nature. 466, 47-55.

Skinner, L. C., Fallon, S., Waelbroeck, C., Michel, E., Barker, S., 2010. Ventilation of the Deep Southern Ocean and Deglacial CO2 Rise. Science. 328, 1147-1151.

Spahni, R., J. Chappellaz, T. F. Stocker, L. Loulergue, G. Hausammann, K. Kawamura, J. Fluckiger, J. Schwander, D. Raynaud, V. Masson-Delmotte, and J. Jouzel (2005), Atmospheric Methane and Nitrous Oxide of the Late Pleistocene from Antarctic Ice
Cores, *Science*, *310*(5752), 1317-1321, doi: 10.1126/science.1120132.

Saenko, O. A., A. Schmittner, and A. J. Weaver, 2004. The Atlantic-Pacific seesaw, J. Clim., 17, 2033–2038.

Speero, H. J. and Lea, D. W., 2002. The Cause of Carbon Isotope Minimum Events on Glacial Terminations. Science. 296, 522-525

Sosdian, S. and Rosenthal, Y., 2009. Deep-Sea Temperature and Ice Volume Changes Across the Pliocene-Pleistocene Climate Transitions. Science. 325, 306-310.

Stott, L., Southon, J., Timmermann, A., and Koutavas, A.: Radiocarbon age anomaly at intermediate water depth in the Pacific Ocean during the last deglaciation, Paleoceanography, 24, PA2223, doi:10.1029/2008PA001690, 2009.

Timmermann, A., Krebs, U., Justino, F., Goosse, H., Ivanochko, T., 2005. Mechanisms for millennial-scale global synchronization during the last glacial period. Paleoceanography. PA4008.

Toggweiler, J. R., 1999. Variation of Atmospheric CO2 by Ventilation of the Ocean's Deepest Water. Paleoceanography. 571.

Toggweiler, J. R. and Russell, J., 2008. Ocean circulation in a warming climate. Nature. 451, 286-288.

Toggweiler, J. R., Russell, J. L., Carson, S. R., 2006. Midlatitude westerlies, atmospheric CO2, and climate change during the ice ages. Paleoceanography. 21, PA2005.

Tziperman, E. and Gildor, H., 2001. On the mid-Pleistocene transition to 100-kyr glacial cycles and the asymmetry between glaciation and deglaciation times. Paleoceanography. 1001.

Tziperman, E., M. E. Raymo, P. Huybers, and C. Wunsch (2006), Consequences of pacing the Pleistocene 100 kyr ice ages by nonlinear phase locking to Milankovitch forcing, *Paleoceanography*, *21*(4), doi: 10.1029/2005pa001241.

Venz, K. A. and Hodell, D. A., 2002. New evidence for changes in Plio–Pleistocene deep water circulation from Southern Ocean ODP Leg 177 Site 1090. Palaeogeography, Palaeoclimatology, Palaeoecology. 182, 197-220.

Wanner, H., Beer, J., Bütikofer, J., Crowley, T. J., Cubasch, U., Flückiger, J., Goosse, H., Grosjean, M., Joos, F., Kaplan, J. O., Küttel, M., Müller, S. A., Prentice, I. C., Solomina, O., Stocker, T. F., Tarasov, P., Wagner, M., Widmann, M., 2008. Mid- to Late Holocene climate change: an overview. Quaternary Science Reviews. 27, 1791-1828.

Yamamoto, M., Yamamuro, M., Tanaka, Y., 2007. The California current system during the last 136,000 years: response of the North Pacific High to precessional forcing. Quaternary Science Reviews. 26, 405-414.

CHAPTER 2

Analytical Methodologies

2.1. Proxies background

2.1.1. Mg/Ca ratio in planktonic foraminifera: a sea surface temperature proxy

As a result of the similar ionic radius and charge of Mg^{+2} and Ca^{+2} ions, Mg^{+2} can substitute for Ca^{+2} during calcite precipitation. In planktonic foraminifera, this incorporation is influenced by the temperature of the water in which the foraminiferal calcite precipitates. Namely, the Mg/Ca ratios of foraminiferal shells increase as the temperature of sea water in which they calcify increases (e.g., *Lea et al., 1999; Anand, et al., 2003; Barker et al., 2005*).

Several studies have demonstrated that the relationship between temperature and planktonic foraminiferal Mg/Ca ratio is exponential (equation 1) and species-specific (e.g., *Mashiotta, et al. 1999; Elderfield and Ganssen. 2000; Regenberg, et al. 2009*), although in some cases multispecies calibration can also yield good results (e.g. 49 Elderfield,H. 2000; Fig 2.1.1) .

$$Mg/Ca \ (mmol \ mol^{-1}) = b* \ e^{a\mathrm{T}} \qquad (1)$$

where b is the pre-exponential constant, a the exponential constant (consistently found to be around 0.09–0.1 which reflects a temperature sensitivity in Mg/Ca of ~10% per 1°C increase in temperature), and T the calcification temperature.

There are different advantages of this proxy over other temperature proxies:

1) Mg/Ca and oxygen isotope ($\delta^{18}O_c$) measurements can be carried out on the exact same signal carrier (i.e., foraminiferal calcite), which precipitated under the exact same environmental conditions (depth habitat, season, etc.). Paired Mg/Ca and $\delta^{18}O_c$ measurements allow reconstruction of past oxygen isotopic composition of sea water ($\delta^{18}O_{sw}$) (*Lea et al., 1999; Mashiotta et al.,1999; Karas et al., 2009*).

2) The residence times of Mg^{2+} and Ca^{2+} are both relatively long. The Mg/Ca ratios in seawater can be considered constant throughout the last ~2000 ka *(Medina-Elizalde et al., 2008)*, thereby enabling seawater temperature reconstructions throughout the Quaternary;

3) It allows reconstructions of vertical water column temperature gradients, as different foraminiferal species dwell in different depths of the upper ocean (e.g. *(Steph et al., 2009; Steinke et al., 2010).*
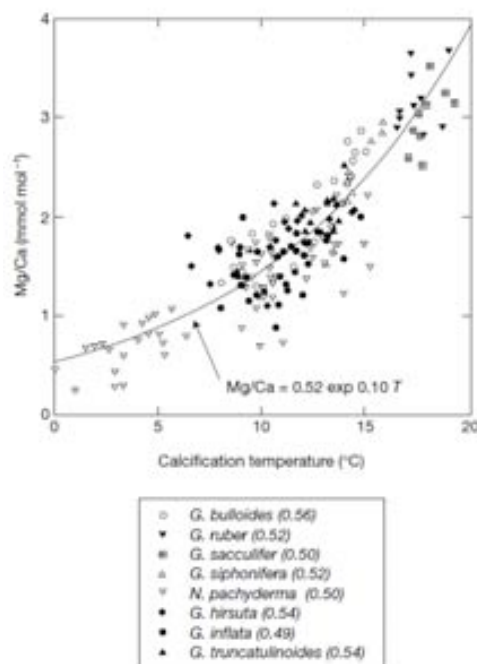
Figure 2.1. Typical Mg/Ca-temperature calibration (taken from *Elderfield and Ganssen, 2000*). It shows a multispecies calibration as well as the species specific influence on the pre-exponential which can be attributed to vital effects.

Although there are many advantages in using foraminiferal Mg/Ca measurements to estimate past ocean temperatures, there are some aspects that must be carefully taken into consideration while interpreting the data. Here we discuss the most relevant issues that can affect this widely-employed proxy, focusing respectively on: (1) specimen selection and sample preparation; (2) Mg/Ca to temperature conversion; and (3) data interpretation.

2.1.1.1 Specimens selection and sample preparation

- Foraminiferal species and morphotypes

As pointed out above, foraminiferal species have different depth habitats depending on their ecological preferences (salinity, temperature, nutrient availability, etc.) (e.g.

(Anand et al., 2003; Regenberg et al., 2009). Consequently, the temperature reconstructed using specific foraminifera species is an integrated temperature signal of the depth range (and season) in which that particular species grew and calcified. Accordingly, species selection should be done with great care according to the specific goal of the study.

Morphotypes of the same species can also show different preferences in terms of depth habitat. For instance, different morphotypes of *Globogirenoides ruber* (white) calcify at different depths *(Wang, 2000; Steinke et al., 2005).* Similar to *G. ruber*, *Neogloboquadrina pachyderma* morphotypes also show different ecological preferences depending on the coiling direction, such that the left coiling morphotype prefers colder environments than the right coiling one, to the extent that the latter morphotype, in some studies, has been ranked as a different species, *Neogloboquadrina incompta (Darling et al., 2006).*

- Size fraction and foraminifera preservation

Elderfield *et al.,* (2002) have shown that in most of the planktonic foraminiferal species, higher Mg/Ca ratios are found when the size of the shell increases. Therefore, ideally foraminifera should be picked from a size fraction window as narrow as possible in order to minimize size-related biases. Furthermore, the picked foraminifera should appear well-preserved under the light microscope to avoid that partially dissolved specimens are measured.

- Cleaning protocol (reductive vs. non-reductive step)

Generally speaking, two different cleaning protocols can be used to clean the samples prior to analysis. They are extremely similar to one another with the exception of one step, which can be added or not depending on the bottom/pore-water chemistry of the study area. Under suboxic conditions, Manganese Oxides (MnO_2) can be reduced to Mn^{2+}. This Mn^{2+} can diffuse upward in the sediment where can be re-oxidized to form again MnO_2 or it can move downward to precipitate as Mn-Ca-Mg and/or Fe-Mn (ferromanganese) coatings on the foraminiferal shells (*Klinkhammer,* 1980; *Pedersen and Price* 1982; *Thomson et al.,* 1986). The aim of including this so-called reductive step is to remove those coatings, which can be enriched with Mg, thereby increasing the foraminiferal Mg/Ca ratio and positively biasing temperatures values derived from them

(Boyle, 1983; Pena et al., 2005). On the other hand, the inclusion of this step in the cleaning protocol can cause foraminiferal dissolution, removing up to 8-10% of the original Mg/Ca in the shells and providing anomalously low temperatures values *(Pena et al., 2005; Barker et al., 2003)*

2.1.1.2. Mg/Ca ratios convertion

There are three approaches to determine the Mg/Ca–calcification temperature relationships in the foraminiferal calcite: a) culture experiments (e.g. *Lea et al., 1999*; *Nürnberg et al., 1996*); b) sediment-trap and water-column studies (e.g., *Anand et al., 2003; Martínez-Botí et al., 2011)*; and c) core-top studies (e.g., *Elderfield and Ganssen, 2000*). Advantages and disadvantages of the different calibrations are summarized in table 1 (summarized from *Barker et al., 2005; Lea, 2003; Mortyn and Martínez-Botí. 2007*). It has been demonstrated that results attained by using the 3 approaches are overall in good agreement.

2.1.1.3. Data interpretation

- Dissolution

During transit to the sea floor, foraminifers undergo different processes that can affect the Mg/Ca ratio of their shells. One of these processes is dissolution, which preferentially removes Mg-enriched calcite from the shells and thus lowers their Mg/Ca ratio (lower temperature; *Lea et al., 1999; Dekens et al., 2002*). Different studies have focused on developing a correction that accounts for the dissolution effect in foraminifera *(Dekens et al., 2002; Rosenthal and Lohmann, 2002; Sadekov et al., 2010)*, but a conclusive approach has yet to be provided.

- Salinity

It has been shown that the uptake of Mg/Ca in planktonic foraminifera can increase when seawater salinity increases above 35 psu. Although this effect on Mg/Ca uptake in foraminifera is not yet fully understood, it should be considered when this proxy is applied in sites located in areas characterized by high salinity gradients, such as the Mediterranean Sea *(Hoogakker et al., 2009; Boussetta et al., 2011; van Raden et al., 2011)*.

- Digenetic overprint

Recent work from similar environments *(Boussetta et al., 2011; van Raden et al., 2011)* has revealed another potentially complicating factor, which is the diagenetic Mg-rich calcite "overprints" to positively bias Mg/Ca ratios. In the Mediterranean Sea, this effect has been revealed beyond a salinity-related Mg/Ca increase to explain exceptionally high values in this region. This lends particular caution to the use of the planktonic foraminiferal Mg/Ca proxy in other regions characterized by restricted circulation, high evaporation, and comparable potential for carbonate overgrowth phases related to diagenesis in sediments.

Table 2.1. Advantages and disadvantages of the different calibration approach.

Approach	Advantages	Disadvantage
Culture experiments	A full suite of environmental factors (e.g., Temperature, salinity, nutrients, light, pH) affecting Mg uptake can be constrained during the experiment	(i) only a limited number of Species (and specimens) can be studied, (ii) foraminiferal reproduction cannot be always achieved under laboratory conditions, and (iii) laboratory conditions may not realistically reproduce the natural environment sufficiently to ensure natural chamber growth
Sediment traps	Season , temperature, and salinity conditions in which foraminifera calcify can be known, so direct comparison between the geochemical signal and the *in-situ* instrumental data is possible	(i) Relatively small amount of foraminifera for analyses, (ii) sample has not gone throughout gametogenic and sedimentary processes, (iii) life cycle stage is not known
Core-tops	Integrates all the processes that take place from the initial foraminiferal chamber formation to residence at the sea floor (e.g., gametogenic calcite)	Complications in calibrating the results may arise if the samples used have undergone post-depositional alteration

2.1.2. Oxygen stable isotope ($\delta^{18}O$) composition of planktonic foraminifera: a combined temperature and salinity signal.

2.1.2.1. Sea water $\delta^{18}O$ composition

Oxygen is present in the nature in the form of three different stable isotopes: ^{16}O, ^{17}O, and ^{18}O, which relative abundances are 99.76%, 0.037%, and 0.19% respectively. Due to their higher abundances compared to ^{17}O (which is known as cumpled isotopes) the ^{18}O and ^{16}O isotopes are the most common forms used in geology. However, the abundance of the ^{18}O isotope is still relatively too small to be accurate measured when using the available analytical techniques. To overcome this limitation, the isotopic composition of a given unknown sample (S) is measured against an external standard (std) with a known isotopic composition *(crf. Rohling and Cooke, 1999)*. This approach is defined as δ (equation 2), and it is reported in parts per thousand (‰):

$$\delta^{18}O_S = ((^{18/16}O_S - {}^{18/16}O_{STD})/{}^{18/16}O_{STD})*1000 \qquad (2)$$

The standard normally use for measuring seawater isotopes composition is Vienna Standard Mean Ocean Water (VSMOW). Processes that influence the partitioning of the oxygen isotopes in seawater ($\delta^{18}O_{SW}$) can be divided in two: those that affect the local $\delta^{18}O_{SW}$ and those that globally modify it.

Locally, the $\delta^{18}O_{SW}$ is highly sensitive to evaporation and precipitation processes (hydrological cycle), ice melting and runoff (e.g. Craig and Gordon, 1965, Rohling and Cook 1999). As shown in Figure 2.2., evaporation processes remove the lighter isotope (^{16}O) preferentially from the seawater while precipitation allows the preferential condensation of the heaviest isotope (^{18}O; e.g. *Dansgaard, 1964*). This process highly accounts for the local distribution of $\delta^{18}O_{SW}$ in low latitudes (Figure 2. 2).

Globally the $\delta^{18}O_{SW}$ is influenced by the latitudinal transport of water vapour and ice volume size *(crf. Rohling and Cooke, 1999)*. Dictated by the Rayleigh distillation *(Garlick, 1974)* the oxygen isotope composition of the sea ice is enriched in ^{16}O with respect to ^{18}O (that is, lighter $\delta^{18}O_{SW}$) during glacial periods, leaving the ocean $\delta^{18}O_{SW}$ values relatively heavier during cold stages. Accordingly, during vapour transport

toward high latitudes, the $\delta^{18}O_{SW}$ of the transported water mass (already depleted in ^{18}O) becomes lighter as precipitation processes take place (e.g. *Dansgaard, 1964*; Fig.2.2). Then, the isotopic composition of the condensed water masses that build up ice in high latitudes is substantially enriched in ^{16}O. To complete the cycle, depleted ^{18}O water masses which form ice, return to the ocean via ice melting and runoff decreasing the $\delta^{18}O_{SW}$ of the surrounding water masses in high latitudes *(crf. Rohling and Cooke, 1999)*. Moreover, the build up of ice in high latitudes reduces the sea level, which further modifies the global mean $\delta^{18}O_{SW}$. It is generally accepted that per metre of sea-level lowering the $\delta^{18}O_{SW}$ change ~0.008‰ in Atlantic deep-sea *(Adkins et al., 2002)*. Different studies have modelled ice volume contribution to global $\delta^{18}O_{SW}$ across long time scales ((e.g. *Bintanja et al., 2005; Stanford et al., 2011*) suggesting similar relations in glacial-interglacial timescales.
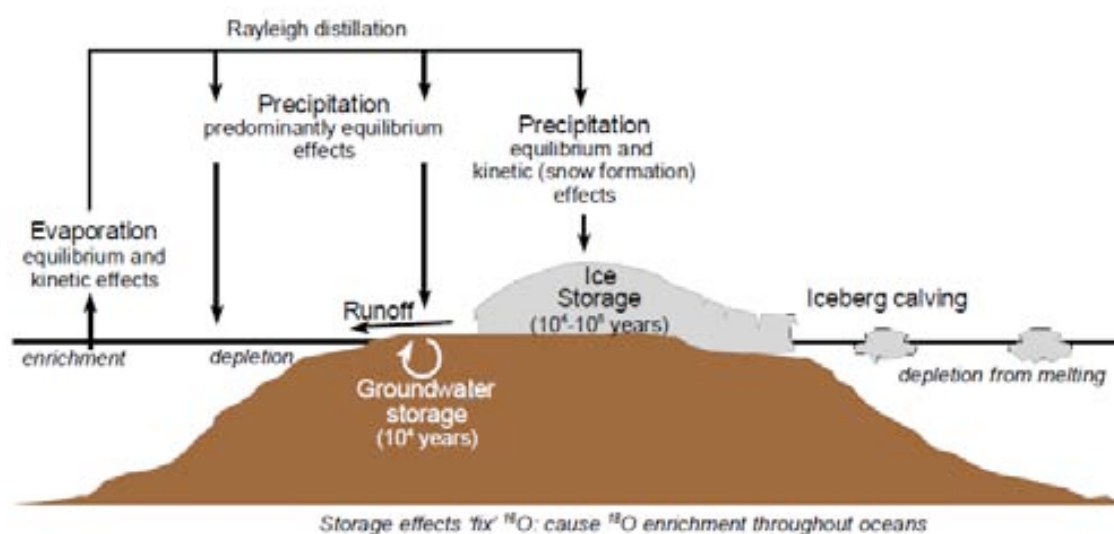
Figure 2.2. Schematic presentation of the processes that produce the fractionation of oxygen isotopic in the ocean (from Rohling and Cooke, 1999).
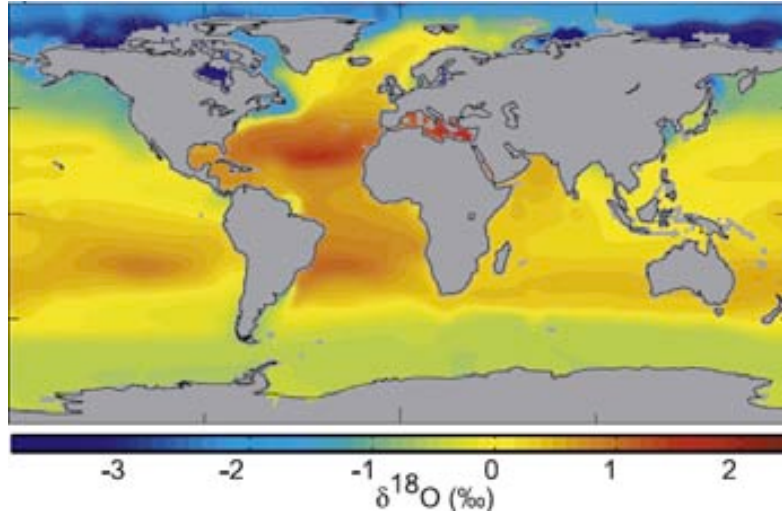
Figure 2.3. Global δ¹⁸O$_{SW}$ distribution *(LeGrande and Schmidt, 2006)*

2.1.2.2. Planktonic foraminifera δ¹⁸O composition

The δ¹⁸O composition in planktonic foraminifera's calcite (δ¹⁸O$_C$) is known to be influenced by the temperature (T; *Uray, 1947*) and the δ¹⁸O$_{SW}$ where it is calcified *(Emiliani, 1955; Epstein et al., 1953)*. This relationship can be expressed by the quadratic equation (3) although the used of the linear component (4) seems to yield also good results *(Bemis, 1998)*.

$$T(\text{°C}) = a - b*(\delta^{18}O_C - \delta^{18}O_{SW}) + c*(\delta^{18}O_C - \delta^{18}O_{SW})^2 \quad (3)$$

$$T(\text{°C}) = a - b*(\delta^{18}O_C - \delta^{18}O_{SW}) \quad (4)$$

where *a* is the temperature when δ¹⁸O$_C$ equals δ¹⁸O$_{SW}$; and *b* is the slope of the equation. The inverse of the slope (1/b) correspond to the rate of δ¹⁸O (in ‰) change per 1°C increase or decrease in temperature. Overall, experiments have shown that δ¹⁸O$_C$ change ~0.27‰ per 1°C (e.g. *Kim and O'Neil, 1997*).

The δ¹⁸O$_C$ is referred to the Pee Dee Belemnite (PDB) which has δ¹⁸O=0 by definition *(Epstein et al., 1953)*. The most commonly used standards are provided by the International Atomic Energy Agency (IAEA); e.g.: IAEA-CO-1 with a δ¹⁸O of -2.4 ±0.1 ‰ PDB, and the NBS19 with a δ¹⁸O of -2.2±0.1‰ PDB. In order to transform PDB to SMOW and vice versa, we use the equation (5).

$$\delta^{18}O_{SW} = \delta^{18}O_C + 0.27 \qquad (5)$$

Eipstein *et al.,* 1953 was the first to propose a paleotemperature equation to be used in paleoclimate reconstructions based on mollusk shell, which was further refined in Craig, 1995 and in other studies that used inorganic calcite precipitation *(O'Neil et al., 1969)*, and culture experiments (e.g. *Erez and Luz 1983; Bemis et al., 2000; Spero et al., 2000*). The first assumption made in the paleotemperature equations (3 and 4) is that planktonic foraminfera calcify in equilibrium with the $\delta^{18}O_{SW}$ of the water mass. However, comparisons between planktonic foraminiferal based equations with inorganic calcite experiments have shown that $\delta^{18}O_C$ is offset from the equilibrium value of the seawater in which the planktonic foraminifera calcify *(Duplessy 1970)*. This is known as "vital effect" and many efforts have been made to develop species specific paleotemperature equations that account for the this (e.g. *Farmer et al., 2007; Mulitza et al., 2004; von Langen et al., 2000; Kim and O'Neil 1997; Shackleton et al., 1974*).

As the Mg/Ca-based temperature proxy inferred from planktonic foraminifera (Section 2.1), the $\delta^{18}O$ is also biased by processes in the water column and during the transit of the shells to the seafloor that can modify their composition (e.g. *Bemis 1998; Spero et al., 1997; Spero and Lea 1996 and 1993*). Among all, the dissolution effect seems to have the most important effect since it removes preferentially the lighter isotope from the shell, positively biasing the $\delta^{18}O_C$ composition *(Dekens et al., 2002)*. For instance, it has been quantified that per km deepening the $\delta^{18}O_C$ increases by ~0.2‰ *(Wu and Berger, 1989; Dekens et al., 2002)* in areas that are known to be extremely affected by dissolution.

2.1.2.3. Deconvolving $\delta^{18}O_{SW}$ records using paired Mg/Ca-$\delta^{18}O_C$ measurements in planktonic foraminifera: paleosalinity reconstruction.

Reconstructing past changes in ocean salinity is of as much importance as reconstructing past ocean temperatures for the paleoclimate community because of the known influence of both variables in ocean circulation. Due to the control of the hydrological cycle on the local partitioning of the $\delta^{18}O_{SW}$ where planktonic foraminifera calcifies (section 2.1.2.1), the $\delta^{18}O_{SW}$ is linearly correlated to local changes in salinity (Fig. 2. 4; *LeGrande and Schmidt, 2006*).

Since there are not yet proxies for reconstructing past ocean salinity changes, the relationship between $\delta^{18}O_{SW}$ and salinity has become a powerful tool for understanding past variations of this oceanic feature (e.g. *Mashiotta et al., 1999; Lea, 2003; Lea et al., 2002*).
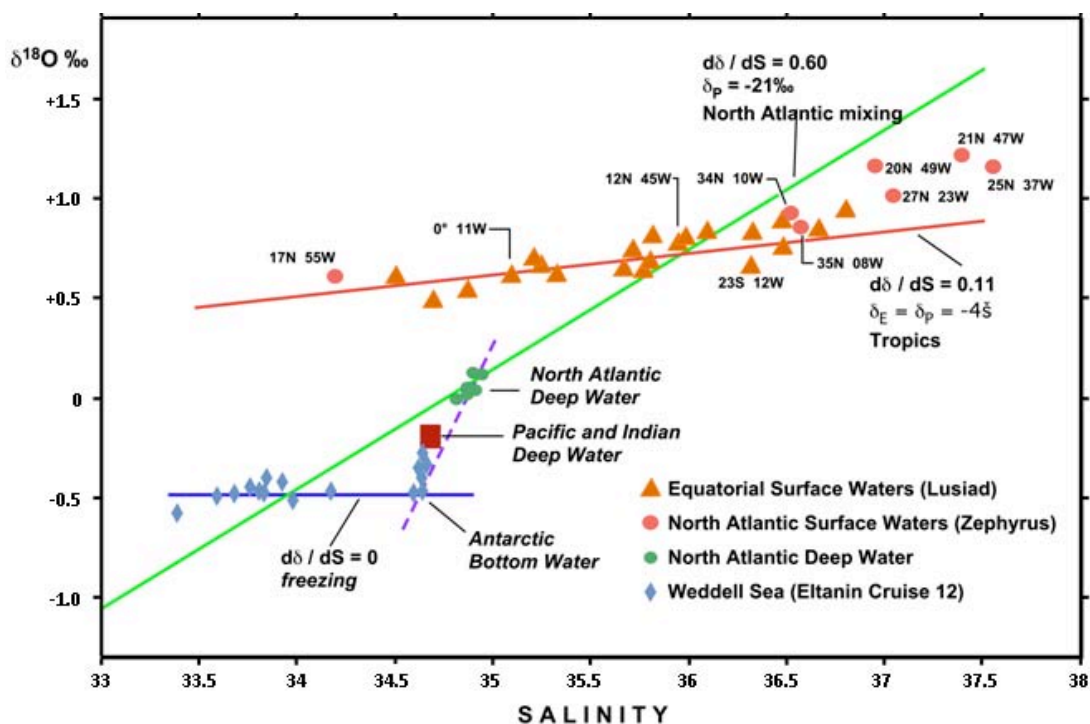
Fig. 2.1.4. $\delta^{18}O_{SW}$ and seawater salinity relation in the Atlantic surface and deep water masses. δe and δp refer to the isotopic composition of evaporating vapour and precipitation (Craig and Gordon, 1965)

Paired Mg/Ca-$\delta^{18}O_C$ measurements in planktonic foraminifera are the best candidate to be used when deconvolving $\delta^{18}O_{SW}$ from equations 3-4. First, because it allows generating temperature and $\delta^{18}O_C$ profiles from the exact same phase and water masses *(Lea, 2003)*, which reduces uncertainties of the $\delta^{18}O_{SW}$ record. Second, because multispecies Mg/Ca-$\delta^{18}O_C$ measurements (using planktonic foraminifera with different depth habitats preferences) can be used to generate downward temperature and $\delta^{18}O_{SW}$ profiles. This allows the understanding of water column physical variations during a given period (e.g. *Regenberg et al., 2009; Karas et al., 2009; Steinke et al., 2010; Steph et al., 2006; Steph et al., 2009*). Nonetheless, some paleoceanography studies have used alkenone-based sea surface temperature (SST) reconstructions to remove the

temperature component from equations 3-4 with fairly sensible results *(Leduc et al., 2007; Sepulcre et al., 2010)*.

In order to better constrained past changes in local $\delta^{18}O_{SW}$, a correction that account for the ice volume contribution to global $\delta^{18}O_{SW}$ changes should be done. Recently, models (Bintanja et al., 2005; Stanford et al., 2011) and proxy data *(Sosdian and Rosenthal, 2009; Elderfield et al., 2012)* studies have made available records that allow to correct for this. In this sense, although ice volume corrected $\delta^{18}O_{SW}$ ($\delta^{18}O_{SW-IVC}$) reconstructions are still far from being accurate; they provide a powerful tool to infer past changes in ocean salinity.

2.2. Analytical methods and sample preparation

2.2.1. Mg/Ca measurements and sample preparation

All the samples analyzed for Mg/Ca in the next chapters underwent analytical and cleaning procedures describe in this section. After picking specie specific planktonic foraminfera (which were carefully selected depending on the study's aim), samples were gently crushed between methanol-cleaned glass microscope slides to break open individual chambers. Afterwards, samples were treated chemically, modifying slightly the cleaning procedures proposed by (Barker et al., 2003). Foraminiferal samples underwent ultra-purified water (milli-Q water) and methanol rinses to remove clay. Then they were cleaned reductively (using anhydrous hydrazine; *Boyle 1983*) to remove Fe-Mn oxide coatings and oxidatively (using H_2O_2) to remove the organic matter. Prior to dissolution, samples were leached once with 0.001 M HNO_3 to remove any adsorbed contaminants *(Barker et al., 2003)*.

Cleaned samples were dissolved in 1% HNO_3. An aliquot of the samples was analysed using an Inductively Coupled Plasma – Mass Spectrometer (ICP-MS, Agilent model 7500ce) to provide a preliminary calcium [Ca^{2+}] determination. The remaining solutions were diluted to 40 ppm [Ca^{2+}] and then injected into the ICP-MS to obtain [Ca^{2+}], magnesium [Mg^{2+}], and other trace metal concentrations *(de Villiers et al., 2002; Yu et al., 2005)*. Analytical precision was monitored calculating the relative standard deviation of two in-house standard solutions analysed after 5 samples, containing Mg/Ca = 2.58 and Mg/Ca= 7.73 mmol mol^{-1} at a [Ca^{2+}] of 40 ppm. The relative

standard deviation was on average 1.3% (N=158). A commonly used limestone standard (ECRM752–1) with a specified Mg/Ca of 3.75 mmol mol^{-1} (Greaves et al., 2008) was also analyzed, yielding values of 3.70±0.9 mmol mol^{-1}. Samples with Al/Ca and Mn/Ca above the commonly used thresholds *(Boyle, 1983; Barker et al., 2003; Ferguson et al., 2008)* were repeated.

An error propagation exercise was carried out for each temperature record generated in the next chapters. It was calculated as follow; the square root of the sum of the second potency of all the errors involved in the Mg/Ca-based temperature records (analytical error, calibration error, and natural variability).

2.2.2. δ¹⁸O$_C$ measurements and sample preparation

Prior to analyses, all the samples were prepared and cleaned following the same procedure. After isolating species specific foraminiferal species, they were crushed, cleaned with methanol, and ultrasonicated for approximately 10 seconds. Then, measurements were performed in two different laboratories.

Cardiff University mass spectrometer

Samples from the ODP Site 190 were analyzed using a Thermofinnigan MAT-252 mass spectrometer coupled online to an automated carbonate sample preparation device. External reproducibility (1σ) of carbonate standards was better than ±0.08‰ for δ^{18}O. Isotope values were calibrated to the Vienna Peedee Belemnite scale (VPDB) with the NBS-19 carbonate standard.

Autonomous University of Barcelona mass spectrometer

Samples from core MD02-2505 were analyzed using a Thermofinnigan MAT-253 mass spectrometer coupled to a Kiel IV device for carbonate sample preparation. External reproducibility (1σ) of carbonate standards was better than ±0.08‰ for δ^{18}O. Isotope values were calibrated to the Vienna Peedee Belemnite scale (VPDB) with the NBS-19 and IAEA-CO-1 carbonate standard.

2.3 References

Adkins, J. F., McIntyre, K., Schrag, D. P., 2002. The Salinity, Temperature, and δ18O of the Glacial Deep Ocean. Science. 298, 1769-1773.

Anand, P., Elderfield, H., Conte, M. H., 2003. Calibration of Mg/Ca thermometry in planktonic foraminifera from a sediment trap time series. Paleoceanography. 18, 1050.

Barker, S., Greaves, M., Elderfield, H., 2003. A study of cleaning procedures used for foraminiferal Mg/Ca paleothermometry. Geochemistry, Geophysics, Geosystems. 4, 8407.

Barker, S., Cacho, I., Benway, H., Tachikawa, K., 2005. Planktonic foraminiferal Mg/Ca as a proxy for past oceanic temperatures: a methodological overview and data compilation for the Last Glacial Maximum. Quaternary Science Reviews. 24, 821-834.

Bemis, B.E., Spero, H.J., Bijma, J., Lea, D.W., 1998. Reevaluation of the oxygen isotopic composition of planktonic foraminifera: Experimental results and revised paleotemperature equations. Paleoceanography 13, 150-160.

Bintanja, R., van de Wal, R. S. W., Oerlemans, J., 2005. Modelled atmospheric temperatures and global sea levels over the past million years. Nature. 437, 125-128.

Boussetta, S., Bassinot, F., Sabbatini, A., Caillon, N., Nouet, J., Kallel, N., Rebaubier, H., Klinkhammer, G., Labeyrie, L., 2011. Diagenetic Mg-rich calcite in Mediterranean sediments: Quantification and impact on foraminiferal Mg/Ca thermometry. Marine Geology. 280, 195-204.

Boyle, E. A. (1983), Manganese carbonate overgrowths on foraminifera tests, Geochimica et Cosmochimica Acta, 47, 1815-1819.

Craig, H., Gordon, L.I., 1965. Isotope oceanography: deuterium and oxygen 18 variations in the ocean and the marine atmosphere. Symposium on Marine Geochemistry, University of Rhode Island Occasional Publications 3, 277-374.

Darling, K. F., Kucera, M., Kroon, D., Wade, C. M., 2006. A resolution for the coiling direction paradox in Neogloboquadrina pachyderma. Paleoceanography. 21, PA2011.

Dansgaard, W., 1964. Stable isotopes in precipitation. Tellus 16, 436-468.

de Villiers, S., Greaves, M., Elderfield, H., 2002. An intensity ratio calibration method for the accurate determination of Mg/Ca and Sr/Ca of marine carbonates by ICP-AES. Geochemistry, Geophysics, Geosystems. 3, 1001.

Dekens, P. S., Lea, D. W., Pak, D. K., Spero, H. J., 2002. Core top calibration of Mg/Ca in tropical foraminifera: Refining paleotemperature estimation. Geochemistry, Geophysics, Geosystems. 3, 1022.

Epstein, S., Buchsbaum, R., Lowenstam, H.A., Urey, H.C., 1953. Revised carbonate-water isotopic temperature scale. Geol. Soc. Am. Bull. 64, 1315-1325.

Elderfield, H. and Ganssen, G., 2000. Past temperature and δ18O of surface ocean waters inferred from foraminiferal Mg/Ca ratios. Nature. 405, 442-445.

Elderfield, H., M. Vautravers, and M. Cooper (2002), The relationship between shell size and Mg/Ca, Sr/Ca, δ^{18}O, and δ^{13}C of species of planktonic foraminifera, *Geochem. Geophys. Geosyst.*, *3*(8), doi:10.1029/2001GC000194.

Elderfield, H., Ferretti, P., Greaves, M., Crowhurst, S., McCave, I. N., Hodell, D., Piotrowski, A. M., 2012. Evolution of Ocean Temperature and Ice Volume Through the Mid-Pleistocene Climate Transition. Science. 337, 704-709.

Emiliani, C., 1955. Pleistocene temperatures: Journal of Geology, v. 63, p. 539-578.

Erez, J., and B. Luz (1983), Experimental paleotemperature equation for planktonic foraminifera, Geochim. Cosmochim. Acta, 47, 1025–1031.

Ferguson, J.E., Henderson, G.M., Kucera, M., Rickaby, R.E.M., 2008. Systematic change of foraminiferal Mg/Ca ratios across a strong salinity gradient. Earth Planet. Sci. Lett. 265, 153–166, http://dx.doi.org/10.1016/j.epsl.2007.10.011.

Garlick, G.D., 1974. The stable isotopes of oxygen, carbon, hydrogen in the marine environment. In: Goldberg, E.D. (Ed.), The Sea, Vol. 5. John Wiley & Sons, New York, pp. 393-425.

Hoogakker, B. A. A., Klinkhammer, G. P., Elderfield, H., Rohling, E. J., Hayward, C., 2009. Mg/Ca paleothermometry in high salinity environments. Earth and Planetary Science Letters. 284, 583-589.

Karas, C., Nurnberg, D., Gupta, A. K., Tiedemann, R., Mohan, K., Bickert, T., 2009. Mid-Pliocene climate change amplified by a switch in Indonesian subsurface throughflow. Nature Geosci. 2, 434-438.

Klinkhammer, G. P. (1980), Early diagenesis in sediments from the eastern equatorial Pacific, II. Pore water metal results, Earth and Planetary Science Letters, 49(1), 81–101.

Lea, D.W., 2003. Elemental and Isotopic Proxies of Past Ocean Temperatures, in: Anonymous . Elsevier Ltd, Treatise on Geochemistry, pp. 365.

Lea, D. W., Martin, P. A., Pak, D. K., Spero, H. J., 2002. Reconstructing a 350 ky history of sea level using planktonic Mg/Ca and oxygen isotope records from a Cocos Ridge core. Quaternary Science Reviews. 21, 283-293.

Lea, D. W., Mashiotta, T. A., Spero, H. J., 1999. Controls on magnesium and strontium uptake in planktonic foraminifera determined by live culturing. Geochimica Et Cosmochimica Acta. 63, 2369-2379.

Leduc, G., Vidal, L., Tachikawa, K., Rostek, F., Sonzogni, C., Beaufort, L., Bard, E., 2007. Moisture transport across Central America as a positive feedback on abrupt climate changes. Nature 445, 908e911. doi:10.1038/nature05578.

LeGrande, A. N. and Schmidt, G. A., 2006. Global gridded data set of the oxygen isotopic composition in seawater. Geophysical Research Letters. 33, L12604.

Martínez-Botí, M. A., Mortyn, P. G., Schmidt, D. N., Vance, D., Field, D. B., 2011. Mg/Ca in foraminifera from plankton tows: Evaluation of proxy controls and comparison with core tops. Earth and Planetary Science Letters. 307, 113-125.

Mashiotta, T. A., Lea, D. W., Spero, H. J., 1999. Glacial–interglacial changes in Subantarctic sea surface temperature and δ18O-water using foraminiferal Mg. Earth and Planetary Science Letters. 170, 417-432.

Medina-Elizalde, M., Lea, D. W., Fantle, M. S., 2008. Implications of seawater Mg/Ca variability for Plio-Pleistocene tropical climate reconstruction. Earth and Planetary Science Letters. 269, 585-595.

Mortyn, P. G., and Martínez-Botí, M. A., 2007. Planktonic foraminifera and their proxies for the reconstruction ofsurface-ocean climate parameters. CONTRIBUTIONS to SCIENCE, 3 (3): 371–383, .

Nürnberg, D., Bijma, J., Hemleben, C., 1996. Assessing the reliability of magnesium in foraminiferal calcite as a proxy for water mass temperatures. Geochimica Et Cosmochimica Acta. 60, 803-814.

O'Neil, J.R., Clayton, R.N., Mayeda, T.K., 1969. Oxygen isotope fractionation on divalent metal carbonates. Journal of Chemical Physics 51, 5547-5558.

Pena, L. D., Calvo, E., Cacho, I., Eggins, S., Pelejero, C., 2005. Identification and removal of Mn-Mg-rich contaminant phases on foraminiferal tests: Implications for Mg/Ca past temperature reconstructions. Geochemistry, Geophysics, Geosystems. 6, Q09P02.

Pedersen, T., and N. Price (1982), The geochemistry of manganese carbonate in Panama Basin sediments, Geochimica et Cosmochimica Acta, 46(1), 59–68.

Regenberg, M., Steph, S., Nürnberg, D., Tiedemann, R., Garbe-Schönberg, D., 2009a. Calibrating Mg/Ca ratios of multiple planktonic foraminiferal species with δ18O-calcification temperatures: Paleothermometry for the upper water column. Earth and Planetary Science Letters. 278, 324-336.

Regenberg, M., Steph, S., Nürnberg, D., Tiedemann, R., Garbe-Schönberg, D., 2009b. Calibrating Mg/Ca ratios of multiple planktonic foraminiferal species with δ18O-calcification temperatures: Paleothermometry for the upper water column. Earth and Planetary Science Letters. 278, 324-336.

Rohling, E.J., Cooke, S., 1999. Stable oxygen and carbon isotope ratios in foraminiferal carbonate. In B.K. Sen Gupta (ed.) Modern Foraminifera, Kluwer Academic, Dordrecht, The Netherlands, pp.239-258.

Rosenthal, Y. and Lohmann, G. P., 2002. Accurate estimation of sea surface temperatures using dissolution-corrected calibrations for Mg/Ca paleothermometry. Paleoceanography. 17, 1044.

Sadekov, A. Y., Eggins, S. M., Klinkhammer, G. P., Rosenthal, Y., 2010. Effects of seafloor and laboratory dissolution on the Mg/Ca composition of Globigerinoides sacculifer and Orbulina universa tests — A laser ablation ICPMS microanalysis perspective. Earth and Planetary Science Letters. 292, 312-324.

Sepulcre, S., Vidal, L., Tachikawa, K., Rostek, F., and Bard, E., 2011. Sea-surface salinity variations in the northern Caribbean Sea across the Mid-Pleistocene Transition, Clim. Past, 7, 75-90, doi:10.5194/cp-7-75-2011.

Spero, H.J., Lea, D.W., 1993. Intraspeci¢c stable isotope variability in the planktic foraminifera Globigerinoides sacculifer: Results from laboratory experiments. Mar. Micropaleontol. 22, 221^234.

Spero, H.J., Lea, D.W., 1996. Experimental determination of stable isotope variability in Globigerina bulloides: Implications for paleoceanographic reconstruction. Mar. Micropaleontol. 28, 231-246.

Spero, H. J., J. Bijma, D. W. Lea, and B. Bemis, 1997. Effect of seawater carbonate chemistry on planktonic foraminiferal carbon and oxygen isotope values, Nature, 390, 497–500.

Sosdian, S. and Rosenthal, Y., 2009. Deep-Sea Temperature and Ice Volume Changes Across the Pliocene-Pleistocene Climate Transitions. Science. 325, 306-310.

Stanford, J. D., Hemingway, R., Rohling, E. J., Challenor, P. G., Medina-Elizalde, M., Lester, A. J., 2011. Sea-level probability for the last deglaciation: A statistical analysis of far-field records. Global and Planetary Change. 79, 193-203.

Steinke, S., Chiu, H., Yu, P., Shen, C., Löwemark, L., Mii, H., Chen, M., 2005. Mg/Ca ratios of two Globigerinoides ruber (white) morphotypes: Implications for reconstructing past tropical/subtropical surface water conditions. Geochemistry, Geophysics, Geosystems. 6, Q11005.

Steinke, S., Mohtadi, M., Groeneveld, J., Lin, L., Löwemark, L., Chen, M., Rendle-Bühring, R., 2010. Reconstructing the southern South China Sea upper water column structure since the Last Glacial Maximum: Implications for the East Asian winter monsoon development. Paleoceanography. 25, PA2219.

Steph, S., Tiedemann, R., Prange, M., Groeneveld, J., Nürnberg, D., Reuning, L., Schulz, M., - Haug, G. H., 2006. Changes in Caribbean surface hydrography during the Pliocene shoaling of the Central American Seaway. - Paleoceanography. - PA4221.

Steph, S., Regenberg, M., Tiedemann, R., Mulitza, S., Nürnberg, D., 2009. Stable isotopes of planktonic foraminifera from tropical Atlantic/Caribbean core-tops: Implications for reconstructing upper ocean stratification. Marine Micropaleontology. 71, 1-19.

Thomson, J., N. Higgs, I. Jarvis, D. Hydes, S. Colley, and T. Wilson, 1986. The behaviour of manganese in Atlantic carbonate sediments, Geochimica et Cosmochimica Acta, 50(8), 1807–1818.

Urey, H. C., 1947. The thermodynamics of isotopes abundances. Jounar of chemichal Sociaty of London. 562-581.

van Raden, U. J., Groeneveld, J., Raitzsch, M., Kucera, M., 2011. Mg/Ca in the planktonic foraminifera Globorotalia inflata and Globigerinoides bulloides from Western Mediterranean plankton tow and core top samples. Marine Micropaleontology. 78, 101-112.

von Langen, P. J., D. K. Pak, H. J. Spero, and D. W. Lea (2005), Effects of temperature on Mg/Ca in neogloboquadrinid shells determined by live culturing, Geochem. Geophys. Geosyst., 6, Q10P03, doi:10.1029/2005GC000989.

Wang, L., 2000. Isotopic signals in two morphotypes of Globigerinoides ruber (white) from the South China Sea: implications for monsoon climate change during the last glacial cycle. Palaeogeography, Palaeoclimatology, Palaeoecology. 161, 381-394.

Wu G. and Berger W. H., 1989. Planktonic foraminifera: differential dissolution and the Quaternary stable isotope record in the west equatorial Pacific. Paleoceanography 4(2), 181–198.

Yu, J., Day, J., Greaves, M., Elderfield, H., 2005. Determination of multiple element/calcium ratios in foraminiferal calcite by quadrupole ICP-MS. Geochemistry, Geophysics, Geosystems. 6, Q08P01.

CHAPTER 3

Glacial Southern Ocean freshening at the onset of the Middle Pleistocene Climate Transition

Abstract

Changes in Southern Ocean hydrography may have played an important role in the Middle Pleistocene Transition (MPT), particularly through their impact on ocean circulation and atmospheric CO_2 concentrations. Here we present foraminiferal Mg/Ca and $\delta^{18}O$ results for the subsurface dwelling planktonic foraminifer *Neogloboquadrina pachyderma* (sinistral) at the Ocean Drilling Program (ODP) Site 1090. Results are used to reconstruct upper ocean temperatures and derive seawater $\delta^{18}O$ in the Subantarctic Atlantic Ocean during the MPT. The new records indicate that, starting at ~1250 ka, glacial temperatures and local (ice volume corrected) seawater $\delta^{18}O$ in the upper water column of the Subantarctic Atlantic Ocean decreased, pointing to cooler (~2ºC) and fresher (~0.4‰) conditions than in the preceding glacial stages. These upper ocean hydrographic changes broadly coincide with the increase in the power of the 100 ky glacial-interglacial cycle in both records and with a shift towards decreased deep ventilation in the glacial Southern Ocean. Our finding suggests that an increase in Southern Ocean stratification, driven by the observed freshening of the upper water column, may have reduced the exchange of carbon between the deep Southern Ocean and the atmosphere during glacial stages. This process may have contributed, in combination with other mechanisms, to lower glacial atmospheric CO_2 concentrations during the MPT.

3.1. <u>Introduction</u>

During the Middle Pleistocene Transition (MPT), between 1250 and 700 ka (Clark et al., 2006), the periodicity of the glacial-interglacial cycles changed from 41 ky to a less frequent, more intense and asymmetric 100 ky rhythm (e.g., Park and Maasch, 1993; Mudelsee and Schulz, 1997; Schmieder et al., 2000; Clark et al., 2006). This fundamental climate reorganization apparently occurred in the absence of any considerable change in orbital forcing, leading to the concept that the MPT involved a change of the climate system's internal feedbacks (Clark et al., 2006), which has yet to be conclusively addressed.

Some of the hypotheses to explain the MPT invoke a decrease in atmospheric carbon dioxide concentrations (pCO$_2$) as the driving mechanism (Raymo et al., 1997; Paillard, 1998; Berger et al., 1999; van de Wal and Bintanja, 2009; Martínez-Garcia et al., 2011). Currently available reconstructions indicate that glacial pCO$_2$ decreased by ~30 ppmv during the MPT, while interglacial pCO$_2$ levels remained relatively unchanged (Hönisch et al., 2009). A ~30 ppmv shift to lower glacial pCO$_2$ levels, likely in combination with other climate feedbacks (Clark et al., 2006), may have played an important role in the climate changes observed across the MPT, given the potentially higher climate sensitivity to pCO$_2$ for a glacial world compared to the present-day (van de Wal and Bintanja, 2009).

The Southern Ocean has been proposed as one of the key regions of the global ocean in modulating pCO$_2$ variations on glacial-interglacial timescales (Sigman and Boyle, 2000; Sigman et al., 2010 and references therein). In the modern Southern Ocean the efficiency of the biological pump to sequester carbon is limited by the scarcity of micro-nutrients, e.g., iron (Fe). Accordingly, an increase in Fe supply by aeolian dust during glacial intervals would stimulate marine export production and enhance major nutrient consumption, contributing to the storage of respired CO$_2$ in the deep ocean (Martin, 1990). The increased export production in the Subantarctic Zone during glacials was closely coupled to changes in aeolian Fe supply (Kumar et al., 1995; Kohfeld et al., 2005; Martínez-Garcia et al., 2009). However, modeling studies and paleoceanographic data suggest that Fe fertilization of the Subantarctic Zone can explain only a fraction of

the complete glacial-interglacial pCO_2 fluctuations of the Late Pleistocene, and hence other mechanisms are required to explain the full amplitude of pCO_2 (90-100 ppmv) shifts (Watson et al., 2000; Kohfeld et al., 2005; Martínez-Garcia et al., 2009) that are observed in the Antarctic ice cores (e.g. Lüthi et al., 2008).

The storage of respired CO_2 at depth in the polar Southern Ocean may be another important mechanism to sequester carbon in the deep ocean during glacial times (Toggweiler, et al., 1999). This process may have been modulated by changes in the position of the westerly wind belt (Toggweiler et al., 2006), in the surface ocean stratification (Francois et al., 1997; Toggweiler, 1999), and in the latitudinal extension and temporal duration of the Antarctic sea-ice cover (Stephens and Keeling, 2000; Keeling and Stephens, 2001; Archer et al., 2003). Indeed, Antarctic sea-ice cover, westerly winds changes, and stratification of the Southern Ocean have been proposed as key factors to reduce the pCO_2, by physically inhibiting the CO_2 outgassing and by decreasing the vertical mixing of the water column in the Southern Ocean, respectively (Francois et al., 1997; Toggweiler, 1999; Stephens and Keeling, 2000; Sigman et al., 2004).

Various studies have provided evidence of major changes in deep water circulation roughly coincident with the onset of the MPT (Schmieder et al., 2000; Hall et al., 2001; Venz and Hodell, 2002; Hodell and Venz-Curtis, 2006) that might reflect an increase in water column stratification in the Southern Ocean (Hodell and Venz-Curtis, 2006). The enhanced sensitivity of the ocean density to salinity changes during glacial stages (Adkins et al., 2002; de Boer et al., 2008) implies that reconstructions of this physical property of ocean waters in the Southern Ocean are instrumental to accurately assess the impact of surface ocean hydrographic changes on ocean circulation and carbon storage. Indeed, upper ocean stratification in the Subantarctic Zone is a fundamental feature to be addressed in order to provide a causal mechanism for both deep Southern Ocean ventilation (Hodell and Venz-Curtis, 2006) and pCO_2 decreases (Hönisch et al., 2009) at the onset of the MPT and for the glacial stages across the transition and beyond.

Here we report continuous and highly resolved reconstructions of the upper ocean temperature and ice volume corrected oxygen isotope composition of ocean

water ($\delta^{18}O_{SW\text{-}IVC}$) from the South Atlantic sector of the Southern Ocean (ODP Site 1090) spanning the entire MPT (1800-580 ka), based on paired Mg/Ca-$\delta^{18}O_C$ measurements on the polar planktonic foraminifer *Neogloboquadrina pachyderma* (sinistral) (*N. pachyderma* (s.)). These reconstructions provide new insights into the hydrography of the Subantarctic Zone of the Southern Ocean during the MPT, allowing their potential impact on the upper ocean stratification and deep Southern Ocean ventilation to be assessed, with implications for the evolution of the global carbon cycle and atmospheric pCO$_2$ across the MPT.

3.2. <u>Material and Methods</u>

3.2.1. Sediment core location and chronology

Site 1090 was drilled during ODP Leg 177 (Gersonde et al., 1999) in the Subantarctic Zone (42°54.8´S, 8°54´E) on the northern flank of the Agulhas Ridge (Fig. 3.1a and b). At a water depth of 3702 m, the site is located at the interface between North Atlantic Deep Water (NADW) and underlying lower Circumpolar Deep Water (CDW). Due to its location, ODP Site 1090 is ideally suited to monitor past dynamics of the Polar Frontal Zone through the Pleistocene glacial-interglacial cycles (Gersonde et al., 1999). Sedimentation rates at the site are on the order of 3-4 cm ky^{-1} (Venz and Hodell, 2002), which implies that temporal resolution for the paleoceanographic records that we generated at this location is potentially high enough to resolve climate variability on orbital timescales (e.g., (Venz and Hodell, 2002; Becquey and Gersonde, 2002; Martínez-Garcia et at., 2009). After inspection with an optical microscope we determined that overall the planktonic foraminifera used for analyses were well preserved and thus discarded dissolution-related artifacts in the interpretation of our records (see below). In this study we use the age model presented in Martínez-García et al. (2010), which was obtained by graphically correlating the benthic $\delta^{18}O$ record of ODP Site 1090 (Venz and Hodell, 2002) to the Lisiecki and Raymo (2005) benthic $\delta^{18}O$ global stack (hereafter LR04, Fig. 3.2a and 3.3a).
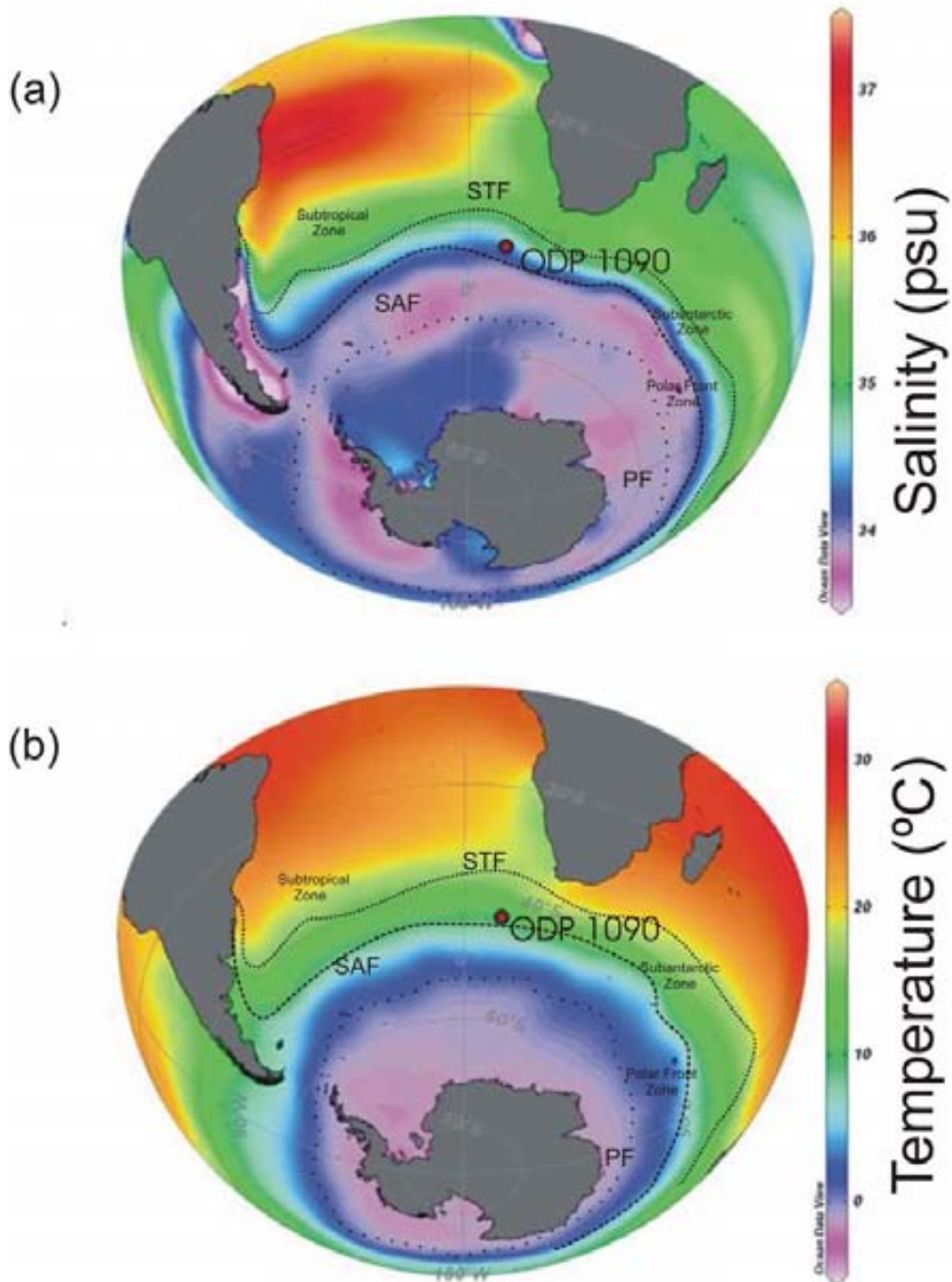
Figure 3.1. Location of ODP Site 1090 (42°54.5′S, 8°54.0′E; water depth 3702 m): World Ocean Atlas 2009 (WOA09) modern annual sea surface (a) salinity and (b) temperature gradients in the Southern Ocean (highly schematic view of the Southern Ocean). Black dashed and dotted lines denote the frontal water mass boundaries: subtropical front (STF), suabantarctic front (SAF) and polar front (PF).

3.2.2 Foraminiferal Mg/Ca

We analyzed a total of 227 samples from the interval between 17.46 to 43.79 meters composite depth, corresponding to an average temporal resolution of ~5 ky over the interval 1800 to 580 ka. A minimum of 60 individuals of *N. pachyderma* (s.) from the 150-250 μm fraction were picked for each sample. *N. pachyderma* (s.) geochemichal

data most likely provide a reconstruction of the austral summer conditions in the upper 130 m of the water column (Mortyn and Charles, 2003; King and Howard, 2003; Fraile et al, 2009). We consider this species ideally suited for this study because: a) it is continuously abundant throughout the core. b) the geochemistry and ecological preferences of *N. pachyderma* (s.) in the Southern Ocean are fairly well known (e.g. Mortyn and Charles. 2003; Nürnberg. 1995; Donner and Wefer. 1994; Hendry, et al. 2009) and c) considering that the modern depth of the mixed-layer in the Southern Ocean (~100-200m; e.g. Monterey and Levitus. 1997), *N. pachyderma* (s.) calcification depth is still shallow enough to faithfully record past changes in the upper water column.

We followed the analytical procedure explained in Chapter 2 section 2.2.1. We replicated samples with high Mn/Ca values. Those replicates that yielded significantly different values were disregarded, while those with consistently high (15 out of 227 samples) values were retained as they do not affect any of those features of the records upon which our conclusions are based. The calibration equation proposed by Elderfield and Ganssen (2000) was selected for converting the *N. pachyderma* (s.) Mg/Ca values for Site 1090 into calcification temperatures. Although this calibration was obtained in the North Atlantic, it gives reasonable temperature values that agree best with both the modern subsurface mean annual summer temperatures and with paleo-records based on coccolithophores and foraminifera assemblages and alkenones (Becquey and Gersonde, 2002; Marino et al., 2009; Martínez- Garcia et al., 2010).

Recently, it has been suggested that Mg/Ca records spanning intervals longer than 1000 ka should be adjusted for the long-term changes in the mean Mg/Ca of seawater (Medina-Elizalde et al., 2008). We applied this adjustment to our record and in the following sections we exclusively refer to these adjusted Mg/Ca values unless otherwise stated.

3.2.3. *N. pachyderma* (s.) stable oxygen isotope ($\delta^{18}O_C$) measurements

For $\delta^{18}O$ analyses on foraminiferal calcite ($\delta^{18}O_C$) ~40 individuals of *N. pachyderma* (s.) were picked from the same size fraction used for Mg/Ca analyses. Analyses of the

samples were carried out at the analitical service of Cardiff University following cleaning procedure and sample preparation described in chapter 2 section 2.2.2.

3.2.4. Seawater oxygen isotope ($\delta^{18}O_{SW}$) calculation

The paleotemperature equation used in this study to reconstruct $\delta^{18}O_{SW}$ from paired Mg/Ca-$\delta^{18}O_c$ measurements on *N. pachyderma* (s) is that of Shackleton (1974) ($\delta^{18}O_{SW} = \delta^{18}O_c + 0.27 - (4.38 - (4.38^2 - 4 \times 0.1 \times (16.9 - T))^{1/2})/(0.1 \times 2))$, which has been employed for other paleoceanographic studies in the Subantarctic (Mashiotta et al., 1999) and Antarctic (Hendry et al., 2009) regions. *N. pachyderma* (s.) is known to exhibit 'vital effects' that offset their $\delta^{18}O$ values from the equilibrium values of the seawater in which they calcify. In order to account for this offset, we follow Hodell et al. (2000), who generated a *N. pachyderma* $\delta^{18}O$ record for a younger interval at the same location, by adjusting the $\delta^{18}O_C$ by -0.4‰ prior to the calculation of $\delta^{18}O_{SW}$.

In order to 'remove' the ice volume component of the $\delta^{18}O_{SW}$ signal we used the Pleistocene record of eustatic sea level changes as modeled by Bintanja and van de Wal (2008). Briefly, we linearly interpolated the Bintanja and van de Wal (2008) record at the time step of the Site 1090 *N. pachyderma* (s.) profile and we then subtracted from the reconstructed $\delta^{18}O_{SW}$ values the mean ocean $\delta^{18}O_{SW}$, which reflects eustatic changes. The local $\delta^{18}O_{SW-IVC}$ linearly correlates with ocean water salinity on regional scales (LeGrande and Schmidt, 2006). Full error propagation yields 1σ uncertainties for our $\delta^{18}O_{SW-IVC}$ data of ±0.3‰ (Fig. 3.3b).

3.3. <u>Results</u>

In Figure 3.2 we compare early to middle Pleistocene Mg/Ca and $\delta^{18}O_C$ profiles for *N. pachyderma* (s.) at Site 1090 with a contemporaneous alkenone-based (U^K_{37}) sea surface temperature (SST) reconstruction from the same location (Martínez-Garcia et al., 2010; Fig. 3.2b). The Mg/Ca-derived temperature profile (Fig. 3.2c) shows a clear pattern of glacial-interglacial variability that is also reflected in the *N. pachyderma* (s.) (Fig. 2d) and benthic foraminiferal $\delta^{18}O$ records (Venz and Hodell, 2002, Fig. 3.2a), and in U^K_{37}-SST (Martínez-Garcia et al., 2010, Fig. 3.2b). Overall, the amplitude of glacial-interglacial changes for Mg/Ca based temperatures, *N. pachyderma* (s.) $\delta^{18}O$, and

benthic $\delta^{18}O$ is markedly larger across the MPT (~4 °C, ~1.2‰, and ~1.3‰, respectively) compared to the preceding interval (~2 °C, ~0.8‰, and ~0.9‰, respectively). This evidence from Site 1090 supports the concept that the amplitude of the glacial-interglacial variability increased at the onset of the MPT (Clark et al. 2006),
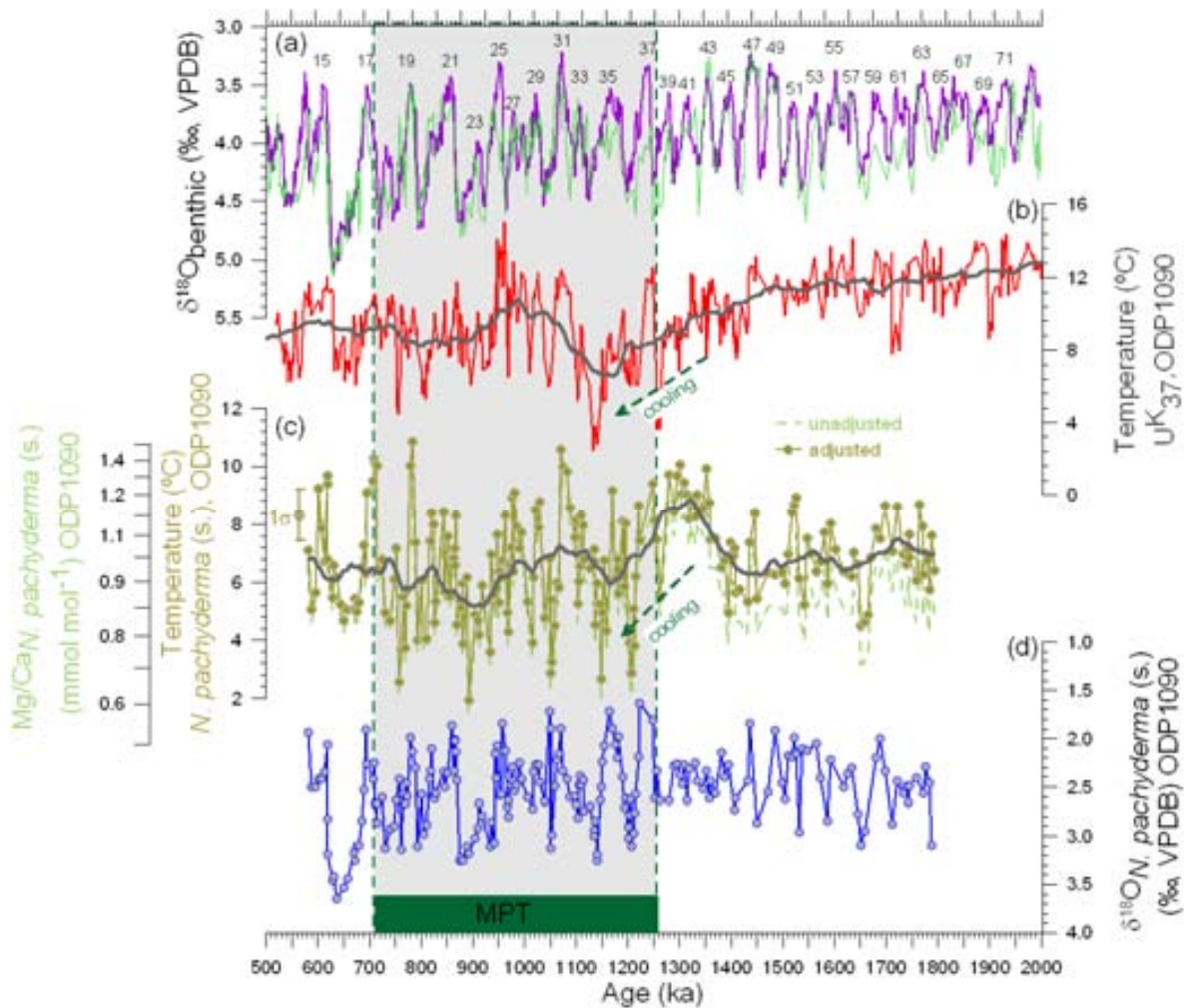
Figure 3.2. (a) *Cibicidoides wuellerstorfi* $\delta^{18}O$ record for ODP 1090 (Venz and Hodell, 2002; green) overlain onto the global benthic $\delta^{18}O$ stack (Lisiecki and Raymo, 2005; purple). (b) Alkenone-based SST (U^K_{37}) reconstruction at ODP Site 1090 (Martínez-Garcia et al., 2010; red). A running average of 100 ky is shown in dark grey. (c) Mg/Ca-derived temperature at Site 1090 obtained from *N. pachyderma* (s.). In green are temperatures obtained by correcting the Mg/Ca record for the long-term Mg/Ca changes in seawater (Mg/Ca$_{SW}$) (Fantle and DePaolo, 2005; Fantle and DePaolo, 2006; Medina-Elizalde et al., 2008); in light green (dashed line) are the Mg/Ca and temperature values unadjusted for such a change. A running average of 100 ky is shown to highlight the long-term trends (grey). Dashed horizontal line corresponds to the average of glacial temperatures before (~5.8°C) and during (~3.9°C) the MPT (d)

Oxygen isotope calcite composition ($\delta^{18}O_C$) of *N. pachyderma* (s.) (blue). Green/grey vertical band highlights the MPT interval according to Clark et al. (2006). Error bars represent the 1σ propagated errors for the Mg/Ca-derived temperature reconstructions. Green arrows denote the major trends discussed in the paper.

in line with several surface and deep-ocean reconstructions from different ocean basins (Wara et al., 2005; Medina-Elizalde and Lea, 2005; Sosdian and Rosenthal, 2009; Martínez-Garcia et al., 2010).

Dissolution is known to significantly affect Mg/Ca ratios in foraminifera (Brown and Elderfield, 1996). However, the relatively low planktonic foraminiferal fragmentation (rarely exceeding 40%) observed at Site 1090 (Becquey and Gersonde, 2002), the lack of correlation between the *N. pachyderma* (s.) shell weight and the Mg/Ca data (Fig. S1a), and the absence of significant changes to the overall structure and values of the Mg/Ca record when applying dissolution corrections (Barker et al., 2009, Fig. S1b), suggest only a minor effect on our planktonic foraminiferal Mg/Ca-based reconstruction.

The low amplitude glacial-interglacial temperature variability (~ 2.4ºC) observed throughout the older part of the record (1800-1200 ka) agrees with the low amplitude glacial-interglacial changes that can be expected for the interval preceding the MPT, the so-called 41ky-world (Fig. 3.2c; Clark et al., 2006). Before the MPT, between 1395 and 1250 ka, the *N. pachyerma* (s.) Mg/Ca record indicates a long-term warming, which preceded a shift towards more severe glaciations. The warming interval featured glacial and interglacial temperatures that were up to 2ºC warmer than in previous glacial-interglacial stages),. In general, across the MPT temperatures reconstructed by using *N. pachyderma* (s.) Mg/Ca show colder glacial and warmer interglacial values than in the 1395 to 1800 ka interval and a glacial-interglacial amplitude change of $\sim$4ºC, with the coldest glacial temperature of the entire record observed during Marine Isotope Stage 22. Direct comparison between Mg/Ca- (Fig. 3.2c) and alkenone-based (Fig. 3.2b) temperature records at Site 1090 reveals a similar structure of the temperature variations throughout the MPT, while for the interval before the transition higher temperature gradients are observed. We speculate that these differences may reflect a change in the structure of the upper water column and the position of the thermocline at the onset of

the MPT, given the different depth habitat of the two signal carriers (alkenone producing Haptophyceae live within the euphotic zone, and *N. pachyderma* (s.) throughout the top ~130 m).

The glacial $\delta^{18}O_{SW-IVC}$ (Figure 3.3b) shows a decrease at ~1250, suggesting a shift towards fresher conditions in the upper water column (from 0.2‰ to -0.2‰) that persist throughout the MPT glaciations. Glacial-interglacial $\delta^{18}O_{SW-IVC}$ amplitude changes during the MPT were clearly larger (0.9‰) than before the transition (0.4‰).

Figure 4 shows the evolutionary power-spectra analyses of the global benthic $\delta^{18}O$ stack (Lisiecki and Raymo, 2005; Fig 4a), *N. pachyderma* (s.) temperature (Fig 4b), and $\delta^{18}O_{SW-IVC}$ (Fig 3.4c) reconstructions. The presence of a strong low frequency cycle in *N. pachyderma* (s.) records (Fig 3.4b-c) makes it difficult to perform robust spectral analyses of these records (even after detrending and prewhitening of the records). However, the expected shift in the dominance of the orbital cycles across the MPT is clearly observed in both temperature and $\delta^{18}O_{SW-IVC}$ reconstructions. The obliquity cycle (~41 ky) in the *N. pachyderma* (s.) temperature reconstruction (Fig. 3.4b) is observed from ~1300 ka, and is followed by a progressive increase of the dominance of variability in the eccentricity band (~100-120 ky) starting at 1200-1100 ka, with a clear intensification at ~900-800 ka. Although, in the $\delta^{18}O_{SW-IVC}$ power spectra (Fig 3.4c) the eccentricity band is partially overlapped by the strong low frequency cycle, it is evident that the increase in the dominance of this cycle starts at 1200-1100 ka in agreement with temperature and LR04 spectral analyses. The power of the precession band (~23 ky) also increases in all the records at the MPT, again, in agreement with the LR04 stack.

Figure 3.3. (a) Global benthic $\delta^{18}O$ stack (Lisiecki and Raymo, 2005; purple). (b) Local $\delta^{18}O_{sw\text{-}ivc}$ changes at ODP Site 1090 were obtained by removing the ice-volume (mean ocean $\delta^{18}O$; Bintanja and van de Wal, 2008) and calcification temperature components from the $\delta^{18}O$ measured on *N. pachyderma* (s.) (pink). A running average of 100 ky is shown to highlight the main trends (red). Dashed horizontal line corresponds to the glacial $\delta^{18}O_{sw\text{-}ivc}$ average before (~0.2‰) and during (~-0.2‰) the MPT (c) Percentage of tetra-unsaturated alkenone relative to the total abundance of unsaturated C_{37} alkenones (%$C_{37:4}$; Martínez-Garcia et al., 2010; dark gray). The 100 ky running average is shown in red. (d) The 50-pt running average of vertical gradients in the South Atlantic (red) and inter-basinal gradients between the (e) South Atlantic and Pacific (blue) and (f) South Atlantic and North Atlantic (Hodell et al., 2006; brown). Green/grey vertical band highlights the MPT interval according to Clark et al. (2006). Error bars represent the 1σ propagated errors for the Mg/Ca-derived temperature reconstructions. Green arrows denote the major trends discussed in the paper.

Figure 3.4. Evolutionary power-spectra analyses for: a) global benthic foraminiferal stack (Lisieke and Raymo, 2004), b) *N. pachyderma* (s.) Mg/Ca-based temperature reconstructions and c) *N. pachyderma* (s.) $\delta^{18}O_{SW-IVC}$. The evolutionary power spectra of all records were computed using MATLAB software with a 500 ky Hamming window and 95% overlap. Before spectral analysis, both series were detrended, prewhitened, and linearly interpolated to 5 ky.

3.4. <u>Discussion</u>

Our upper ocean *N. pachyderma* (s.) Mg/Ca record from Site 1090 reveals the occurrence of more pronounced temperature decreases and generally colder conditions during the glacial stages across the MPT than before the transition (Fig. 3.2c). The good agreement with SST reconstructions based on alkenone paleothermometer from the same site corroborates the picture of a major cooling of the Southern Ocean glacial climate starting at 1250 ka, that is, at the onset of the MPT (Martínez-Garcia et al., 2010). Importantly, our results also indicate a hitherto unrecognized negative ~0.4‰ glacial shift of the $\delta^{18}O_{SW\text{-}IVC}$ at ~1250 ka, implying that the upper ocean waters in the Subantarctic Zone during glacials cooled and freshened in tandem at the onset of the MPT, and that overall fresher and cooler conditions persisted throughout, at least, glacial periods of the MPT (Fig. 3.2c and 3.3b).

Modern hydrographic studies show that across the Polar Frontal Zone, surface waters gradually cool and freshen towards the south, between Subantarctic Surface Water (SASW) and Antarctic Surface Water (AASW) (Fig. 3.1a-b, Rintoul et al., 2001; Antonov et al., 2010; Locarnini et al., 2010). We therefore interpret our data as indicative of the meridional expansion of the Southern Ocean Polar Frontal Zone (PFZ), coincident with the onset of the MPT. This confirms previous inferences based on organic biomarkers (relative abundance of $C_{37:4}$ alkenone, Fig. 3.3c) that indicate a northward expansion of the Southern Ocean fronts and increased advection of polar waters to Site 1090 during the glacial stages of the MPT (Martínez-García et al., 2010). These changes marked the establishment at around 1200 ka of a glacial Antarctic polar system configuration and sea ice field that were likely comparable to that of the last glacial maximum (Martínez-Garcia et al., 2010). This view is also supported by other paleoceanographic studies based on diatom (Kemp et al., 2010) and coccolithophorid assemblages (Marino et al., 2009).

The northward expansion of the Antarctic PFZ could have been associated with the long-term global cooling (Lisiecki and Raymo, 2005), which caused the expansion of the Antarctic ice sheet. Sediments retrieved from the Ross Sea in Antarctica show an increase in glacial type lithologies before MIS 31 (Naish et al., 2009), i.e., virtually in parallel with the cooling and freshening that we observe at Site 1090, at 42°S in the

Atlantic Ocean. This suggests a strong link between seaward expansion of the West Antarctic ice sheet and hydrographic changes in Subantarctic Zone at the onset of the MPT. We note, however, that a northward shift of the southern westerlies would have had virtually similar impacts on the temperature and salinity of the upper water column in the Southern Ocean, in that the westerly wind field in the Southern Hemisphere controls the upwelling of deep waters offshore Antarctica that modulates the meridional extension of sea ice in the Southern Ocean (e.g. Toggweiler et al. 2006).

Previous studies have emphasized the close interaction between the northward expansion of the Antarctic Ocean frontal systems, the northward expansion of the sea ice cover and westerly winds, the stratification of the upper Southern Ocean (triggered by surface ocean freshening), and the storage of respired CO_2 in the deep Southern Ocean (Archer et al., 2003; Stephens and Keeling, 2000; Keeling and Stephens, 2001). Freshening of the upper ocean might have thus contributed to promote the build up of respired CO_2 in the deep ocean by enhancing stratification and, in turn, reducing the vertical mixing in the Southern Ocean (Francois et al. 1997; Sigman and Boyle, 2000; Sigman et al., 2010).

Notably, the cooling and freshening of the upper Southern Ocean waters that is revealed by our records (Figs. 3.2c and 3.3b) occurred roughly in step with the change toward reduced deep water ventilation (circulation) in the Southern Ocean. The isolation of the deep water masses impacts their $\delta^{13}C$ composition, by enriching them in ^{12}C and, in turn, yielding lighter $\delta^{13}C$ values. Exceptionally light benthic $\delta^{13}C$ values have been reported for the glacial stages of the MPT at Site 1090 (Venz and Hodell, 2002). Hodell et al. (2006) emphasized a change in the vertical $\delta^{13}C$ gradient in the South Atlantic (Fig. 3.3d, red profile) during this period, by comparing $\delta^{13}C$ benthic values of the ODP 1090 against the ODP 1088 $\delta^{13}C$ benthic record (Southern Ocean intermediate depth). This change was linked to a shift in the $\delta^{13}C$ gradient between the Pacific (ODP 849) and South Atlantic (1090) oceans (Fig. 3.3e, blue profile), and between the North and the South Atlantic (Fig. 3.3f, brown profile). Hence, Hodell et al. (2006) demonstrated that a marked decrease in the ventilation of the deep Southern Ocean followed the onset of the MPT (Fig. 3.3d-f) and promoted the build-up of respired CO_2 in the deep Southern Ocean. We interpret this change in the deep ocean as the response to the

meridional expansion of the polar front zone, and the concomitant freshening and cooling of the Subantarctic Zone of the Southern Ocean, which together may have been instrumental in reducing the ventilation of the deep Southern Ocean and in isolating deep water masses enriched in respired CO_2.

Indeed, Figure 3.5 suggests a close relationship between hydrographic changes in the Southern Ocean and pCO_2 measurements from Antarctic ice cores (Lüthi et al., 2008) in two glacial-interglacial cycles after the MPT. We propose that the increase in the northward advection of Antarctic waters and Southern Ocean stratification could have accounted for the observed pCO_2 drawdown across the MPT (Hönisch et al. 2009) in two different ways. First, by increasing the residence time of major nutrients in the Southern Ocean surface waters (Francois et al., 1997) that together with the coeval increase in Fe fertilization at the onset of the MPT (Martínez-Garcia et al., 2011) could have accounted for enhancing Southern Ocean major nutrient consumption and glacial primary biological productivity in the Subantarctic Zone (Martínez-Garcia et al., 2009). Second by restricting CO_2 outgassing, and allowing the build-up of respired carbon in the deep ocean.

Several studies have suggested that sea ice expansion and Southern Ocean stratification are key mechanisms for explaining the full glacial-interglacial pCO_2 shifts of the Late Pleistocene (Toggweiler, 1999; Watson et al., 2000; Stephens and Keeling, 2000). A recent model study, however, has demonstrated that stratification and sea ice expansion can also promote the release of CO_2 to the atmosphere by increasing deep ocean alkalinity, thus counteracting the CO_2 uptake of the biological pump (Hain et al., 2010). Separately, stratification and sea ice expansion can reduce pCO_2 by 36 ppmv, while the biological pump can account for a pCO_2 decrease of 58 ppmv. Notably, when these physical and biological mechanisms operate together the resultant pCO_2 decrease is in the order of 36 ppmv (Hain et al., 2010), which is remarkably similar to the amplitude change of the pCO_2 drawdown (~30ppmv) observed between pre- and post- MPT glacials (Hönisch et al., 2009). We speculate that this pCO_2 change could be explained by the combined effect of increasing both Southern Ocean stratification (this study) and wind-blown Fe supply to the Subantarctic Zone (Martínez-Garcia et al., 2011) at the onset of the MPT. In this respect the observed increase in the power of the 100 ky cycle

in both, $\delta^{18}O_{SW\text{-}IVC}$ (Figure 3.4c) and Fe deposition in the Southern Ocean (Martínez-Garcia et al., 2011), argues in favour of a shift in the periodicity and amplitude of glacial-interglacial atmospheric CO_2 cycles during the MPT. This inference could be tested in the future with high-resolution proxy CO_2 records when they become available.
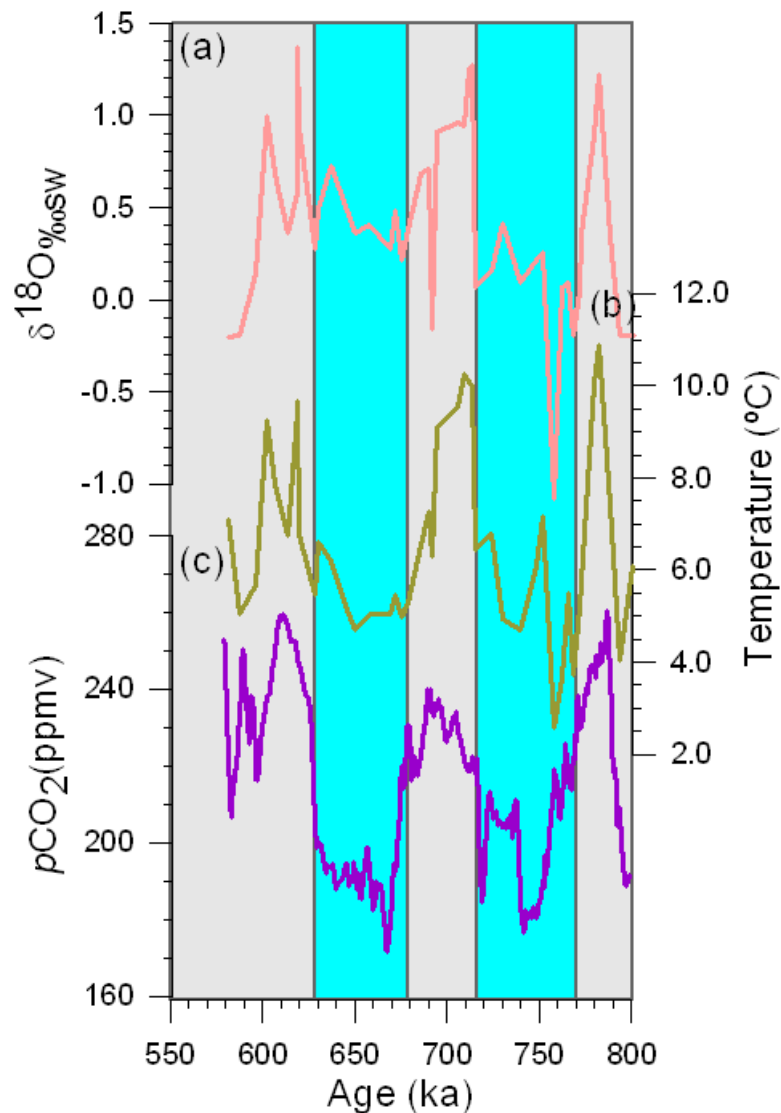
Figure 3.5. *N. pachyderma (s.)* foraminiferal species reconstructions from site 1090: (a) $\delta^{18}O_{SW\text{-}IVC}$, and (b) temperature reconstructions compared to *p*CO_2 measurements (c) from Antarctic ice cores (solid purple line, Lüthi et al., 2008) from 500 to 800 ka. Blue box areas highlight glacial periods where freshening and cooling at Site 1090 correspond with lower *p*CO_2.

Hence, our paired Mg/Ca-$\delta^{18}O$ *N. pachyderma* (s.) results indicate that the upper Southern Ocean was cooler and fresher at the onset, and during the glacial periods

throughout the MPT, compared to the pre-MPT. We associate the observed freshening of the upper Southern Ocean to sea ice expansion and stratification of the water column, which could have accounted for the coeval reduction of glacial deep ocean ventilation (Hodell and Venz-Curtis, 2006). These physical mechanisms, in combination with an increase in Fe supply to the Southern Ocean at the onset and glacial periods of the MPT (Martínez-Garcia et al., 2011) could have accounted for the glacial pCO$_2$ drawdown during the MPT indicated by Hönisch et al. (2009) and possible during glacial periods after the transition (Fig. 3.5a-c).

3.5. <u>Conclusions</u>

N. pachyderma (s.) Mg/Ca- and δ^{18}O-based reconstructions from ODP Site 1090 suggest a major hydrographic reorganization (towards cooler and fresher conditions) of the upper glacial ocean in the Subantarctic Zone of the Atlantic Ocean at the onset of the MPT (i.e. around 1250 ka). These observations point to the northward expansion of the Antarctic Zone during glacials, in line with an independent organic biomarker reconstruction (Martínez-Garcia et al., 2010). The magnitude of the glacial cooling and freshening increased considerably at 1250 ka and overall cooler and fresher glacial conditions persisted throughout the MPT, coinciding with the intensification of the 100 ky cycle in the temperature and δ^{18}O$_{SW-IVC}$ in our records. The increased upper Southern Ocean stratification during glacial stages of the MPT that we deduce from these changes provides a mechanism to isolate deep water masses and reduce the exchange of carbon with the atmosphere. These physical changes in the Southern Ocean upper water column, in combination with other biological processes driven by major reorganizations in the micro-nutrient supply to the Southern Ocean (Martínez-Garcia et al., 2011), might explain the lower pCO$_2$ levels observed during the glacial stages from the onset of the MPT onwards (Hönisch et al., 2009). Therefore, the MPT may be seen as a time when glacial intensity considerably increased with development of the more pronounced glacial pCO$_2$ decreases, which possibly occurred as the result of the close interaction of physical and biological changes taking place within the Southern Ocean.

3.6. References

Adkins, J. F., McIntyre, K., Schrag, D. P., 2002. The Salinity, Temperature, and $\delta^{18}O$ of the Glacial Deep Ocean. Science. 298, 1769-1773. doi: 10.1126/science.1171477.

Antonov, J. I., D. Seidov, T. P. Boyer, R. A. Locarnini, A. V. Mishonov, and H. E. Garcia, 2010. World Ocean Atlas 2009 Volume 2: Salinity. S. Levitus, Ed., NOAA Atlas NESDIS 69, U.S. Government Printing Office, Washington, D.C., 184 pp.

Archer, D. E., Martin, P. A., Milovich, J., Brovkin, V., Plattner, G., Ashendel, C., 2003. Model sensitivity in the effect of Antarctic sea ice and stratification on atmospheric pCO$_2$. Paleoceanography. 18, 1012. doi: 10.1029/2002PA000760

Barker, S., Greaves, M., Elderfield, H., 2003. A study of cleaning procedures used for foraminiferal Mg/Ca paleothermometry. Geochemistry, Geophysics, Geosystems. 4, 8407. doi:10.1029/2003GC000559.

Barker, S., Diz, P., Vautravers, M. J., Pike, J., Knorr, G., Hall, I. R., Broecker, W. S., 2009. Interhemispheric Atlantic seesaw response during the last deglaciation. Nature. 457, 1097-1102. doi:10.1038/nature07770.

Becquey, S. and Gersonde, R., 2002. Past hydrographic and climatic changes in the Subantarctic Zone of the South Atlantic – The Pleistocene record from ODP Site 1090. Palaeogeography, Palaeoclimatology, Palaeoecology. 182, 221-239. doi:10.1016/S0031-0182(01)00497-7.

Berger, A., Li, X. S., Loutre, M. F., 1999. Modelling northern hemisphere ice volume over the last 3 Ma. Quaternary Science Reviews. 18, 1-11. doi: 10.1016/S0277-3791(98)00033-X.

Bintanja, R. and van de Wal, R. S. W., 2008. North American ice-sheet dynamics and the onset of 100,000-year glacial cycles. Nature. 454, 869-872. doi:10.1038/nature07158.

Boyle, E.A., 1983. Manganese carbonate overgrowths on foraminifera tests. Geochim. cosmochim. Acta 47, 1815–1819. doi:10.1016/0016-7037(83)90029-7.

Brown, S. J., and H. Elderfield, Variations in Mg/Ca and Sr/Ca ratios of planktonic foraminifera caused by postdepositional dissolution: Evidence of shallow Mg- dependent dissolution, Paleoceanography, 11, 543–551, 1996.

Clark, P. U., Archer, D., Pollard, D., Blum, J. D., Rial, J. A., Brovkin, V., Mix, A. C., Pisias, N. G., Roy, M., 2006. The middle Pleistocene transition: characteristics, mechanisms, and implications for long-term changes in atmospheric pCO$_2$. Quaternary Science Reviews. 25, 3150-3184. doi:10.1016/j.quascirev.2006.07.008.

de Boer, A. M., Toggweiler, J. R., Sigman, D. M., 2008. Atlantic Dominance of the Meridional Overturning Circulation. Journal of Physical Oceanography.435.

de Villiers, S., Greaves, M., Elderfield, H., 2002. An intensity ratio calibration method for the accurate determination of Mg/Ca and Sr/Ca of marine carbonates by ICP-AES. Geochemistry, Geophysics, Geosystems. 3, 1001. doi:10.1029/2001GC000169.

Donner, B. and Wefer, G., 1994. Flux and stable isotope composition of Neogloboquadrina pachyderma and other planktonic foraminifers in the Southern Ocean (Atlantic sector). Deep Sea Research Part I: Oceanographic Research Papers. 41, 1733-1743.

Elderfield, H., Ganssen, G., 2000. Past temperature and $\delta^{18}O$ of surface ocean waters inferred from foraminiferal Mg/Ca ratios. Nature 405, 442–445. doi:10.1038/35013033.

Fantle, M. S. and DePaolo, D. J., 2005. Variations in the marine Ca cycle over the past 20 million years. Earth and Planetary Science Letters. 237, 102-117. doi:10.1016/j.epsl.2005.06.024.

Fantle, M. S. and DePaolo, D. J., 2006. Sr isotopes and pore fluid chemistry in carbonate sediment of the Ontong Java Plateau: Calcite recrystallization rates and evidence for a rapid rise in seawater Mg over the last 10 million years. Geochimica Et Cosmochimica Acta. 70, 3883-3904. doi:10.1016/j.gca.2006.06.009.

Fraile, I., Mulitza, S., Schulz, M., 2009. Modeling planktonic foraminiferal seasonality: Implications for sea-surface temperature reconstructions. Marine Micropaleontology. 72, 1-9. doi:10.1016/j.marmicro.2009.01.003

Francois, R., Altabet, M. A., Yu, E. F., Sigman, D. M., Bacon, M. P., Frank, M., Bohrmann, G., Bareille, G., and Labeyrie, L. D.,1997, Contribution of Southern Ocean surface-water stratification to low atmospheric CO_2 concentrations during the last glacial period, Nature, 389(6654), 929– 935, doi:10.1038/40073.

Ferguson, J.E., Henderson, G.M., Kucera, M., Rickaby, R.E.M., 2008. Systematic change of foraminiferal Mg/Ca ratios across a strong salinity gradient. Earth Planet. Sci. Lett. 265, 153–166. doi:10.1016/j.epsl.2007.10.011.

Gersonde, R., Hodell, D. A., blum, P., et al., 1999. Leg 177 Summary: Southern Ocean Paleoceanography. Init. Repts. 177: College Station, (TX).

Greaves, M., et al. (2008), Interlaboratory comparison study of calibration standards for foraminiferal Mg/Ca thermometry, Geochem. Geophys. Geosyst., 9, Q08010, doi:10.1029/2008GC001974.

Hain, M. P., Sigman, D. M., Haug, G. H., 2010. Carbon dioxide effects of Antarctic stratification, North Atlantic Intermediate Water formation, and subantarctic nutrient drawdown during the last ice age: Diagnosis and synthesis in a geochemical box model. Global Biogeochemical Cycles. 24, GB4023. doi:10.1029/2010GB003790.

Hall, I. R., McCave, I. N., Shackleton, N. J., Weedon, G. P., Harris, S. E., 2001. Intensified deep Pacific inflow and ventilation in Pleistocene glacial times. Nature. 412, 809-812. doi:10.1038/35090552.

Hendry, K. R., Rickaby, R. E. M., Meredith, M. P., Elderfield, H., 2009. Controls on stable isotope and trace metal uptake in Neogloboquadrina pachyderma (sinistral) from an Antarctic sea-ice environment. Earth and Planetary Science Letters. 278, 67-77. doi:10.1016/j.epsl.2008.11.026.

Hodell, D. A., Charles, C. D., Ninnemann, U. S., 2000. Comparison of interglacial stages in the South Atlantic sector of the southern ocean for the past 450 kyr: implifications for Marine Isotope Stage (MIS) 11. Global and Planetary Change. 24, 7-26. doi: 10.1016/S0921-8181(99)00069-7.

Hodell, D. A. and Venz-Curtis, K. A., 2006. Late Neogene history of deepwater ventilation in the Southern Ocean. Geochemistry, Geophysics, Geosystems. 7, Q09001. doi:10.1029/2005GC001211

Hönisch, B., Hemming, N. G., Archer, D., Siddall, M., McManus, J. F., 2009. Atmospheric Carbon Dioxide Concentration Across the Mid-Pleistocene Transition. Science. 324, 1551-1554. doi: 10.1126/science.1171477

Keeling, R. F. and Stephens, B. B., 2001. Antarctic sea ice and the control of Pleistocene climate instability. Paleoceanography. 16, 112-131. doi:10.1029/2000PA000529.

Kemp, A. E. S., Grigorov, I., Pearce, R. B., Naveira Garabato, A. C., 2010. Migration of the Antarctic Polar Front through the mid-Pleistocene transition: evidence and climatic implications. Quaternary Science Reviews. 29, 1993-2009. doi:10.1016/j.quascirev.2010.04.027.

King, A. L. and Howard, W. R., 2003. Planktonic foraminiferal flux seasonality in Subantarctic sediment traps: A test for paleoclimate reconstructions. Paleoceanography. 18, 1019. doi: 10.1029/2002PA000839.

Kohfeld, K. E., Quere, C. L., Harrison, S. P., Anderson, R. F., 2005. Role of Marine Biology in Glacial-Interglacial CO_2 Cycles. Science. 308, 74-78. doi: 10.1126/science.1105375.

Kumar, N., Anderson, R. F., Mortlock, R. A., Froelich, P. N., Kubik, P., Dittrich-Hannen, B., Suter, M., 1995. Increased biological productivity and export production in the glacial Southern Ocean. Nature. 378, 675-680. doi:10.1038/378675a0.

LeGrande, A. N. and Schmidt, G. A., 2006. Global gridded data set of the oxygen isotopic composition in seawater. Geophysical Research Letters. 33, L12604. doi:10.1029/2006GL026011.

Lisiecki, L. E. and Raymo, M. E., 2005. A Pliocene-Pleistocene stack of 57 globally distributed benthic δ18O records. Paleoceanography. 20, PA1003. doi:10.1029/2004PA001071.

Locarnini, R. A., A. V. Mishonov, J. I. Antonov, T. P. Boyer, and H. E. Garcia, 2010. World Ocean Atlas 2009, Volume 1: Temperature. S. Levitus, Ed., NOAA Atlas NESDIS 68, U.S. Government Printing Office, Washington, D.C., 184 pp.

Lüthi, D., Le Floch, M., Bereiter, B., Blunier, T., Barnola, J., Siegenthaler, U., Raynaud, D., Jouzel, J., Fischer, H., Kawamura, K., Stocker, T. F., 2008. High-resolution carbon dioxide concentration record 650,000-800,000 years before present. Nature. 453, 379-382. doi:10.1038/nature06949.

Marino, M., Maiorano, P., Lirer, F., Pelosi, N., 2009. Response of calcareous nannofossil assemblages to paleoenvironmental changes through the mid-Pleistocene revolution at Site 1090 (Southern Ocean). Palaeogeography, Palaeoclimatology, Palaeoecology. 280, 333-349. doi:10.1016/j.palaeo.2009.06.019

Martin, J. H., 1990. Glacial-Interglacial CO_2 Change: The Iron Hypothesis. Paleoceanography. 5, 1-13. doi:10.1029/PA005i001p00001.

Martínez-Garcia, A., Rosell-Melé, A., Geibert, W., Gersonde, R., Masqué, P., Gaspari, V., Barbante, C., 2009. Links between iron supply, marine productivity, sea surface temperature, and CO_2 over the last 1.1 Ma. Paleoceanography. 24, PA1207. doi:10.1029/2008PA001657.

Martínez-García, A., Rosell-Melé, A., McClymont, E. L., Gersonde, R., Haug, G. H., 2010. Subpolar Link to the Emergence of the Modern Equatorial Pacific Cold Tongue. Science. 328, 1550-1553. doi:10.1126/science.1184480

Martínez-García, A., Rosell-Melé, A., Jaccard, S. L., Geibert, W., Sigman, D. M., Haug, G. H., 2011. Southern Ocean dust-climate coupling over the past four million years. Nature. 476, 312-315. doi:10.1038/nature10310

Mashiotta, T. A., Lea, D. W., Spero, H. J., 1999. Glacial–interglacial changes in Subantarctic sea surface temperature and δ^{18}O-water using foraminiferal Mg. Earth and Planetary Science Letters. 170, 417-432. doi: 10.1016/S0012-821X(99)00116-8.

Medina-Elizalde, M. and Lea, D. W., 2005. The Mid-Pleistocene Transition in the Tropical Pacific. Science. 310, 1009-1012. doi: 10.1126/science.1115933.

Medina-Elizalde, M., Lea, D. W., Fantle, M. S., 2008. Implications of seawater Mg/Ca variability for Plio-Pleistocene tropical climate reconstruction. Earth and Planetary Science Letters. 269, 585-595. doi: 10.1016/j.epsl.2008.03.014.

Monterey, G. and Levitus, S., 1997: Seasonal Variability of Mixed Layer Depth for the World Ocean. NOAA Atlas NESDIS 14, U.S. Gov. Printing Office, Wash., D.C., 96 pp. 87 figs.

Mortyn, P. G. and Charles, C. D., 2003. Planktonic foraminiferal depth habitat and δ^{18}O calibrations: Plankton tow results from the Atlantic sector of the Southern Ocean. Paleoceanography. 18, 1037. doi: 10.1029/2001PA000637.

Mudelsee, M. and Schulz, M., 1997. The Mid-Pleistocene climate transition: onset of 100 ka cycle lags ice volume build-up by 280 ka. Earth and Planetary Science Letters. 151, 117-123. doi: 10.1016/S0012-821X(97)00114-3.

Naish, T., Powell, R., Levy, R., Wilson, G., Scherer, R., Talarico, F., Krissek, L., Niessen, F., Pompilio, M., Wilson, T., Carter, L., DeConto, R., Huybers, P., McKay, R., Pollard, D., Ross, J., Winter, D., Barrett, P., Browne, G., Cody, R., Cowan, E., Crampton, J., Dunbar, G., Dunbar, N., Florindo, F., Gebhardt, C., Graham, I., Hannah, M., Hansaraj, D., Harwood, D., Helling, D., Henrys, S., Hinnov, L., Kuhn, G., Kyle, P., Laufer, A., Maffioli, P., Magens, D., Mandernack, K., McIntosh, W., Millan, C., Morin, R., Ohneiser, C., Paulsen, T., Persico, D., Raine, I., Reed, J., Riesselman, C., Sagnotti, L., Schmitt, D., Sjunneskog, C., Strong, P., Taviani, M., Vogel, S., Wilch, T., Williams, T., 2009. Obliquity-paced Pliocene West Antarctic ice sheet oscillations. Nature. 458, 322-328.

Nürnberg, D., 1995. Magnesium in tests of Neogloboquadrina pachyderma sinistral from high northern and southern latitudes. The Journal of Foraminiferal Research. 25, 350-368.

Paillard, D., 1998. The timing of Pleistocene glaciations from a simple multiple-state climate model. Nature. 391, 378-381. doi:10.1038/34891.

Park, J. and Maasch, K. A., 1993. Plio—Pleistocene Time Evolution of the 100-kyr Cycle in Marine Paleoclimate Records. J. Geophys. Res. 98, 447-461.

Raymo, M. E., Oppo, D. W., Curry, W., 1997. The Mid-Pleistocene Climate Transition: A Deep Sea Carbon Isotopic Perspective. Paleoceanography. 12, 546-559. doi:10.1029/97PA01019.

Rintoul SR, Hughes C, and Olbers D (2001) The Antarctic Circumpolar Current system. In: Siedler G, Church J, and Gould J (eds.) Ocean Circulation and Climate, pp. 271--302. London: Academic Press.

Schmieder, F., von Dobeneck, T., Bleil, U., 2000. The Mid-Pleistocene climate transition as documented in the deep South Atlantic Ocean: initiation, interim state and terminal event. Earth and Planetary Science Letters. 179, 539-549. doi:10.1016/S0012-821X(00)00143-6.

Sigman, D. M. and Boyle, E. A., 2000. Glacial/interglacial variations in atmospheric carbon dioxide. Nature. 407, 859-869. doi:10.1038/35038000.

Sigman, D. M., Jaccard, S. L., Haug, G. H., 2004. Polar ocean stratification in a cold climate. Nature. 428, 59-63. doi:10.1038/nature02357.

Sigman, D. M., Hain, M. P., Haug, G. H., 2010. The polar ocean and glacial cycles in atmospheric CO_2 concentration. Nature. 466, 47-55. doi:10.1038/nature09149

Shackleton, N.J., 1974. Attainment of isotopic equilibrium between ocean water and the benthonic foraminifera genus Uvigerina: isotopic changes in the ocean during the last glacial. Cent. Nat. Rech. Sci. Colloq. Int. 219, 203–209.

Sosdian, S. and Rosenthal, Y., 2009. Deep-Sea Temperature and Ice Volume Changes Across the Pliocene-Pleistocene Climate Transitions. Science. 325, 306-310. doi: 10.1126/science.1169938.

Stephens, B. B. and Keeling, R. F., 2000. The influence of Antarctic sea ice on glacial-interglacial CO_2 variations. Nature. 404, 171-174. doi:10.1038/35004556.

Toggweiler, J. R., 1999. Variation of Atmospheric CO_2 by Ventilation of the Ocean's Deepest Water. - Paleoceanography. 14, 571, PA1999. doi:10.1029/1999PA900033.

Toggweiler, J. R., Russell, J. L., Carson, S. R., 2006. Midlatitude westerlies, atmospheric CO_2, and climate change during the ice ages. Paleoceanography. 21, PA2005. doi:10.1029/2005PA001154.

van de Wal, R. S. W. and Bintanja, R., 2009. Changes in Temperature, Ice, and CO_2 During the Mid-Pleistocene Transition. Science published online.

Venz, K. A. and Hodell, D. A., 2002. New evidence for changes in Plio–Pleistocene deep water circulation from Southern Ocean ODP Leg 177 Site 1090. Palaeogeography, Palaeoclimatology, Palaeoecology. 182, 197-220. doi:10.1016/S0031-0182(01)00496-5.

Wara, M. W., Ravelo, A. C., Delaney, M. L., 2005. Permanent El Niño-Like Conditions During the Pliocene Warm Period. Science. 309, 758-761. doi:10.1126/science.1112596.

Watson, A. J., Bakker, D. C. E., Ridgwell, A. J., Boyd, P. W., Law, C. S., 2000. Effect of iron supply on Southern Ocean CO_2 uptake and implications for glacial atmospheric CO_2. Nature. 407, 730-733. doi:10.1038/35037561.

Yu, J., Day, J., Greaves, M., Elderfield, H., 2005. Determination of multiple element/calcium ratios in foraminiferal calcite by quadrupole ICP-MS. Geochemistry, Geophysics, Geosystems. 6, Q08P01. doi:10.1029/2005GC000964.

3.7. Supplementary information
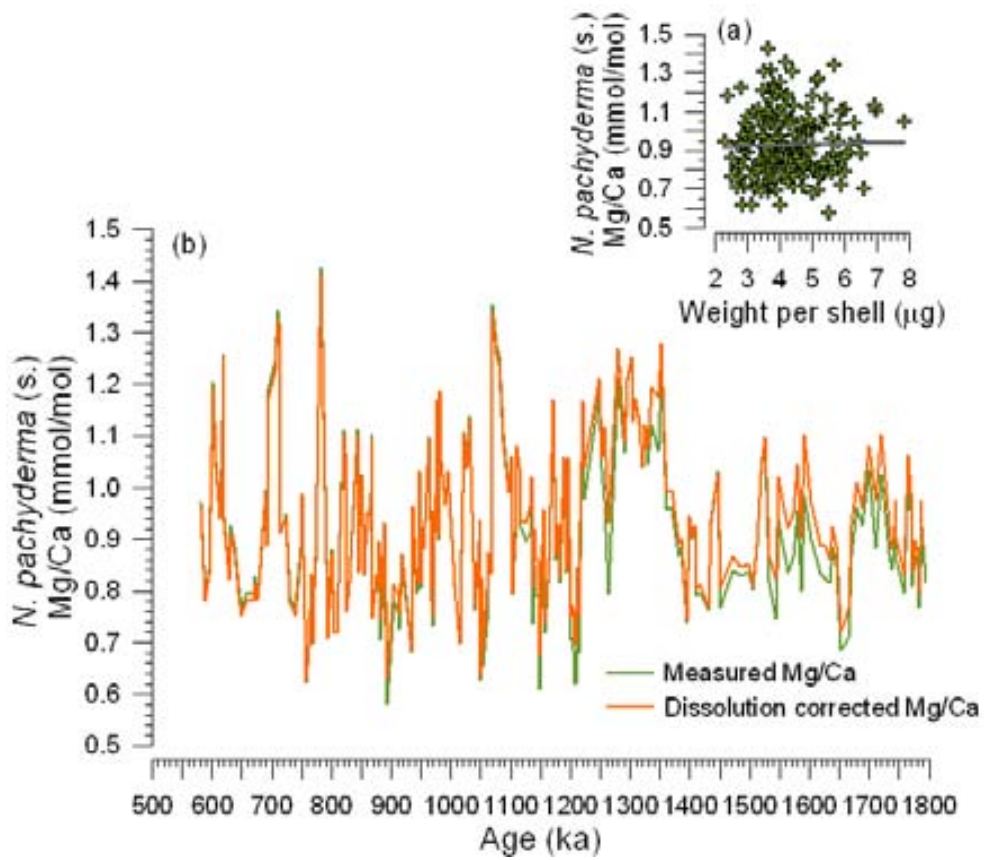
Figure S1. (a) Correlation between *N. pachyderma* (s.) Mg/Ca and *N. pachyderma* (s.) shell weight. (b) Comparison between the *N. pachyderma* (s.) Mg/Ca raw data (green), and *N. pachyderma* (s.) Mg/Ca when the dissolution correction proposed by Barker et al. (2009) is applied.
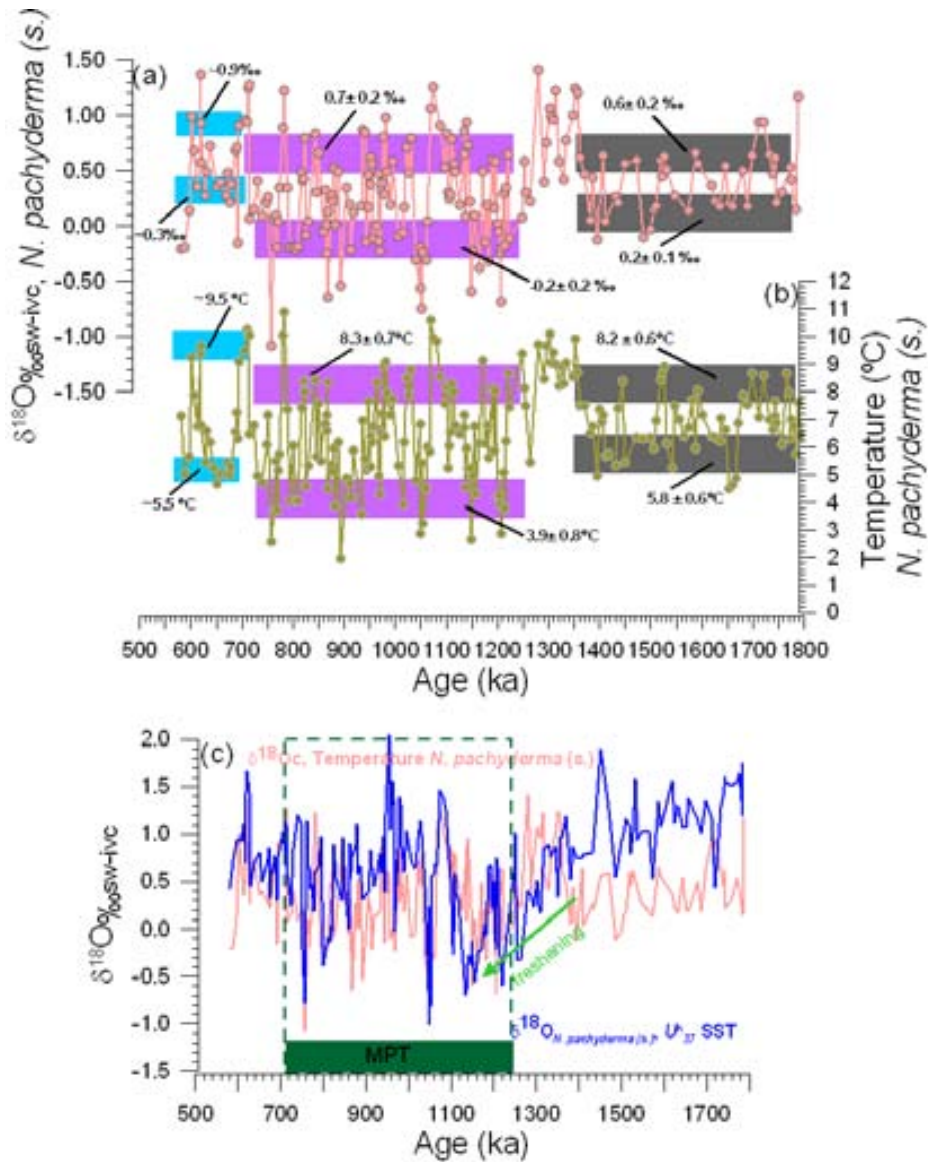
Figure S2. *N. pachyderma* (s.)-based reconstructions from ODP site 1090: (a) $\delta^{18}O_{SW\text{-}IVC}$ (b) Temperature. Horizontal box areas are shown to highlight the glacial periods (lower boxes) considered to calculate the average of glacial temperature and $\delta^{18}O_{SW\text{-}IVC}$ for each interval: before MPT (gray), during MPT (purple) and the only one glacial-interglacial cycle after the MPT (blue). Although not discussed in the main text, we also show interglacial changes (upper boxes). Numbers connected to each box correspond to the average and standard deviation of the temperature, and $\delta^{18}O_{SW\text{-}IVC}$ reconstructions within the boxed area. (c) Local $\delta^{18}O_{SW\text{-}IVC}$ changes at ODP Site 1090 obtained by removing the ice-volume mean ocean $\delta^{18}O$ (Bintanja and van de Wal, 2008) and calcification temperature components from the $\delta^{18}O$ measured on *N. pachyderma* (s.) (pink). For comparison, it is also shown the local $\delta^{18}O_{SW\text{-}IVC}$ obtained by removing the ice-volume mean ocean $\delta^{18}O$ (Bintanja and van de Wal, 2008) and U^{K}_{37} temperature reconstructions (Martínez-Garcia et al., 2010) from $\delta^{18}O$ measured on *N. pachyderma* (s.)(blue).

CHAPTER 4

Subantarctic Zone thermocline shoaling at the onset of the Middle Pleistocene Transition: improving conditions for glacial marine productivity in the region?

Abstract

Paleoceanographic studies in the Southern Ocean have provided evidence of meridional expansion of the Antarctic Polar Frontal system at the onset of the Middle Pleistocene Transition (MPT), and successive fluctuations in its positioning during glacial-interglacial stages around the Subantarctic Zone. Here we provide insights on the influence of the expansion of the Antarctic Polar Frontal system on the physical structure of the water column in that region across the MPT. Mg/Ca-temperature and $\delta^{18}O_{SW-IVC}$ profiles inferred from *Globigerina bulloides*, *Neogloboquadrina pachyderma* (sinistral), and *Globorotalia crassaformis* allowed reconstructing past changes in the positions of the thermocline/halocline in the Subantarctic Zone (ODP Site 1090), spanning the entire MPT (1800-580 ka). Our results suggest that from 1500-1300 ka these oceanographic features shoaled and that shallower conditions persisted throughout the MPT. This also implies that environmental conditions at Site 1090 shifted from Subtropical (deeper thermocline/halocline) to Subantarctic (shallower thermocline/halocline) before the onset of the MPT. Using modern conditions in the region as an analog, we suggest that the observed physical structure changes of the water column probably was associated to increases in macro-nutrient availability in the region. This likely conditioned the Subantarctic Zone for increased primary productivity during periods of high eolian Fe-supply. Therefore, synchronous changes in the upper water column conditions and sharp increases in Fe-supply to the region at the onset of the MPT provides a plausible mechanism (absent before the MPT) to explain the observed boost in primary productivity at 1200 ka in the Subantarctic Zone. We suggest that the new Subantarctic Zone glacial arrangement, in combination with Southern Ocean stratification, maintained low pCO$_2$ and temperatures in glacial stages after the MPT, further accentuating climate sensitivity to Fe-fertilization under cold conditions.

4.1. <u>Introduction</u>

The Middle Pleistocene Transition (MPT) was a period between 1250 and 700 ka *(Clark et al., 2006)* where glacial changes in ice volume became more prominent *(Elderfield et al., 2012)* and the periodicity of the glacial-interglacial cycles changed from 41 to 100 ky with apparently no changes in solar incoming radiation *(Clark et al. 2006; Park and Maasch, 1993)*. Although the causes of the transition still remain elusive, most of the theories point to atmospheric carbon dioxide (pCO_2) concentration changes to have acted as an important feedback for the transition *(Clark et al., 2006; van de Wal and Bintanja, 2009)*. It has been widely accepted that the combination of biological and physical processes in the Southern Ocean have highly influenced pCO_2 concentrations over glacial-interglacial timescales *(Sigman et al, 2010 and references therein)*, and by extension during the MPT. Thus, a reinforcement of the glacial biological pump in the Subantarctic Zone, which in the modern ocean features High Nutrient Low Chlorophyll (HNLC) conditions, triggered by the eolian transport of Fe *(Martin, 1980)*, would have increased the uptake of pCO_2 during glacial periods. Additionally, the strengthening of Southern Ocean processes that physically inhibited the outgassing of respired CO_2, such as upper ocean stratification *(Francois et al., 1990; Francois, 2004)* and sea ice expansion *(Stephens and Keeling, 2000; Keeling and Stephens, 2001; Archer et al., 2003)*, would have further improved conditions for more efficiently storing Carbon (C) at depth during glaciations.

Different paleoceanographic studies have indeed provided evidence of oceanic reorganization in the Southern Ocean during the MPT with important implications for the C cycle across and after the transition. Recently, Rodríguez-Sanz *et al.,* (2012) have shown that the Southern Ocean upper water column cooled and freshened at the onset of the MPT (~1250 ka) due to the expansion of the Antarctic Polar Fronts and that those conditions persisted in the following glacial stages. Based on the sensitivity of ocean density to changes in salinity under cold conditions *(Adkins et al., 2002; de Boer et al., 2008)* the authors suggested that the observed freshening increased glacial upper Southern Ocean stratification and that this in combination with biological processes could have possibly accounted for the ~30ppm drop in pCO_2 across the MPT *(Hönisch et al., 2009)*. Southern Ocean studies focused on the MPT undoubtedly support the

notion of the northward advection of polar waters to latitudes closer to the Subantarctic Zone during glacial stages since the onset of the transition. By using different approaches, summer sea surface temperature (SST) reconstructions based on planktonic foraminifera abundances *(Becquey and Gersonde, 2002)* and coccolithofore and diatom assemblages *(Flores and Sierro, 2007; Kemp et al., 2010)* have demonstrated successive glacial-interglacial variations in the position of the Antarctic polar frontal across the MPT. Furthermore, a study based on biomarkers *(Martínez-Garcia et al., 2010)* has identified that the advection of surface polar waters to the Subantarctic Zone increased during glaciations after 1250 ka (the onset of the MPT), further supporting the view of the Antarctic Polar Front expansion. None of the studies, however, have focused on understanding the implications of the expansion of the polar fronts on the physical structure of the water column, and coupling of this physical feature with sharp increases in micro-nutrient availability at the onset of the MPT *(Martinez-Garcia et al., 2011)* to explain past cycles in productivity.

Here we present new geochemical results from the South Atlantic sector of the Southern Ocean (ODP Site 1090) spanning the entire MPT (1800-580 ka) to understand the influence of the expansion of the Antarctic Polar Fronts on the physical structure of the Subantarctic water column. Although proxy records to reconstruct past temperature and salinity are inherently limited in their precision because of the large error associated with them, they still provide valuable information on the amplitude of changes associated to both oceanic features in the surface ocean water column. Therefore, paired Mg/Ca-$\delta^{18}O_C$ measurements on three planktonic foraminiferal species having distinctly different depth habitat preferences; *Globigerina bulloides* (surface dweller), *Neogloboquadrina pachyderma* (s.) (subsurface dweller, *(Rodríguez-Sanz et al., 2012)*, and *Globorotalia crassaformis* (thermocline), yield depth-specific temperature and ice volume corrected seawater $\delta^{18}O$ profiles. Collectively these data allow us to reconstruct the thermocline and halocline across the MPT and gain new insight on the structure of the water column and its combined effect with biological processes to characterize past productivity in relation to carbon sequestration.

4.2. <u>Material and Methods</u>

4.2.1. Sediment core location, chronology

Site 1090 was drilled during ODP Leg 177 *(Gersonde et al., 1999)* in the Subantarctic Zone (42°54.8´S, 8°54´E) on the northern flank of the Agulhas Ridge (Fig. 1a and b). It is located at a water depth of 3702 m, and it has sedimentation rates on the order of 3-4 cm kyr^{-1}*(Venz and Hodell, 2002)*. In this study we use the age model reported in *(Martínez-Garcia, et al. 2010),* which was obtained by graphically correlating the benthic $\delta^{18}O$ record of ODP Site 1090 *(Venz and Hodell, 2002)* to the Lisiecki and Raymo (2005) global stack (hereafter LR04, Fig. 2a). The site is located at the interface between North Atlantic Deep Water (NADW) and underlying lower Circumpolar Deep Water (CDW) *(Gersonde, et al. 1999)*. In the region, the upper 600 m austral temperatures ranged between ~10-6ºC and salinity ~35-34 psu (Fig. 1a-d; *Antonov et al., 2010; Locarnini et al., 2010*).

4.2.2. Oceanographic setting

ODP Site 1090 is especially suited to monitor changes in the positions of the Southern Ocean fronts, as surface temperature and salinity (Fig. 1a-b) can vary drastically on glacial-interglacial timescales. A cross section from the Equator to 60°S at 0°W in the South Atlantic (Fig. 1a-b) shows that the depth of surfaces with the same temperature and salinity shoal toward the Polar Front *(Antonov et al., 2010; Locarnini et al., 2010)*, hence resulting in a deeper thermocline/pycnocline in the Subtropical Zone than in the Subantarctic Zone. The feature observed in the iso-surfaces of the Southern Ocean is forced by the upwelling processes close to the Antarctic continent (Fig.1, *Rintoul et al., 2001*), which also influence nutrient distribution both at local and global scales *(Marinov et al., 2006)*. Nutrient availability clearly decreases from the upwelling region (Antarctic Zone; *Garcia et al., 2010*) toward lower latitudes, then leaving the Subantarctic Zone more enriched in nutrients than the Subtropical Zone (Fig. 1c). Productivity in the Antarctic Zone primarily consumes the outcropped micro-nutrients (Fe and Si), while leaving an excess of the macro-nutrients (Nitrate and Phosphate) in the region. The excess of macro-nutrients is either returned to the deep Southern Ocean or exported northward through circulation processes *(Rintoul et al., 2001)*. The northward advection of water masses with high macro-nutrient contents but low Fe

concentration to the Subantarctic Zone accounts for the HNLC character of the region, making biological productivity there susceptible to eolian supply of micro-nutrients. Nutrients in the Subantarctic Zone are eventually redistributed to low latitudes by circulation processes that involve the SAMW and AAIW *(Sarmiento et al., 2004)*, hence influencing primary productivity in those regions.
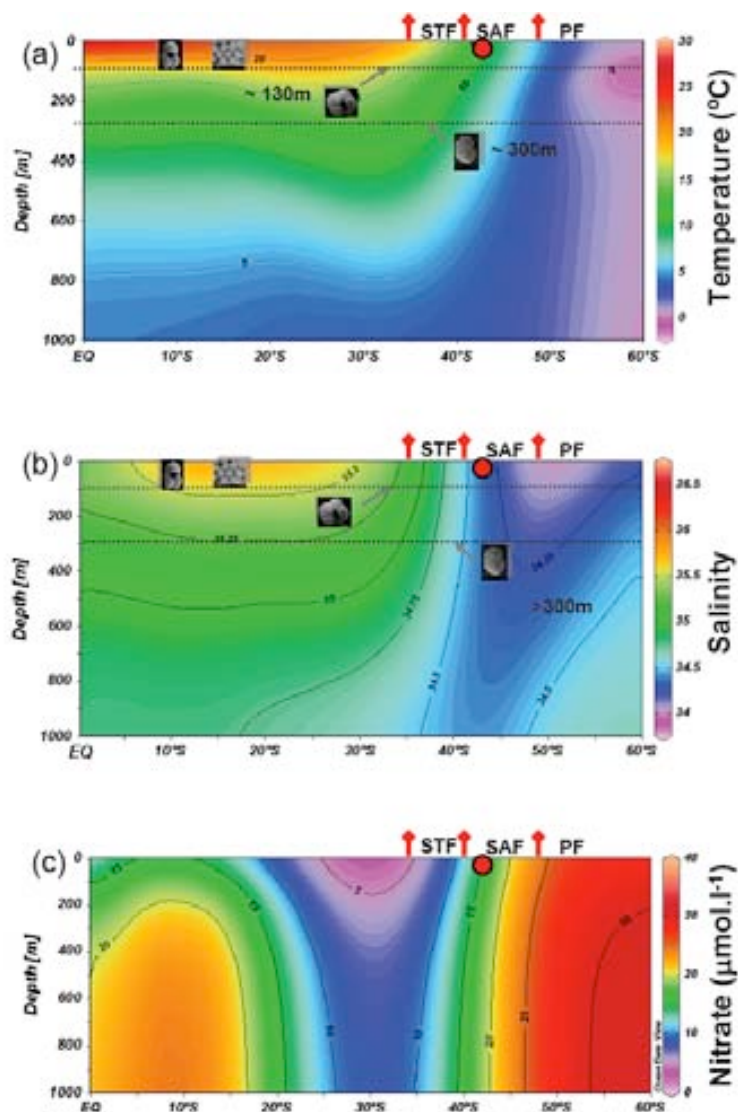
Figure 4.1. Cross section from the Equator to 60°S at 0°W in the South Atlantic showing Austral summer temperatures (a), salinity (b) and (c) macro-nutrients distribution. Dashed lines show the approximate depth habitat of the proxy signal carriers (foraminifera) used in this study. A schematic view of the modern position of the Subtropical front (STF), Subantarctic Front (SAF) and Polar Front (PF) with respect to the core site (red dot) is shown by red arrows.

4.2.3. Foraminiferal Mg/Ca

We have generated Mg/Ca-based temperature records inferred from two different foraminiferal species: the surface dweller *G. bulloides* and the deep dweller *G. crassaformis* spanning the entire MPT (1800 to 580 ka) with a temporal resolution of ~6-7ky. For Mg/Ca analyses, a minimum of ~20 individuals of each species were picked from the 250-350 μm size fraction. Foraminiferal shells were crushed and cleaned according to the analytical procedure explained in Chapter 2 section 2.2.1. Samples with Al/Ca and Mn/Ca above the commonly used thresholds *(Boyle, 1983; Barker et al., 2003; Ferguson et al., 2008)* were replicated. Those replicates that yielded significantly different values were discarded, while those with consistently high (~15 % of the total samples in both, *G. bulloides* and *G. crassaformis*, records) values were retained as they do not affect any of those features upon which our conclusions are based. Furthermore, the correlation between Mg/Ca and Mn/Ca measurements was poor $(r^2 \sim 0.4)$, suggesting that high Mn/Ca values were not affecting our Mg/Ca measurements. The calibrations selected for converting Mg/Ca values into temperature in this study were *(Mashiotta et al., 1999)* for *G. bulloides* and *(Regenberg et al., 2009)* for *G. crassaformis*. We applied the adjustment suggested by Medina-Elizalde *et al.,* (2008) to account for the long-term changes in the Mg/Ca of seawater for intervals older than 1000 ka. In the discussion we exclusively refer to the adjusted values unless otherwise stated.

4.2.4. Stable isotope measurements

Approximately 20 individuals of *G. crassaformis* were picked from the same size fraction used for Mg/Ca analyses to perform stable oxygen isotope ($\delta^{18}O_C$) measurements following cleaning procedure and sample preparation described in chapter 2 section 2.2.2. Analyses of the samples were carried out at the analitical service of Cardiff University.

4.2.5. Sea water isotope composition based on *G. bulloides* and *G. crassaformis*

Based on paired Mg/Ca-$\delta^{18}O_C$ measurements on *G. crassaformis* we calculated the sea water isotope composition ($\delta^{18}O_{SW}$) using the paleotemperature equation reported by

Shackleton (1974) ($\delta^{18}O_{SW} = \delta^{18}O_c + 0.27 - (4.38 - (4.38^2 - 4 \times 0.1 \times (16.9 - T))^{1/2})/(0.1 \times 2)$), which has been employed recently in Rodríguez-Sanz *et al.*, (2012). We have also calculated $\delta^{18}O_{SW}$ based on *G. bulloides*. We used the Mg/Ca$_{G. \; bulloides}$- based SST reconstruction reported in this study, and the previously published $\delta^{18}O_C$ inferred from the same species and performed at the same core site *(Venz and Hodell, 2002)*. We have resampled *G. bulloides* $\delta^{18}O_C$ *(Venz and Hodell, 2002)* to the same temporal resolution than Mg/Ca$_{G. \; bulloides}$- based SST record and then we calculated the $\delta^{18}O_{SW}$ using Shackleton, (1974). We employed the same paleotemperature equation for all $\delta^{18}O_{SW}$ records to facilitate comparison between them. Therefore, we ensure that differences observed in trends are real and not an artifact introduced by using different equations.

We 'remove' the ice volume component of the $\delta^{18}O_{SW}$ signal in both reconstructions using the Pleistocene record of eustatic sea level changes as modeled by *(Bintanja and van de Wal, 2008)*. We linearly interpolated the Bintanja and van de Wal (2008) record at the time step of the Site 1090 *G. bulloides* and *G. crassaformis* profiles and we then subtracted from the reconstructed $\delta^{18}O_{SW}$ values the mean ocean $\delta^{18}O_{SW}$ eustatic changes. The $\delta^{18}O_{SW-IVC}$ is known to be linearly correlated with ocean water salinity on regional scales *(LeGrande and Schmidt, 2006)*. A full error propagation exercise yields 1σ uncertainties for the two new ice-volume corrected $\delta^{18}O_{SW-IVC}$ data of 0.3‰.

4.2.6. Planktonic foramiferal species as recorders of past changes of the physical structure of the water column

In order to reconstruct changes of the thermocline and halocline in the Subantarctic Zone across the MPT we present a reconstruction of Mg/Ca-based temperature and $\delta^{18}O_{SW-IVC}$ (which is linearly correlated with local salinity *(LeGrande and Schmidt, 2006)* variations derived from three planktonic foraminiferal species having different ecological habitat (depth) preferences. *G. bulloides* reflects austral summer surface ocean conditions in the upper ~80m of the water column, with maximal abundances coinciding with phytoplankton blooms *(Fraile et al., 2009; Mortyn and Charles, 2003)*. Plankton tow studies have suggested that *N. pachyderma* (s.) is commonly found between the deep chlorophyll maximum and pycnocline to shallower depths in the Southern Ocean *(Mortyn and Charles, 2003)*. *G. crassaformis* is a recorder of deeper

ocean conditions (~250-400 m; *Niebler, 1995; Regenberg, et al. 2009; Steph, et al., 2009*) in subtropical areas, and is known to dwell below the thermocline *(Ravelo and Fairbanks, 1992)*, with apparently no seasonal preferences *(Tedesco et al., 2007)*. The identification of this species at the core site required a more exhaustive micropaleontological analysis, which has been added as supplementary information (S1). Most of the ecological information of the species has been provided by studies carried out in tropical-subtropical areas (e.g. *Regenberg et al., 2009; Steph et al., 2009*). Therefore, since *G. crassaformis* dwells at the base of the thermocline, we contend that in the modern ocean its depth habitat tends to shoal southward toward the Subantarctic Zone following Southern Ocean isothermals (Fig. 1a). The same reasoning has been followed to understand its recorded signal across the MPT, where the location of Site 1090 allows tracking the interplay between the Subtropical and Subantarctic Fronts in the region during glacial-interglacial cycles *(Gersonde et al., 1999)*. Hence, non-surface dwelling foraminifera used here allow us to address the past dynamics of the thermocline and halocline (hence pycnocline) position, which are compared with surface conditions obtained from the separate signal carriers (alkenone- and *G. bulloides*-based SST).

4.3. Results

Figure 2 shows the LR04 stack (Fig. 2a), which we use here as a reference for the Early to Middle Pleistocene ice volume and/or deep ocean temperature variations *(Bintanja et al., 2005; Elderfield et al., 2012)*, along with a suite of upper water column temperature reconstructions from ODP Site 1090 (Fig. 2b-c). Between ~1800 and 1500 ka the offset between surface and subsurface temperatures at Site 1090 was larger than in the remainder of the records (Figure S2).

Alkenone- and Mg/Ca$_{G.\ bulloides}$-based SST reconstructions at Site 1090 (Fig. 2b), show overall comparable trends throughout the time interval spanned by our records. However, the amplitude of the glacial-interglacial SST variations derived from the Mg/Ca$_{G.\ bulloides}$ record remains similar (~3±1ºC) throughout, while the alkenones indicate larger glacial-interglacial SST changes after the MPT (~7±1ºC) than before the transition (~5±1ºC). We suggest that this is due to the lower temporal resolution of Mg/Ca$_{G.\ bulloides}$ caused by the low to zero abundance of *G. bulloides* during the coldest

glacial periods, for which SST was plausibly too cold for this species to proliferate (cfr. Niebler and Gersonde, 1998). As a result, glacial conditions are somewhat undersampled in the 1090 Mg/Ca$_{G.\ bulloides}$ record, explaining why it underestimates the glacial-interglacial variability in certain intervals of the MPT.
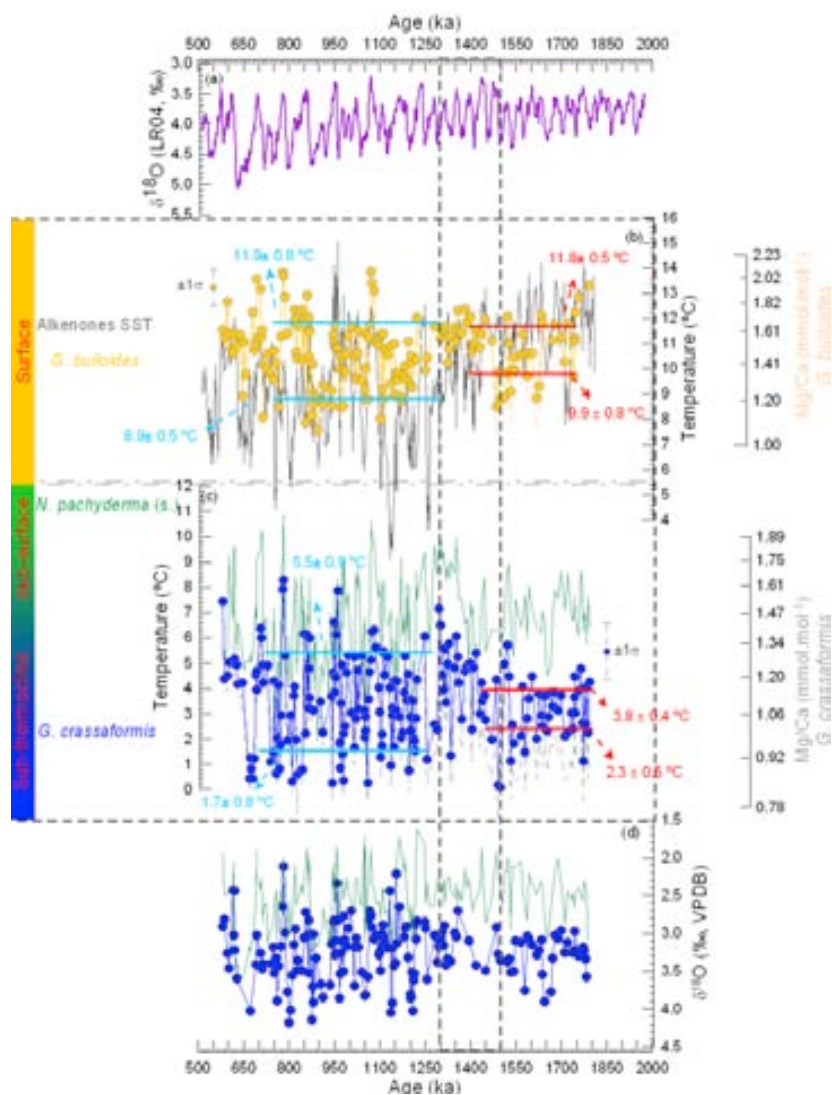
Figure 4.2. (a) Global benthic δ18O stack *(Lisieke and Raymo, 2005)*. (b) Alkenone-based SST (UK37) reconstruction at ODP Site 1090 (grey; *Martínez-Garcia et al., 2010*) and Mg/Ca-derived SST at Site 1090 obtained from *G. bulloides* (purple). (c) Mg/Ca-derived temperature from *N. pachyderma* (s.) (green, *Rodríguez-Sanz et al., 2012*) and *G. crassaformis* (blue). (d) Calcite oxygen isotope composition (δ18O$_C$) of *N. pachyderma* (s.) (green) and *G. crassaformis* (blue). Horizontal red and blue lines and numbers show the average glacial and interglacial temperatures before and during the MPT, respectively. Boxed dashed area highlights the progressive shoaling of the thermocline (1500-1300 ka), the position of which persisted throughout the MPT.

We compare Mg/Ca$_{N.pachyderma}$- and Mg/Ca$_{G.\ crassaformis}$-based temperature reconstructions in Figure 2c. Despite its deeper habitat (~250-400 m, *Niebler, 1995; Regenberg, et al. 2009; Steph, et al., 2009*) and contrary to the pre-MPT interval, Mg/Ca $_{G.\ crassaformis}$ during the MPT shows glacial-interglacial temperature shifts (4±1ºC) that are similar in amplitude to those derived from the Mg/Ca$_{N.pachyderma}$ profile (~5±1ºC). This feature was preceded by a sustained warming from 1500 to 1300 ka observed in both Mg/Ca-temperature reconstructions (Fig. 2c) but absent in the SST records (Fig. 2b). Depth habitat preferences of *N. pachyderma* (s.) (above; *Mortyn and Charles, 2003*) and *G. crassaformis* (below; *Ravelo and Fairbanks, 1992; Regenberg et al., 2009*) with respect to the thermocline make them ideal to monitor past changes in the position of this oceanographic feature. Indeed, Mg/Ca $_{G.crassaformis}$-based reconstructions have been already used elsewhere for this purpose (e.g. *Karas et al., 2009*). Hence, the Mg/Ca-based temperature increases shown by the relatively deeper dwelling planktonic foraminiferal species, in the vicinity of the thermocline, attest to the upward migration of this feature between 1500 and 1300 ka. Warmer interglacial temperatures (1.7±0.6ºC) across the MPT derived from the deepest Mg/Ca$_{G.\ crassaformis}$ profile compared to the interval from 1800 to 1300 ka, together with similar glacial-interglacial amplitude shifts than Mg/Ca$_{N.pachyderma}$ from 1200-580 ka (Fig. 2c), suggest that shallower thermocline conditions persisted throughout the MPT. *N. pachyderma* (s.)- and *G. crassaformis*-$\delta^{18}O_C$ also feature similar glacial-interglacial amplitude changes only after the MPT, further supporting the notion of changes in environmental conditions in the habitat of the foraminiferal species at the onset of the MPT.

The thermocline and halocline are tightly linked in the Southern Ocean (Fig 1a-b). Comparisons between the three planktonic foraminiferal species $\delta^{18}O_{SW-IVC}$ reconstructions (Fig. 3a-c) suggest that the halocline shoaled together with the thermocline, which is a coupling in line with modern observations. That is, *N. pachyderma* (s.)- (Fig. 3b) and *G. crassaformis*-$\delta^{18}O_{SW-IVC}$ (Fig. 3c) show a sustained increase in salinity, that is absent in *G. bulloides*-$\delta^{18}O_{SW-IVC}$ (Fig. 3a), and which parallels the warming before the MPT suggested by both relatively deeper dwelling foraminiferal temperature records (Fig. 2c).
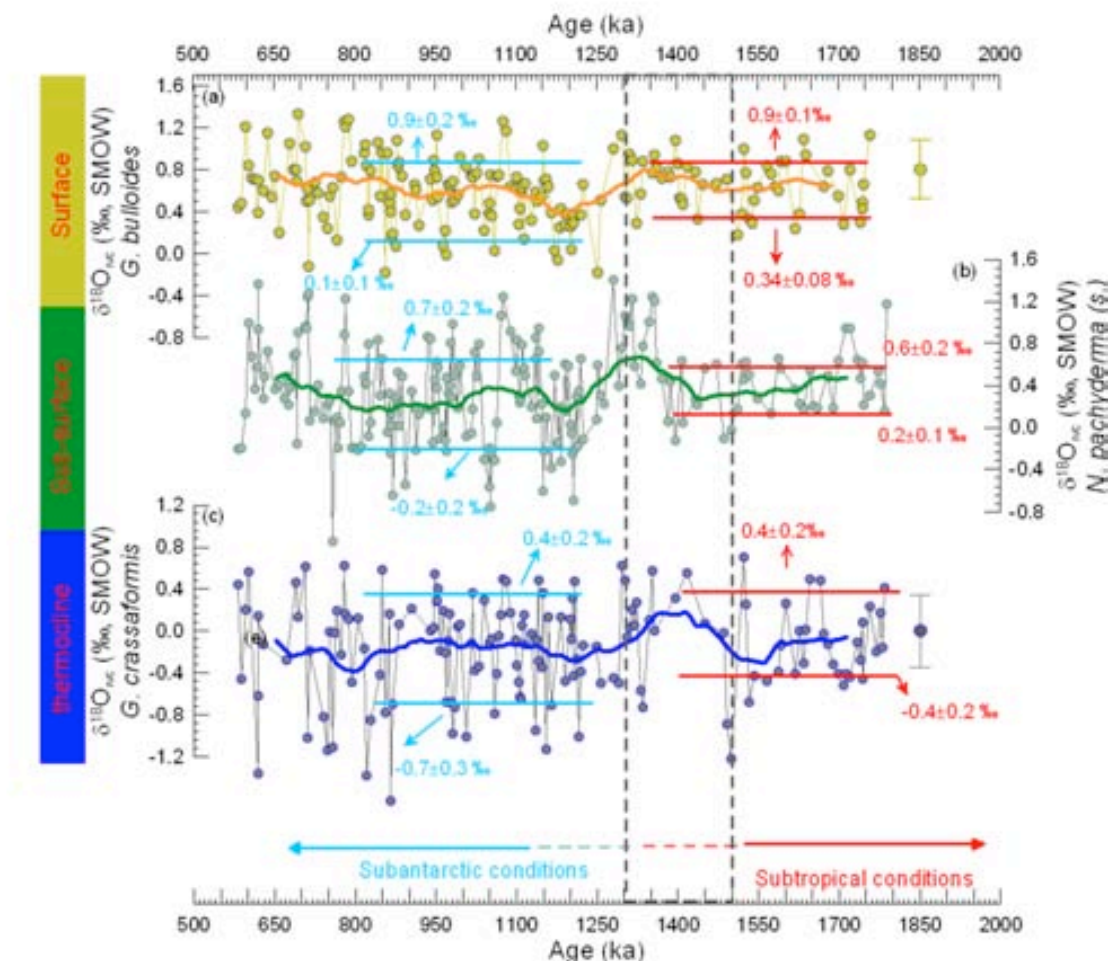
Figure 4.3. (a) Global benthic $\delta^{18}O$ stack *(Lisieke and Raymo, 2005)*. Local $\delta^{18}O_{SW-IVC}$ changes at ODP Site 1090 were obtained by removing the ice-volume mean ocean $\delta^{18}O$ *(Bintanja and van de Wal, 2008)* and calcification temperature components from the $\delta^{18}O$ measured on (b) *G. bulloides*, (c) *N. pachyderma* (s.), and (d) *G. crassaformis*. Boxed dashed area highlights the progressive shoaling of the halocline (1500-1300 ka), the position of which persisted throughout the MPT.

4. **Discussion**

The temperature and $\delta^{18}O_{SW-IVC}$ developments derived from paired Mg/Ca-$\delta^{18}O$ measurements on the upper and lower thermocline foraminifera *N. pachyderma* and *G. crassaformis* (Fig. 2c-d and 3b-c) provide robust evidence of the shoaling of the thermocline and halocline prior to the onset of the MPT in the Subantarctic Zone of the Atlantic Ocean. Overall shallower positions of both oceanic features persisted throughout the MPT at the same site.

81

In the modern Southern Ocean the depth of the thermocline and halocline are influenced by the upwelling of deep waters offshore Antarctica *(Rintoul et al., 2001)*, which collectively causes the isothermal and isohaline surfaces to shoal southwards *(Antonov et al., 2010; Locarnini et al., 2010)*. Accordingly, the equatorward expansion of the oceanic fronts during the more severe glaciations of the MPT *(Kemp et al., 2010; Martínez-Garcia et al., 2010; Marino et al., 2009; Rodríguez-Sanz et al., 2012)* would cause a shoaling of the thermocline and halocline, as documented in our upper and lower thermocline temperature (Fig. 2c) and in $\delta^{18}O_{SW-IVC}$ proxies (Fig. 3b-c). Our data further suggest that the northward position of the Antarctic Polar Front during the MPT shifted environmental conditions at ODP Site 1090 from Subtropical (deeper thermocline/halocline) to more Subantarctic (shallower thermocline/halocline). The shift in the response of the Subantarctic Zone climate from precession-driven (low latitude insolation) to more obliquity-driven (high latitude insolation) observed in Martínez-Garcia *et al.,* (2010) around 1600 ka also corroborates our finding. Thus, the equatorward expansion of the polar fronts had important repercussions in the physical structure, and possibly also in the chemical composition, of the upper water column of the Subantarctic Zone, likely having implications for marine productivity in the region after the transition.

4.4.1. Interaction between upper water column changes, iron supply, and marine primary productivity

It has been suggested that the northward expansion of the Antarctic Polar Fronts during glacial periods is coupled with the equatorward migration of the westerly wind belt in the Southern Hemisphere *(Toggweiler et al., 2006)*. This change in the atmospheric circulation occurred as a consequence of meridional shift of the band of the strongest thermal gradient between low and high latitudes (crf. *Toggweiler and Russell, 2008*). During the glacial phases of the MPT the expansion of the polar fronts was also associated with the compression of the subtropical areas of the global ocean *(Martínez-Garcia et al., 2010)*. This affected global atmospheric patterns *(McClymont and Rosell-Mele, 2005; Etourneau et al., 2009)*, in turn promoting drier conditions over South America and Africa during the MPT than observed in previous geological periods as the Pliocene *(Wara et al., 2005; Brierley et al., 2009)*. Such a wind field configuration together with more arid conditions in South America during the MPT should have

enabled enhanced eastward transport and fluxes of dust to the Subantarctic sector of the Atlantic Ocean (e.g. *Iriondo, 2000; Lambert et al., 2009*), in line with the sharp increase of glacial Fe supply to Site 1090 at the onset of the MPT *(Martinez-Garcia et al., 2011)*.

Glacial increases of Fe-supply to areas of the ocean where productivity is limited by micro-nutrients, HNLC regions, might have strengthened the biological pump, in turn, increasing the uptake and storage of C in the deep ocean *(Martin, 1990)*. This mechanism seemed to have had an important role in modulating pCO$_2$ concentration during the glacial stages over the last 1100 ky *(Watson et al., 2000; Kohfeld et al., 2005; Martínez-Garcia et al., 2009)*. Beyond the coverage of Antarctic ice core pCO$_2$ records, Fe-supply to the Southern Ocean featured two large amplitude pulses centred at ~2700 and ~1250 ka, that is, at the onset of the Northern Hemisphere glaciations and at the MPT, respectively (Fig. 4a; *Martinez-Garcia et al., 2011*). However, while primary productivity at the higher latitudes of the Southern Ocean responded to Fe-supply during both pulses (Fig. 4b-c), increases at ~1250 ka mark the only pulse showing a tight coupling between Fe-fertilization and marine primary productivity in the Subantarctic Zone (Fig. 4d). This suggests that besides Fe concentration availability other factors were preventing primary productivity in the Subantarctic Zone before the MPT.

We speculate that the expansion of the Antarctic Polar Fronts not only triggered physical changes, but also increased macro-nutrient availability changes in the Subantarctic Zone water column, improving conditions in the region to exploit primary productivity under high Fe concentration periods. Accordingly, the Antarctic Polar Front expansion reached its closest position to ODP 1090 at the onset of the MPT (~1250 ka; *Martínez-Garcia et al., 2010*) and it was a recurrent phenomena that took place during glacial stages after 1250 ka *(Rodríguez-Sanz et al., 2012)*. This promoted a shift from Subtropical to Subantarctic conditions at ODP 1090, triggering the observed shoaling of the thermocline/halocline and changes in the response to orbital parameters in the region *(Martínez-Garcia et al., 2010)*. In the modern ocean the Subantarctic Zone features shallower thermocline/pycnocline conditions than the Subtropical Zone (Fig. 1a-b), but also higher concentrations of macro-nutrients due to the advection of polar waters to the core site (Fig. 1c). Using this as an analog, a more Subantarctic ODP

1090 after 1250 ka might have also resulted in an increase in macro-nutrient availability during glacial stages of the MPT than before. Fe concentrations would then become the only limiting factor to enhance primary productivity in the region after the transition, explaining the tight link between them only after 1250 ka (Fig. 4a and d).
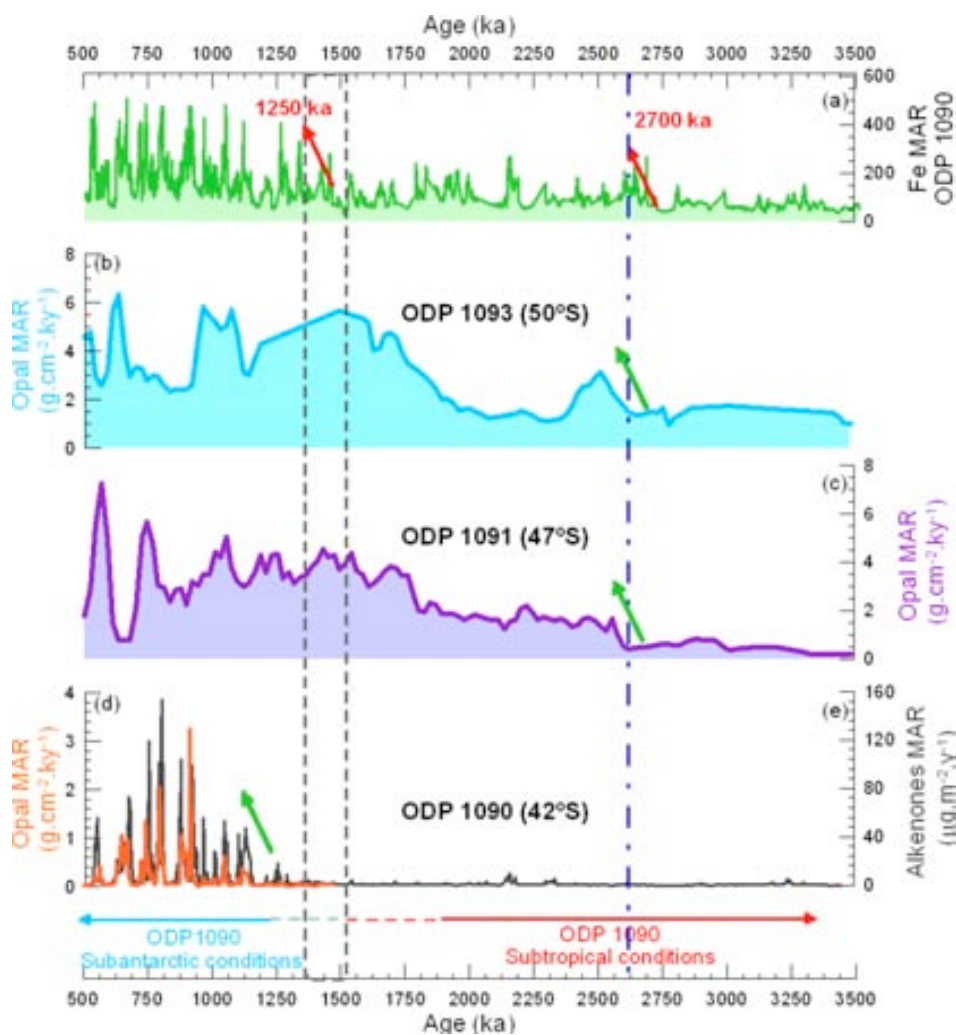
Figure 4.4. (a) ODP Site 1090 dust flux (n-alkanes mass accumulation rate; MAR) *(Martinez-Garcia et al., 2011)*. Opal MAR from a Southern Ocean transect *(Cortese et al., 2004)*: (b) Polar Front (ODP 1093), (c) Polar Front Zone (ODP 1091), and (d) Subantarctic Zone (ODP 1090; orange). Alkenones MAR in the Subantarctic Zone Site 1090 is also shown in gray in panel (d) *(unpublished data)*. Boxed dashed area highlights the progressive shoaling of the halocline (1500-1300 ka), the position of which persisted throughout the MPT. Red arrows highlight the pulses of increased Fe-fertilizations while green arrows the response of marine primary productivity to them in each zone of the Southern Ocean. Dark blue vertical dashed line shows the increase in Fe-supply and productivity response at 2700 ka.

Hence, the new MPT Subantarctic Zone water column configuration after 1250 ka increased the sensitivity of the region to glacial Fe-fertilization with concomitant enhancements in primary productivity during glacial stages. This in combination with glacial Southern Ocean stratification allowed the more efficient uptake and storage of C in the deep ocean with respect to glacial stages before 1250 ka *(Hodell and Venz-Curtis, 2006; Rodríguez-Sanz et al., 2012)*. This mechanism maintained low pCO$_2$ *(Hönisch et al., 2009)* concentrations and temperatures during MPT glacial stages after 1250 ka, helping to maintain glacial arid conditions in South America. We speculate that simultaneous changes at the onset of the MPT of the Subantarctic Zone water column structure, westerly winds configuration associated to Antarctic Polar Frontal system expansion, and conditions in South America acted as a positive feedback to enhance the observed climate sensitivity to Fe-fertilization under glacial conditions after ~1250 ka *(Ridgwell and Watson, 2002; Lambert et al., 2009; Martinez-Garcia, et al. 2011)*.

4.5. <u>Conclusions</u>

Multispecies reconstructions of Mg/Ca-temperature and δ^{18}O$_{SW-IVC}$ at ODP Site 1090 inferred from planktonic foraminifera with different depth habitat preferences has provided insights on the influence of the Antarctic Polar Frontal system northward expansion on the physical structure of the Subantarctic Zone across the MPT. Our results suggest the thermocline and halocline of the region shoaled from 1500 to 1300 ka in response to the northward expansion of the fronts and that those conditions remained throughout the transition. The shoaling of these oceanic features suggest that at the onset of the MPT Site 1090 shifted from Subtropical to Subantarctic conditions in agreement with the change in the dominance of the orbital cycles observed in the alkenone-SST reconstruction from the same site *(Martínez-Garcia et al., 2010)*. We speculate that new conditions of Site 1090 after the MPT not only prompted the shoaling of the thermocline and halocline but also an increase of macro-nutrient concentrations, in concordance with modern oceanic differences between the Subtropical and Subantarctic Zone. These changes at Site 1090 were roughly in tandem with a sharp increase of Fe-supply to the Southern Ocean *(Martinez-Garcia et al., 2011)*, providing a holistic (physical/chemical) mechanism to explain increases in marine primary productivity during glacial stages after ~1250 ka. Synchronous physical changes and characteristics of the upper water column, Fe-supply, and efficiency of the

biological pump in the Subantarctic Zone glacial stages across the MPT, possibly acted as a positive feedback to enhance climate sensitivity to Fe-fertilization under glacial conditions after the MPT *(Ridgwell and Watson, 2002; Martinez-Garcia et al., 2011)*.

4.6. <u>References</u>

Adkins, J. F., McIntyre, K., Schrag, D. P., 2002. The Salinity, Temperature, and δ18O of the Glacial Deep Ocean. Science. 298, 1769-1773.

Antonov, J. I., D. Seidov, T. P. Boyer, R. A. Locarnini, A. V. Mishonov, and H. E. Garcia, 2010. World Ocean Atlas 2009 Volume 2: Salinity. S. Levitus, Ed., NOAA Atlas NESDIS 69, U.S. Government Printing Office, Washington, D.C., 184 pp.

Archer, D. E., Martin, P. A., Milovich, J., Brovkin, V., Plattner, G., Ashendel, C., 2003. Model sensitivity in the effect of Antarctic sea ice and stratification on atmospheric pCO$_2$. Paleoceanography. 18, 1012.

Barker, S., Greaves, M., Elderfield, H., 2003. A study of cleaning procedures used for foraminiferal Mg/Ca paleothermometry. Geochemistry, Geophysics, Geosystems. 4, 8407.

Becquey, S. and Gersonde, R., 2002. Past hydrographic and climatic changes in the Subantarctic Zone of the South Atlantic – The Pleistocene record from ODP Site 1090. Palaeogeography, Palaeoclimatology, Palaeoecology. 182, 221-239.

Bintanja, R. and van de Wal, R. S. W., 2008. North American ice-sheet dynamics and the onset of 100,000-year glacial cycles. Nature. 454, 869-872.

Bintanja, R., van de Wal, R. S. W., Oerlemans, J., 2005. Modelled atmospheric temperatures and global sea levels over the past million years. Nature. 437, 125-128.

Boyle, E.A., 1983. Manganese carbonate overgrowths on foraminifera tests. Geochim. cosmochim. Acta 47, 1815–1819. doi:10.1016/0016-7037(83)90029-7.

Brierley, C. M., Fedorov, A. V., Liu, Z., Herbert, T. D., Lawrence, K. T., LaRiviere, J. P., 2009. Greatly Expanded Tropical Warm Pool and Weakened Hadley Circulation in the Early Pliocene. Science. 323, 1714-1718.

Clark, P. U., Archer, D., Pollard, D., Blum, J. D., Rial, J. A., Brovkin, V., Mix, A. C., Pisias, N. G., Roy, M., 2006. The middle Pleistocene transition: characteristics, mechanisms, and implications for long-term changes in atmospheric pCO2. Quaternary Science Reviews. 25, 3150-3184.

Cortese, G., R. Gersonde, C. D. Hillenbrand, and G. Kuhn (2004), Opal sedimentation shifts in the World Ocean over the last 15 Myr, *Earth And Planetary Science Letters*, *224*(3-4), 509-527, doi: 10.1016/j.epsl.2004.05.035.

de Boer, A. M., Toggweiler, J. R., Sigman, D. M., - Atlantic Dominance of the Meridional Overturning Circulation. - Journal of Physical Oceanography. - 435.

Elderfield, H., Ferretti, P., Greaves, M., Crowhurst, S., McCave, I. N., Hodell, D., Piotrowski, A. M., 2012. Evolution of Ocean Temperature and Ice Volume Through the Mid-Pleistocene Climate Transition. Science. 337, 704-709.
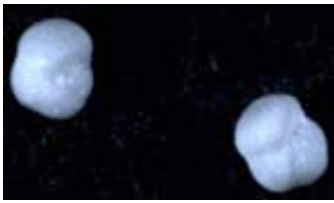
Etourneau, J., Martinez, P., Blanz, T., Schneider, R., 2009. Pliocene–Pleistocene variability of upwelling activity, productivity, and nutrient cycling in the Benguela region. Geology. 37, 871-874.

Ferguson, J.E., Henderson, G.M., Kucera, M., Rickaby, R.E.M., 2008. Systematic change of foraminiferal Mg/Ca ratios across a strong salinity gradient. Earth Planet. Sci. Lett. 265, 153–166. doi:10.1016/j.epsl.2007.10.011.

Flores, J. and Sierro, F. J., 2007. Pronounced mid-Pleistocene southward shift of the Polar Front in the Atlantic sector of the Southern Ocean. Deep Sea Research Part II: Topical Studies in Oceanography. 54, 2432-2442.

Fraile, I., Mulitza, S., Schulz, M., 2009. Modeling planktonic foraminiferal seasonality: Implications for sea-surface temperature reconstructions. Marine Micropaleontology. 72, 1-9.

Francois, R., M. A. Altabet, E. F. Yu, D. M. Sigman, M. P. Bacon, M. Frank, G. Bohrmann, G. Bareille, and L. D. Labeyrie, 1997. Contribution of Southern Ocean surface-water stratification to low atmospheric CO2 concentrations during the last glacial period, Nature, 389(6654), 929– 935, doi:10.1038.

Garcia, H. E., R. A. Locarnini, T. P. Boyer, and J. I. Antonov, 2010. World Ocean Atlas 2009, Volume 4: Nutrients (phosphate, nitrate, and silicate). S. Levitus, Ed., NOAA Atlas NESDIS 71, U.S. Government Printing Office, Washington, D.C., 398 pp.

Gersonde, R., Hodell, D. A., blum, P., et al., 1999. Leg 177 Summary: Southern Ocean Paleoceanography. Init. Repts. 177: College Station, (TX), .

Hodell, D. A. and Venz-Curtis, K. A., 2006. Late Neogene history of deepwater ventilation in the Southern Ocean. Geochemistry, Geophysics, Geosystems. 7, Q09001.

Hönisch, B., Hemming, N. G., Archer, D., Siddall, M., McManus, J. F., 2009. Atmospheric Carbon Dioxide Concentration Across the Mid-Pleistocene Transition. Science. 324, 1551-1554.

Iriondo, M., 2000. Patagonian dust in Antarctica. Quaternary international 68, 83–86.

Karas, C., Nurnberg, D., Gupta, A. K., Tiedemann, R., Mohan, K., Bickert, T., 2009. Mid-Pliocene climate change amplified by a switch in Indonesian subsurface throughflow. Nature Geosci. 2, 434-438.

Keeling, R. F. and Stephens, B. B., 2001. Antarctic sea ice and the control of Pleistocene climate instability. Paleoceanography. 16, 112-131.

Kemp, A. E. S., Grigorov, I., Pearce, R. B., Naveira Garabato, A. C., 2010. Migration of the Antarctic Polar Front through the mid-Pleistocene transition: evidence and climatic implications. Quaternary Science Reviews. 29, 1993-2009.

Kohfeld, K. E., Quere, C. L., Harrison, S. P., Anderson, R. F., 2005. Role of Marine Biology in Glacial-Interglacial CO2 Cycles. Science. 308, 74-78.

Lambert, F., B. Delmonte, J. R. Petit, M. Bigler, P. R. Kaufmann, M. A. Hutterli, T. F. Stocker, U. Ruth, J. P. Steffensen, and V. Maggi (2008), Dust-climate couplings over the past 800,000 years from the EPICA Dome C ice core, Nature, 452(7187), 616 – 619, doi:10.1038/nature06763.

LeGrande, A. N. and Schmidt, G. A., 2006. Global gridded data set of the oxygen isotopic composition in seawater. Geophysical Research Letters. 33, L12604.

Lisiecki, L. E. and Raymo, M. E., 2005. A Pliocene-Pleistocene stack of 57 globally distributed benthic δ18O records. Paleoceanography. 20, PA1003.

Locarnini, R. A., A. V. Mishonov, J. I. Antonov, T. P. Boyer, and H. E. Garcia, 2010. World Ocean Atlas 2009, Volume 1: Temperature. S. Levitus, Ed., NOAA Atlas NESDIS 68, U.S. Government Printing Office, Washington, D.C., 184 pp.

Marino, M., Maiorano, P., Lirer, F., Pelosi, N., 2009. Response of calcareous nannofossil assemblages to paleoenvironmental changes through the mid-Pleistocene revolution at Site 1090 (Southern Ocean). Palaeogeography, Palaeoclimatology, Palaeoecology. 280, 333-349.

Marinov, I., A. Gnanadesikan, J. R. Toggweiler, and J. L. Sarmiento (2006), The Southern Ocean biogeochemical divide, Nature, 441, 964 – 967, doi:10.1038/nature04883.

Martin, J. H., 1990. Glacial-Interglacial CO2 Change: The Iron Hypothesis. Paleoceanography. 5, 1-13.

Martínez-Garcia, A., A. Rosell-Mele´, W. Geibert, R. Gersonde, P. Masque´, V. Gaspari, and C. Barbante (2009), Links between iron supply, marine productivity, sea surface temperature, and CO2 over the last 1.1 Ma, Paleoceanography, 24, PA1207, doi:10.1029/2008PA001657.

Martinez-Garcia, A., Rosell-Mele, A., Jaccard, S. L., Geibert, W., Sigman, D. M., Haug, G. H., 2011. Southern Ocean dust-climate coupling over the past four million years. Nature. advance online publication, .

Martínez-Garcia, A., Rosell-Melé, A., McClymont, E. L., Gersonde, R., Haug, G. H., 2010. Subpolar Link to the Emergence of the Modern Equatorial Pacific Cold Tongue. Science. 328, 1550-1553.

Mashiotta, T. A., Lea, D. W., Spero, H. J., 1999. Glacial–interglacial changes in Subantarctic sea surface temperature and δ18O-water using foraminiferal Mg. Earth and Planetary Science Letters. 170, 417-432.

McClymont, E. L. and Rosell-Mele, A., 2005. Links between the onset of modern Walker circulation and the mid-Pleistocene climate transition. Geology. 33, 389-392.

Medina-Elizalde, M., Lea, D. W., Fantle, M. S., 2008. Implications of seawater Mg/Ca variability for Plio-Pleistocene tropical climate reconstruction. Earth and Planetary Science Letters. 269, 585-595.

Mortyn, P. G. and Charles, C. D., 2003a. Planktonic foraminiferal depth habitat and δ18O calibrations: Plankton tow results from the Atlantic sector of the Southern Ocean. Paleoceanography. 18, 1037.

Mortyn, P. G. and Charles, C. D., 2003b. Planktonic foraminiferal depth habitat and δ18O calibrations: Plankton tow results from the Atlantic sector of the Southern Ocean. Paleoceanography. 18, 1037.

Niebler, H.-S., Hubberten, H.-W., Gersonde, R., 1999. Oxygen isotope values of planktic foraminifera: a tool for the reconstruction of surfacewater stratification. In: Fischer, G., Wefer, G. (Eds.), Use of Proxies in Paleoceanography: Examples from the South Atlantic. Springer-Verlag, Berlin, pp. 165–189.

Park, J. and Maasch, K. A., 1993. Plio—Pleistocene Time Evolution of the 100-kyr Cycle in Marine Paleoclimate Records. J. Geophys. Res. 98, 447-461.

Ravelo, A. C. and Fairbanks, R. G., 1992. Oxygen Isotopic Composition of Multiple Species of Planktonic Foraminifera: Recorders of the Modern Photic Zone Temperature Gradient. Paleoceanography. 815, 7, 6. doi:10.1029/92PA02092.

Regenberg, M., Steph, S., Nürnberg, D., Tiedemann, R., Garbe-Schönberg, D., 2009a. Calibrating Mg/Ca ratios of multiple planktonic foraminiferal species with δ18O-calcification temperatures: Paleothermometry for the upper water column. Earth and Planetary Science Letters. 278, 324-336.

Ridgwell, A. J. and - Watson, A. J., 2002. Feedback between aeolian dust, climate, and atmospheric CO2 in glacial time. Paleoceanography. 1059, 11PP. doi:10.1029/2001PA000729.

Rintoul, S. R., C. Hughes and D. Olbers, 2001. The Antarctic Circumpolar Current System. In:*Ocean Circulation and Climate*, G. Siedler, J. Church, and J. Gould, (Eds.), Academic Press, 271-302.

Rodríguez-Sanz, L., Graham Mortyn, P., Martínez-Garcia, A., Rosell-Melé, A., Hall, I. R., 2012. Glacial Southern Ocean freshening at the onset of the Middle Pleistocene Climate Transition. Earth and Planetary Science Letters. 345–348, 194-202.

Sarmiento, J. L., Gruber, N., Brzezinski, M. A., Dunne, J. P., 2004. High-latitude controls of thermocline nutrients and low latitude biological productivity. Nature. 427, 56-60.

Shackleton, N.J., 1974. Attainment of isotopic equilibrium between ocean water and the benthonic foraminifera genus Uvigerina: isotopic changes in the ocean during the last glacial. Cent. Nat. Rech. Sci. Colloq. Int. 219, 203–209.

Sigman, D. M., Hain, M. P., Haug, G. H., 2010. The polar ocean and glacial cycles in atmospheric CO2 concentration. Nature. 466, 47-55.

Steph, S., Regenberg, M., Tiedemann, R., Mulitza, S., Nürnberg, D., 2009. Stable isotopes of planktonic foraminifera from tropical Atlantic/Caribbean core-tops: Implications for reconstructing upper ocean stratification. Marine Micropaleontology. 71, 1-19.

Stephens, B. B. and Keeling, R. F., 2000. The influence of Antarctic sea ice on glacial-interglacial CO 2 variations. Nature. 404, 171-174.

Tedesco, K., Thunell, R., Astor, Y., Muller-Karger, F., 2007. The oxygen isotope composition of planktonic foraminifera from the Cariaco Basin, Venezuela: Seasonal and interannual variations. Marine Micropaleontology. 62, 180-193.

Toggweiler, J. R. and Russell, J., 2008. Ocean circulation in a warming climate. Nature. 451, 286-288.

Toggweiler, J. R., Russell, J. L., Carson, S. R., 2006. Midlatitude westerlies, atmospheric CO2, and climate change during the ice ages. Paleoceanography. 21, PA2005.

van de Wal, R. S. W. and Bintanja, R., 2009. Changes in Temperature, Ice, and CO_2 During the Mid-Pleistocene Transition. Science published online.

Venz, K. A. and Hodell, D. A., 2002. New evidence for changes in Plio–Pleistocene deep water circulation from Southern Ocean ODP Leg 177 Site 1090. Palaeogeography, Palaeoclimatology, Palaeoecology. 182, 197-220.

Wara, M. W., Ravelo, A. C., Delaney, M. L., 2005. Permanent El Niño-Like Conditions During the Pliocene Warm Period. Science. 309, 758-761.

Watson, A. J., Bakker, D. C. E., Ridgwell, A. J., Boyd, P. W., Law, C. S., 2000. Effect of iron supply on Southern Ocean CO2 uptake and implications for glacial atmospheric CO2. Nature. 407, 730-733.

4.7. <u>Supplementary information</u>

Sample	Max diam (μm)	Spiral height (µm)	ratio d/h
1	450,38	294,19	1,53
2	449,73	335,23	1,34
3	485,52	349,36	1,39
4	488,11	348,36	1,40
5	515,97	344,06	1,50
6	449,29	337,58	1,33
7	475,94	320,07	1,49
8	476,11	337,64	1,41
9	486,02	310,20	1,57
10	449,71	320,23	1,40
11	475,14	343,22	1,38
12	459,64	298,33	1,54
13	494,89	348,21	1,42
14	474,24	344,37	1,38
15	494,84	337,60	1,47

Figure S1. We had difficulties for the deeper dwelling foraminiferal species identification. Hence we have taken images in a Scanning Electronic Microscope and carried out morphometric analyses of the species (above). All the species had more than 3.5 chambers in agreement with *G. crassaformis*.
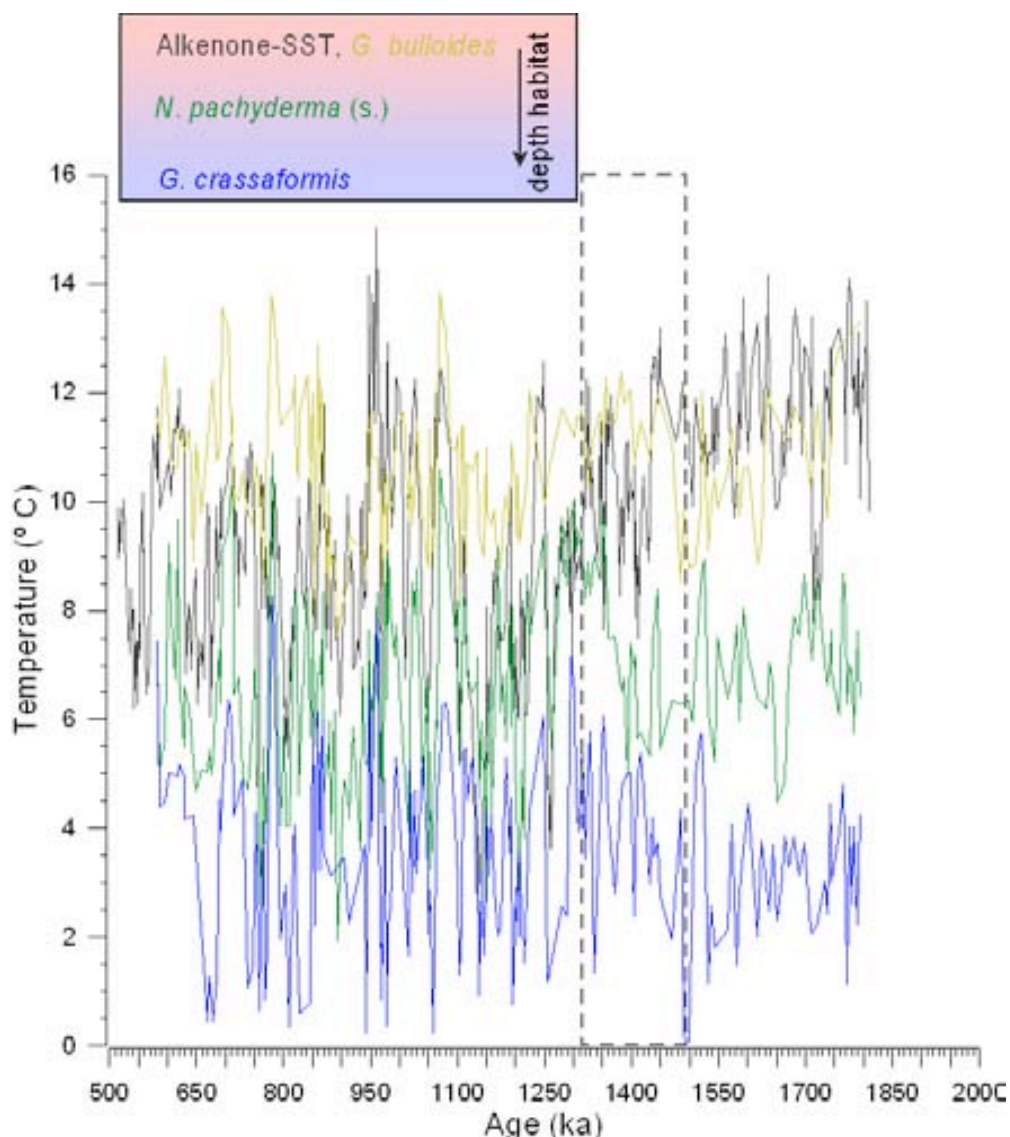
Figure S2. Comparison of aal the temperature reconstruccions performed at the Site 1090; Alkenone-based SST (U^{K}_{37}) reconstruction at ODP Site 1090 (grey; *Martínez-Garcia et al., 2010*) and Mg/Ca-derived SST at Site 1090 obtained from *G. bulloides* (yellow). (c) Mg/Ca-derived temperature from *N. pachyderma* (s.) (green, *Rodríguez-Sanz et al., 2012*) and *G. crassaformis* (blue). Boxed dashed area highlights the progressive shoaling of the thermocline (1500-1300 ka), the position of which persisted throughout the MPT.

CHAPTER 5

Salinity increases in the southern California Current in tandem with Northern Hemisphere cold events

Abstract

Increases of deep water formation in the Pacific Ocean have been proposed as a mechanism to partially maintain the heat and salt transport to the Northern Hemisphere (NH) during periods where the Atlantic Meridional Overturning Circulation (AMOC) was weakened, that is, the Younger Dryas (YD) and stadial Heinrich 1 (stadial-H1). Millennial-scale $\delta^{18}O_{SW-IVC}$ (a proxy for salinity changes) changes in the tropical Pacific Ocean point to salinity increases in tandem with YD and stadial-H1. However the causes have been mainly attributed to local changes in the evaporation-precipitation processes in the tropical Pacific Ocean, rather than regional salinity variations. *Globigerinoides ruber* (sensu lato) and (sensu stricto)- sea surface temperature (SST) and $\delta^{18}O_{SW-IVC}$ reconstructions from a core located in the southern part of the California Current (CC) at 25ºN allowed us to understand salinity changes in the Pacific Ocean beyond the tropical sector of this basin. Our *G.ruber*-$\delta^{18}O_{SW-IVC}$ record shows pronounced increases (~0.7‰) during YD and stadial-H1 in concordance with tropical-$\delta^{18}O_{SW-IVC}$ reconstructions. We propose that the millennial-scale $\delta^{18}O_{SW-IVC}$ profiles in the tropics and at 25ºN in the Pacific Ocean are better explained by a combined effect of weakening local processes that relatively decrease salinity (such as, weakening the CC at 25ºN) and overall saltier conditions in the Pacific Ocean during those events. Our SST profile supports this view; in that, it suggests the weakening of the CC during the YD and stadial-H1 and relative warming of the region during NH-cold events. Although we cannot assess if these salinity increases drove deep-water formation in the Pacific Ocean, our results provide evidence of the relative warming and synchronous salinity increases during NH-cold events in the tropical and sub-tropical ocean basin. This agrees well with the notion of increasing heat and salt transport to the ocean basin as a response of AMOC collapse proposed by different climatic models.

5.1. <u>Introduction</u>

Termination 1 (T1) was the most recent period of large scale and high amplitude warming that the Earth has undergone before entering into the present interglacial period (Holocene). This warming is characteristically different in each hemisphere; periods of rapid cooling in the Northern Hemisphere (NH), such as the Younger Dryas (YD, ~12 ka *(Denton et al., 2010)* and stadial Heinrich 1 (stadial-H1; *Denton et al., 2010*), were paralleled by warming in the Southern Hemisphere (SH) leading to the concept of the "the bipolar see-saw" *(Broecker, 1998; Barker et al., 2009)*. For the "bipolar see-saw" hypothesis the weakening of the Atlantic Meridional Overturning Circulation (AMOC) during the YD and stadial-H1 *(McManus et al., 2004)* is associated with reduced heat transport to the high latitudes of the NH, while increasing it to the SH thereby leading to a gradual warming, due to the heat capacity of the Southern Ocean. These two NH cold stadials were interrupted by a rapid warming period known as the Bölling-Allerod (B-A, ~14.5 ka; *Liu et al., 2009*) during which the AMOC resumed while the SH showed signs of cooling (Antarctic Cold Reversal, ACR). In addition, the SH gradual warming, associated to the YD and stadial-H1, apparently allowed for some melting of the Antarctic ice sheet, leading to an increase in upwelling *(Anderson et al., 2009)* of old, deep water masses *(Skinner et al., 2010)* around the SH probably aided by a southern poleward migration of the SH westerlies. This allowed the outgassing of respired CO_2 from the deep ocean, increasing atmospheric CO_2 *(EPICA, 2004)* and therefore feeding back on the warming during the deglaciation (cfr. *Toggweiler and Russell, 2008*).

Model and proxy data studies that have attempted to understand the response of the Pacific Ocean to the collapse of the NADW suggest deep water formation in the western North Pacific *(Okazaki et al., 2005; Okazaki et al., 2010)* and hence the strengthening of the Pacific Meridional Overturning Circulation (PMOC) *(e.g. Saenko et al., 2004; Timmermann et al., 2005; Okazaki et al., 2010; Chikamoto, et al. 2012)*. Saenko *et al.,* (2004) suggest that, throughout an Atlantic-Pacific seesaw mechanism, periods of freshwater inputs into the North Atlantic might have resulted in the increase of heat and salt transport to the Pacific Ocean with the Southern Ocean acting as a pivot. Then, when salinity in the North Pacific Ocean passed a threshold the conditions were apparently suitable for the formation of relatively deep-water masses in the northern

part of the basin, maintaining the heat transport to high latitudes. Reconstructions of $\delta^{18}O_{SW-IVC}$ (a proxy for local salinity changes *(LeGrande and Schmidt, 2006)* in the Eastern Equatorial Pacific (EEP; *Benway et al.,2006; Leduc et al., 2007; Pena, et al., 2008*) and Western Equatorial Pacific (WEP; *Rosenthal et al., 2003; Mohtadi, et al. 2010*) indeed provided evidence of saltier conditions during YD and stadial-H1. However, these studies invoked the position of the Intertropical Convergence Zone (ITCZ) and its link to moisture transport across the Atlantic to the Pacific Ocean, and to the Eastern Asian Monsoon to explain fluctuations in the tropical Pacific $\delta^{18}O_{SW-IVC}$. This then implies that the observed tropical Pacific salinity anomalies during NH-cold events were mostly restricted to those regions of the basin that were somehow affected by the ITCZ, and not to regional changes of salinity. Here we provide new insights on the salinity changes in a core located a 25ºN North-East Pacific (NEP) where the influence of the ITCZ is negligible. Our sea surface temperature (SST) and $\delta^{18}O_{SW-IVC}$ reconstructions, using separately the two morphotypes (sensu stricto and sensu lato) of *Globigerinoide ruber* white, spanning T1 and into the mid-Holocene (19 to 3 ka) suggest that indeed salinity changes at that latitude paralleled those in the EEP and WEP.

5.2. <u>Material and Methods</u>

5.2.1 Sediment core location and chronology

The core MD02-2505 was retrieved from the San Lázaro Basin (SLB) at 25ºN, 112ºW from 535m depth. It is located at the southernmost part of the CCS *(Esparza-Alvarez et al., 2007)* where it is mainly bathed by the fresh, cold and nutrient-rich California Current (CC). The CC is strengthened during boreal summer and spring when the North Pacific High (NPH) migrates northward (e.g. *Cheshire et al., 2005*) and drives the meridional winds along the western North American coast. During winter the southward movement of the NPH, that is winter and fall and/or during El Niño events, leads to the subsidence of the winds along the coast and allows for the SLB to be bathed by the warmer, saltier and more nutrient-poor tropical to subtropical water masses (Fig. 1; *(Durazo and Baumgartner, 2002)*. The CCS is one of the largest upwelling regions in the ocean where subsurface subtropical water masses (California Undercurrent, CU),

which result from a mixture with water masses from southern higher latitudes, upwell. The upwelling of this relatively salty and high nutrient CU water mass, fueled by the prevailing northwesterly wind, favors the relatively high primary productivity in the SLB, contributing to the high sedimentation rates observed in the basin (1m/ky). Sediments retrieved from the SLB feature excellent carbonate preservation *(Marchitto et al., 2010)* and laminated sequences that suggest the absence of any bioturbation of the sediment on the sea floor *(Esparza-Alvarez et al., 2007; van Geen et al., 2003)*. All the characteristics above collectively make the SLB ideal to study variations of the CCS at high-resolution timescales, allowing us to effectively compare their records with other high resolution ones in the NEP. The MD02-2505 age model was based on 11 radiocarbon measurements on planktonic foraminifera (Table S1 and Figure S1), which were recalibrated using the program Calib 6.0html and the Marine09 calibration curve using a reservoir age correction (ΔR) of 200 ±100 *(Hughen et al., 2004)*. The age model reveals that sediment levels ranging from 295 to 2112 cm depth (used in this study) cover the T1 into the early Holocene from 19.9 to 3 ka. Sampling has been done every 5 cm, yielding a temporal resolution up to ~50 yr.

5.2.2. *Globigerinoides ruber* Mg/Ca reconstructions

Overall, abundances of the planktonic foraminiferal species selected for this study were very variable, ranging from periods of moderate abundance to periods of nonappearance of the species, hindering the generation of continuous Mg/Ca and $\delta^{18}O_C$ records. We have established a threshold of 15 specimens for any determination, above which samples would go through paired Mg/Ca-$\delta^{18}O_C$ measurements. Below that threshold samples were analyzed either for Mg/Ca or $\delta^{18}O_C$, depending on the resolution of the records that were being generated. For this study we have analyzed separately the two morphotypes of the surface-dwelling, symbiont-bearing species *G. ruber* white, sensu lato (s.l.) and sensu stricto (s.s). *G.ruber* (s.s) and (s.l) were picked from the size fraction 250-350 μm, and gently crushed between two glass slides that were previously cleaned with methanol. After crushing, samples were split into two (when it was possible) for Mg/Ca and $\delta^{18}O_C$ cleaning and then analyzed; otherwise samples were entirely cleaned and analyzed following only one of the two procedures.
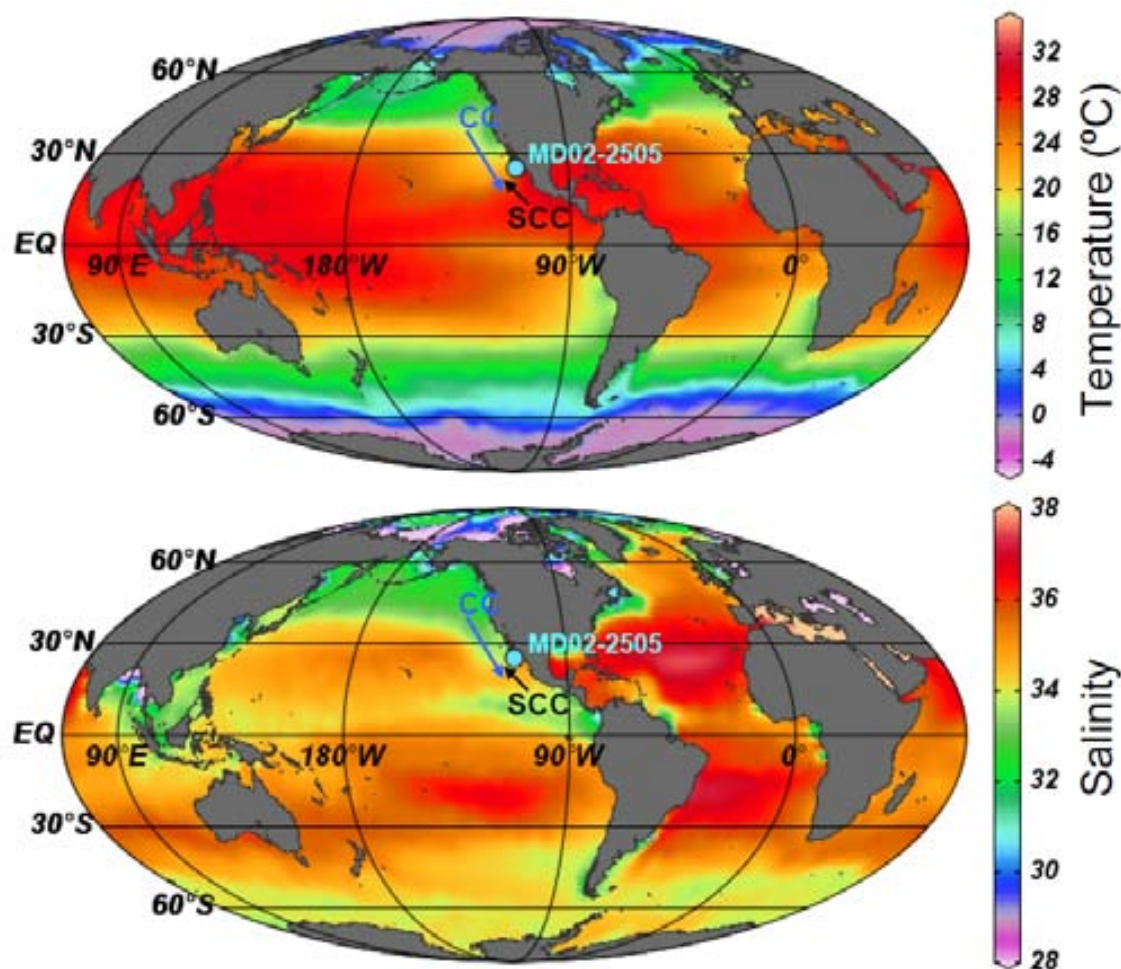
Figure 5.1. Location of the MD05-2505 (light blue dot) in the Pacific Ocean (25ºN, 112ºW, water depth 535 m). World Ocean Atlas 2005 (WOA05) modern summer sea surface (a) temperature and (b) salinity gradients. Blue arrow denotes the flow of the California Current (CC), while the black arrow shows the course of the Southern California Countercurrent (SCC).

For Mg/Ca cleaning we followed the analytical procedure explained in Chapter 2 section 2.2.1. Except for some Fe/Mg values (22 out of 175 in the *G. ruber* (s.l.) record), all the ratios that we have used for testing potential contamination phases yielded values that were well below the proposed thresholds *(Boyle, 1983; Barker et al., 2003; Ferguson et al., 2008).* The lack of correlation between Fe/Mg and Mg/Ca ratios (r^2=0.1) excludes the possibility of any bias introduced by clay contamination. The relative standard deviation was on average 2% (N=45). A commonly used limestone standard (ECRM752–1) with a specified Mg/Ca of 3.75 mmol.mol^{-1} *(Greaves et al., 2008)* was also analyzed, yielding values of 3.70±0.09 mmol.mol^{-1}. The calibration used to convert Mg/Ca into temperature was *(Dekens et al., 2002),* which has been shown to

faithfully reproduce summer temperatures when using *G. ruber* white morphotypes to reconstruct Mg/Ca-based temperatures *(Mortyn et al., 2011)*. A full error propagation exercise suggests uncertainties of ±1°C associated with our sea surface temperature (SST) reconstructions.

5.2.3. Calcite stable oxygen isotope ($\delta^{18}O_C$) measurements and seawater oxygen isotope ($\delta^{18}O_{SW}$) calculation

For $\delta^{18}O$ analyses on foraminiferal calcite ($\delta^{18}O_C$) we followed the cleaning procedure and sample preparation described in chapter 2 section 2.2.2. Analyses of the samples were carried out at the Autonomous University of Barcelona. In order to generate the seawater $\delta^{18}O$ composition ($\delta^{18}O_{SW}$) record based on the paired Mg/Ca-$\delta^{18}O_C$ measurements we used Bemis et al., 1998 (T= 16.5 − 4.80*($\delta^{18}O_C$ -$\delta^{18}O_{SW}$)). We selected this paleotemperature equation based on the proximity of that calibration study to our study region. We used the sea level reconstruction of *(Stanford et al., 2011)* to remove the ice volume ($\delta^{18}O_{SW-IVC}$) component from the calculated $\delta^{18}O_{SW}$. We linearly interpolated the Stanford *et al.*, 2011 record to the same temporal resolution than our records and then we subtracted from the $\delta^{18}O_{SW}$ profile. An error propagation exercise yielded 1σ uncertainties for our data of ±0.3‰.

5.3. Results

Figure 2 displays Greenland (Fig. 2a) and Antarctic (Fig. 2b) ice core data compared to the Mg/Ca and $\delta^{18}O_C$ records from the NEP inferred from each *G. ruber* morphotype (Fig. 2c-e). Both *G. ruber* (s.s.) and (s.l.) $\delta^{18}O_C$ (Fig. 2c) reconstructions show an amplitude change of ~1.6‰ toward lighter values across T1. Overall, the *G. ruber* (s.s.) profile records lighter values than *G. ruber* (s.l.), suggesting a shallower depth habitat for the former in agreement with modern observations (e.g., *Wang, 2000; Steinke et al., 2005*). The lack of *G. ruber* (s.s.) species in the sediment during the NH stadial-H1 and across T1 makes it difficult to generate a continuous SST record based on this morphotype (Fig. 2d). On the other hand *G. ruber* (s.l.), although less abundant during the Holocene compared to *G. ruber* (s.s.), was abundant enough to generate a complete SST record (Fig. 2e). The new *G. ruber* (s.l.)-SST profile features a progressive warming (~2±1°C) during T1 which was interrupted at ~12 ka BP by a subtle cooling correlative to the ACR event in Antarctica.
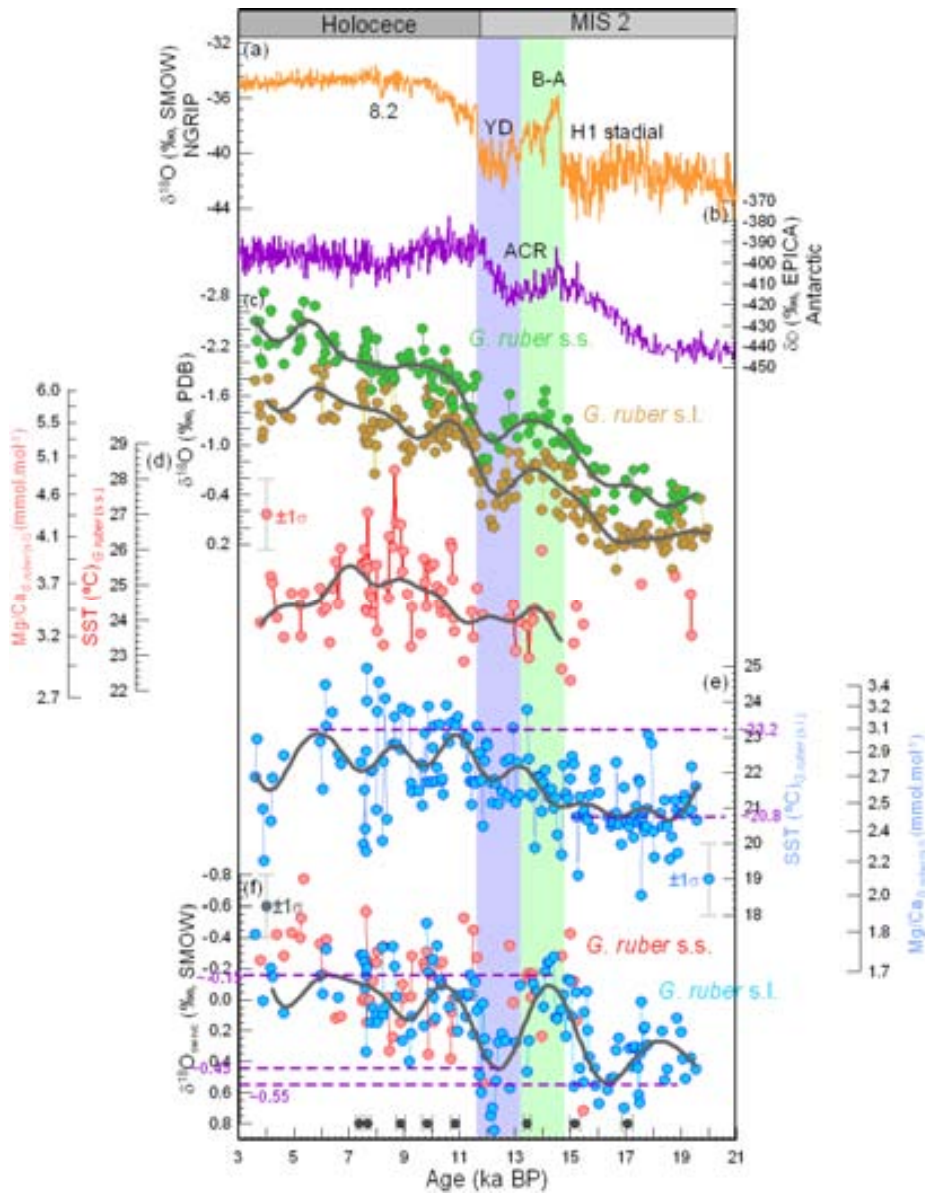
Figure 5.2. (a.) $\delta^{18}O$ in the NGRIP ice core record of Greenland *(NGRIP members, 2004)*. (b) Deuterium (δD) record from the EPICA ice core *(EPICA, 2004)*. Records from core MD05-2505 inferred using *G. ruber* (s.s) and (s.l) morphotypes: (c) $\delta^{18}Oc$, green and gold respectively, (d) *G. ruber* (s.s) Mg/Ca-based SST (red), (e) *G. ruber* (s.l) Mg/Ca-based SST (blue). (f) Local $\delta^{18}O_{SW-IVC}$ changes at MD05-2505, obtained by removing the ice-volume (mean ocean $\delta^{18}O_{SW}$; *Standford et al., 2010*) and calcification temperature from the $\delta^{18}O_C$ measured on *G. ruber* (s.s.) and (s.l.); red and blue respectively. Smoothing using a low pass filter with a cutoff frequency of 0.1Hz is shown in gray in records from c to f to highlight the main trends. Light purple and green vertical boxed areas denote the Younger Dryas (YD) stadial and Bølling-Allerød (B-A) interestadial in the Northern Hemisphere, respectively.

$\delta^{18}O_{SW\text{-}IVC}$ records based on *G. ruber* (s.s.) and (s.l.) show similar patterns and amplitude changes during the end of T1 and into the early Holocene (Fig. 2f). Since we know that $\delta^{18}O_C$ is a mixed signal between the temperature and $\delta^{18}O_{SW}$ of the water mass where foraminifers calcified, the observed consistency between the $\delta^{18}O_{SW\text{-}IVC}$ records might suggest that differences in morphotype abundances are mainly controlled by temperature preferences in the water column. The *G. ruber*-$\delta^{18}O_{SW\text{-}IVC}$ (Fig. 2f) profile displays a progressive change toward lighter values (freshening) across the time span of this study. It also shows a pattern of millennial scale variability that partly resembles the Greenland ice core (Fig. 2a), suggesting a change of ~0.6-0.7‰ toward heavier values (salinity increases) roughly coinciding with NH-cold events (YD and stadial-H1).

5.4. **Discussion**

Our SST-*G.ruber* (s.l.) time series from the SLB suggests that the southern part of the CCS warmed gradually, ~1.5-2ºC, across the T1 (Fig. 2e). In contrast, an alkenone-based SST record from a northern position of the CCS, at 34ºN (ODP 1016, *(Yamamoto et al., 2007)* shows larger amplitude changes across T1 (~6ºC). This difference between the SST profile trends resulted in a larger north to south gradient (~10ºC) across T1 than during the Holocene when the gradient was smaller (~7˚C; Fig. 3a). Since alkenone producers and *G. ruber* fluxes have both been shown to occur during summer in the region *(Thunell et al., 1983)*, the differences observed should then be due to factors other than seasonality. The resolution of the alkenone record does not allow us to further infer millennial scale SST gradient variability during the summer season across T1. However, *Globigerina bulloides* SST records from ODP 1017 (34ºN; *Pak et al., 2012*) and from the SLB (25ºN, *Marchitto et al., 2010; Tello et al., 2009*) allow understanding millennial-scale variations in the north to south SST gradient in the CCS during the spring season, when the CC is still intensified *(Durazo and Baumgartner. 2002)*. The spring SST gradient suggests similar features than the summer counterpart, that is, different trends across the T1 and larger north to south SST gradient in the CCS but only during NH-cold periods (Fig. 3b). Modern ocean observations have shown that the intensification of the CC happens during spring and summer seasons due to the northward movement of the NPH *(Espinosa-Carreon et al., 2004)*. This, in combination

with upwelling processes that are triggered by the northwesterly winds (*Linacre et al., 2010)*, buffers the SST off the coast of California during the year's warmest seasons (spring and summer) and hence equals the latitudinal SST gradient in the CCS. Accordingly, the observed increase in the north to south SST-CCS gradient suggested by the SST reconstructions (Fig. 3a-b) during T1, particularly during NH-cold stages (Fig. 3b), points to a weaker CC and to an overall progressive intensification of the current into the Holocene. The weakening of the CC has always been associated with an increase in the advection of warm, nutrient-poor tropical water masses to the core site (e.g. *Herbert et al., 2001*). Opal percentages in the Guaymas Basin in the Gulf of California *(McClymont et al., 2012)* agree well with increasing the advection of tropical waters during YD and stadial-H1 since it shows nutrient and silica availability in the region during most of the time span except for those periods. In this sense, decreases in the influence of the CC in the southern part of the CCS might have reduced its temperature buffering effect in the region and possibly allowed the advance of tropical water masses during YD and stadial-H1. This therefore facilitated the relative warming of the SLB compared to the SST at 34ºN across T1, and especially during NH-cold stages in the seasons when the CC intensity likely increased.
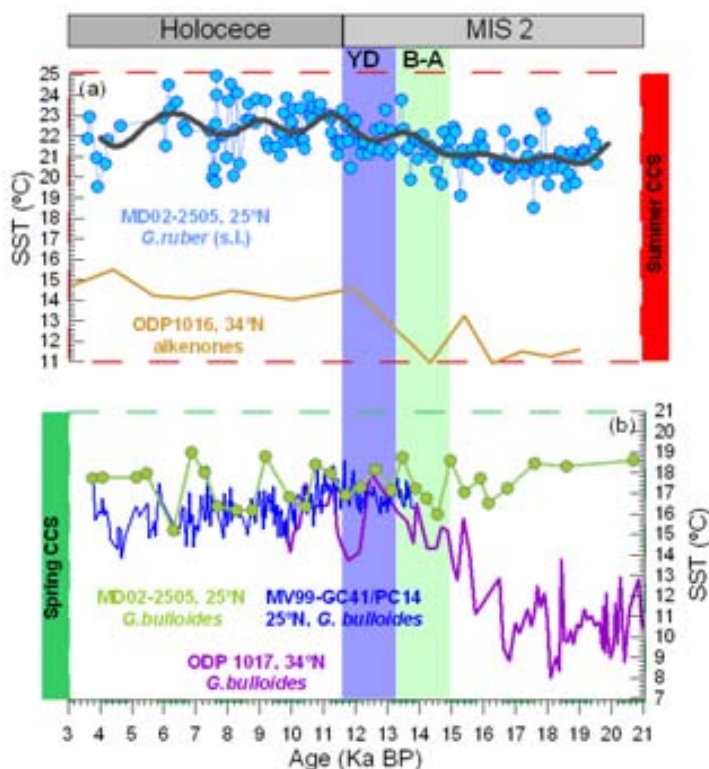

Figure 5.3. Comparison of the North to South SST gradient in the California Current System (CCS) during seasons when the California Current (CC) intensifies; that is, summer (a); *G. ruber* (s.l)- (25ºN; this study) and alkenone-SST (34ºN; Yamamoto et al., 2005) and spring (b); *G. bulloides*-SSTs at 25ºN (Tello-Ramia, 2009; Marchitto et al., 2010) and 34ºN (Pak et al., 2012).

Developments of the *G.ruber*-$\delta^{18}O_{SW\text{-}IVC}$ (Fig. 2f and 4c) record further agree with a gradual intensification of the fresh CC toward the Holocene and additional weakening of the current during YD and stadial-H1, as it suggests an overall slow change toward fresher conditions from T1 into the Holocene and clear increases of *G.ruber*-$\delta^{18}O_{SW\text{-}IVC}$ (relatively salty) during NH-cold events. This pattern of variability agrees well with other reconstructions from the tropical Pacific *(Rosenthal et al., 2003; Benway et al., 2006; Leduc et al., 2007; Pena et al., 2008)*, especially those from the EEP *(Benway et al., 2006; Leduc et al., 2007)*, in that the amplitude changes (~0.5-0.7‰) observed during YD and stadial-H1 are similar to those in the SLB (~0.6-0.7‰). Some hypotheses to explain $\delta^{18}O_{SW\text{-}IVC}$ fluctuations in the EEP profiles invoked the influence of the ITCZ position in the exchange of moisture from the Atlantic to the Pacific Ocean (e.g. Leduc et al., 2007). Accordingly, NH-cold (warm) events triggered a southward (northward) displacement of the ITCZ, reducing (increasing) humidity transport between the ocean basins, hence increasing (decreasing) salinity in the EEP. Indeed, similarities between $\delta^{18}O_{SW\text{-}IVC}$ reconstructions (Fig. 4b-d) and the $\delta^{18}O$ record from the Botuverá stalagmite in the South of Brazil (Fig. 43; *Wang et al., 2007*), i.e., the position of the ITCZ, are irrefutable. These observations clearly show the importance of the ITCZ position as a key process in the observed changes in the EEP Pacific $\delta^{18}O_{SW\text{-}IVC}$ records. We infer that, as in the tropical Pacific, the millennial scale $\delta^{18}O_{SW\text{-}IVC}$ changes in the SLB were also a consequence of weakening a process that, when operating, relatively decreased the surface salinity by freshening the region, that is, minor influence of the CC during NH-cold events.

We noticed, however, that a positive ~0.7‰ *G.ruber*-$\delta^{18}O_{SW\text{-}IVC}$ amplitude change in the CCS during YD and stadial-H1 corresponds to a ~2 psu increase in the region (when using Spero and Lea, 1996 $\delta^{18}O_{SW\text{-}IVC}$-S equation), which is considerably high to be only triggered by CC weakening *(Schneider et al., 2005)*. Hence, we do not exclude that a mechanism other than the CC influence could have been at play in the observed $\delta^{18}O_{SW\text{-}IVC}$ millennial scale changes in the southern CCS during the NH-cold events. Furthermore, synchronous $\delta^{18}O_{SW\text{-}IVC}$ millennial scale changes in the EEP *(Benway et al., 2006; Leduc et al., 2007; Pena et al., 2008)*, north-equatorial western Pacific (e.g. Fig. 4d; *Rosenthal et al., 2003; Steinke et al., 2008; Mohtadi et al., 2010*) and CCS at 25ºN further support this observation. We speculate that the surface/subsurface water

masses advected to the north tropical Pacific Ocean were perhaps relatively salty during NH-cold stages than for the rest of the deglaciation. Thereby, the weakening of local processes that relatively counteract salinity increases in those regions of the Pacific Ocean, such as the ITCZ (tropical), CC intensity (CCS), Asian Monsoon (west-tropical), etc., could have simply acted as a positive feedback to amplify that signal.
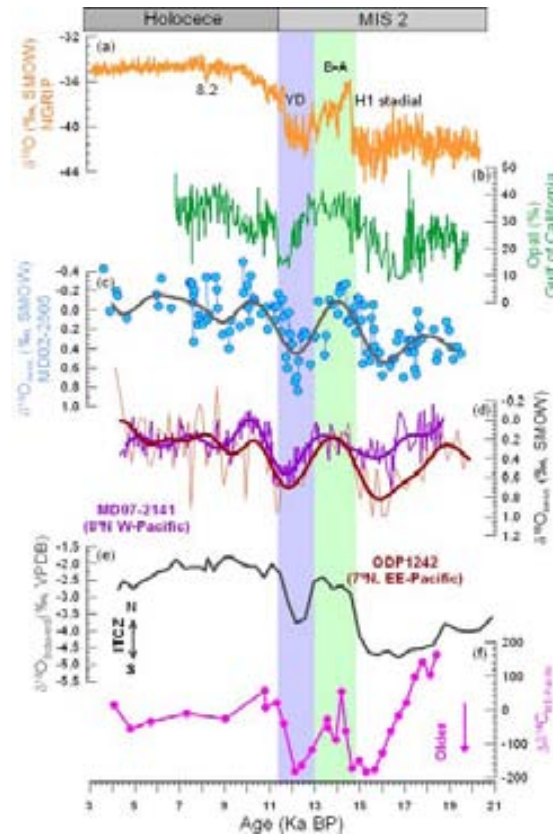
Figure 5.4. Comparison of *G. ruber* (s.l.) records from MD05-2505 with a set of SST and $\delta^{18}O_{SW-IVC}$ reconstructions performed in the Pacific Ocean. (a) $\delta^{18}O$ in the NGRIP ice core record of Greenland is shown as reference (NGRIP members, 2004). (b) Opal percentage from the Guaymas Basin in the Gulf of California (MD02-2515; *McClymont et al., 2012*). (c) $\delta^{18}O_{SW-IVC}$ reconstruction from core MD05-2505 $\delta^{18}O_{SW-IVC}$. (d) Tropical Pacific $\delta^{18}O_{SW-IVC}$ reconstructions from MD97-2141 (purple; *Rosenthal et al., 2003*) and ODP 1242 (dark red, *Benway et al., 2006*). (e) $\delta^{18}O$ record from the Botuverá stalagmite in the South of Brazil (Fig. 43; *Wang et al., 2007*). (f) $\Delta\delta^{14}C$ in the NE-Pacific across T1 *(Marchitto et al., 2007)*. Smoothing using a low pass filter with a cutoff frequency of 0.1Hz is shown in gray in records c-d to highlight the main trends. Purple and green vertical boxed areas denote the Younger Dryas (YD) stadial and Bølling-Allerød (B-A) interstadial in the Northern Hemisphere, respectively.

Radiocarbon records from intermediate water masses at the NEP (Fig. 4f; *Marchitto et al., 2007*) suggest the arrival of very old water masses with a Southern Ocean origin *(Basak et al., 2010)* during NH-cold events coinciding with saltier upper tropical Pacific Ocean conditions. Further evidence of very old intermediate water masses in the EEP and West Pacific have been provided by Stott *et al.,* 2009 and Sikes *et al.,* 2000 respectively. This suggests simultaneous changes in the characteristics of the upper and intermediate water masses in the tropical-subtropical Pacific Ocean. In the modern ocean, water masses formed in the Subantarctic and Polar Zone, the SAMW and AAIW *(Rintoul et al., 2001)*, of the Southern Ocean are known to feed the Pacific Ocean interior (e.g. *Spero and Lea, 2002*). In this sense, synchronous changes in the upper and intermediate Pacific water masses properties suggest major variations in the features of the Southern Ocean water masses during periods of weakening of the NADW *(McManus et al., 2004)*. Modelling studies that attempted to understand the response of the Pacific Ocean to the AMOC weakening further support our inferences on the overall relatively salty conditions in the Pacific Ocean (*Saenko et al., 2004; Timmermann et al., 2005)* through circulation and atmospheric readjustments with the Southern Ocean acting as the pivot *(Saenko et al., 2004)*.

Hence, the relative warming of the southern part of the CCS (Fig. 3a-b) compared to the northern counterpart suggests the weakening of the cold and fresh CC during YD and stadial-H1. We speculate that the combination of overall saltier conditions in the Pacific Ocean and decreased influence of the fresh CC in the SLB accounted for the 0.6-0.7‰ *G.ruber*-$\delta^{18}O_{SW-IVC}$ change observed during those NH-cold events. Similarly, changes in the position of the ITCZ *(Wang et al., 2007)* acted to amplify the Pacific Ocean salinity anomaly, resulting in synchronous salinity increases in the tropical Pacific Ocean (e.g. *Rosenthal et al., 2003; Benway et al., 2006*) and at 25ºN (this study) during NH-cold events. Although we cannot assess whether these salinity increases were sufficient to activate PMOC during AMOC weakening, our results provide evidence that, beyond the equatorial Pacific, the salinity anomaly was extended to 25ºN in the NEP during YD and stadial-H1. In addition, simultaneous variations in upper Pacific Ocean salinity and intermediate water masses changes *(Sakes et al., 2000; Marchitto et al., 2007; Stott et al., 2009)*, of southern latitude origin *(Basak et al., 2010)* during YD and stadial-H1, point to major oceanic water masses characteristic changes in the Southern Ocean. All these observations collectively are in concordance with model

studies that suggest Pacific Ocean salinity increases during periods of weakening of the AMOC due to wind and thermocline processes that involved the Southern Ocean *(Timmermann et al., 2005).*

5.5. <u>Conclusion</u>

Comparison between our summer *G. ruber*-SST record with an alkenone-SST reconstruction from a core located at 34ºN *(Yamamoto et al., 2007)* suggests different warming trends across the deglaciation resulting in a larger SST gradient across the T1. The same North to South comparison in the CCS, but using SST reconstructions based on the spring *G. bulloides* species *(Tello-Ramia, 2009; Marchitto et al., 2010; Pak et al., 2012)*, suggests that the gradient is especially intensified during YD and stadial-H1. In the modern ocean the CC intensifies during summer and spring as a consequence of the northward position of the NPH (e.g. *Hendy et al., 2010*). Therefore, we interpret our results as a weakening of the CC during T1 and especially NH-cold events across the deglaciation. Our new *G. ruber*-$\delta^{18}O_{SW-IVC}$ record shows increases (relatively salty conditions) in tandem with YD and stadial-H1 when the CC was apparently weakened further supporting that concept. We also observed a large *G.ruber*-$\delta^{18}O_{SW-IVC}$ amplitude change during those events, up to 0.7‰ (that is 2 psu), and clear similarities with $\delta^{18}O_{SW-IVC}$ reconstructions from the EEP and WEP. Based on this, we do not exclude that local processes that modulate salinity in those areas (such as ITCZ position, CC intensity, Asian Monsoon, etc.) were acting in concert with regional ones (e.g. overall saltier conditions in the ocean basin) to explain the observed millennial-scale salinity changes in the Pacific Ocean. Our results agree well with model studies *(Saenko et al., 2004; Timmermann et al., 2005)* that suggest increases in Pacific Ocean salinity in response to the weakening of the AMOC via processes that involved the Southern Ocean.

5.6. References

Anderson, R. F., Ali, S., Bradtmiller, L. I., Nielsen, S. H. H., Fleisher, M. Q., Anderson, B. E., Burckle, L. H., 2009. Wind-Driven Upwelling in the Southern Ocean and the Deglacial Rise in Atmospheric CO2. Science. 323, 1443-1448.

Barker, S., Diz, P., Vautravers, M. J., Pike, J., Knorr, G., Hall, I. R., Broecker, W. S., 2009. Interhemispheric Atlantic seesaw response during the last deglaciation. Nature. 457, 1097-1102.

Basak, C., Martin, E. E., Horikawa, K., Marchitto, T. M., 2010. Southern Ocean source of 14C-depleted carbon in the North Pacific Ocean during the last deglaciation, Nature Geoscience, 3, 770-773.

Benway, H. M., Mix, A. C., Haley, B. A., Klinkhammer, G. P., 2006. Eastern Pacific Warm Pool paleosalinity and climate variability: 0–30 kyr. Paleoceanography. PA3008.

Boyle, E.A., 1983. Manganese carbonate overgrowths on foraminifera tests. Geochim. cosmochim. Acta 47, 1815–1819. doi:10.1016/0016-7037(83)90029-7.

Broecker, W. S., 1998. Paleocean Circulation during the Last Deglaciation: A Bipolar Seesaw? - Paleoceanography.119. doi:10.1029/97PA03707.

Cheshire, H., J. Thurow and A.J. Nederbragt (2005), Late Quaternary climate change record from two long sediment cores from Guaymas Basin, Gulf of California, *Journal of Quaternary Science*, 20, 457-469.

Chikamoto, M. O., Menviel, L., Abe-Ouchi, A., Ohgaito, R., Timmermann, A., Okazaki, Y., Harada, N., Oka, A., Mouchet, A., 2012. Variability in North Pacific intermediate and deep water ventilation during Heinrich events in two coupled climate models. Deep Sea Research Part II: Topical Studies in Oceanography. 61–64, 114-126.

Dekens, P. S., Lea, D. W., Pak, D. K., Spero, H. J., 2002. Core top calibration of Mg/Ca in tropical foraminifera: Refining paleotemperature estimation. Geochemistry, Geophysics, Geosystems. 3, 1022.

Denton, G. H., Anderson, R. F., Toggweiler, J. R., Edwards, R. L., Schaefer, J. M., Putnam, A. E., 2010. The Last Glacial Termination. Science. 328, 1652-1656.

Durazo, R. and Baumgartner, T. R., 2002. Evolution of oceanographic conditions off Baja California: 1997–1999. Progress in Oceanography. 54, 7-31.

EPICA Community Members (2004), Eight glacial cycles from an Antarctic ice core, *Nature*, *429*(6992), 623-628, doi: 10.1038/nature02599.

Esparza-Alvarez, M. A., Herguera, J. C., Lange, C., 2007. Last century patterns of sea surface temperatures and diatom (> 38 μm) variability in the Southern California current. Marine Micropaleontology. 64, 18-35.

Espinosa-Carreon, T. L., Strub, P. T., Beier, E., Ocampo-Torres, F., Gaxiola-Castro, G., 2004. Seasonal and interannual variability of satellite-derived chlorophyll pigment, surface height, and temperature off Baja California. J. Geophys. Res. - C03039.

Ferguson, J.E., Henderson, G.M., Kucera, M., Rickaby, R.E.M., 2008. Systematic change of foraminiferal Mg/Ca ratios across a strong salinity gradient. Earth Planet. Sci. Lett. 265, 153–166. doi:10.1016/j.epsl.2007.10.011.

Greaves, M., Caillon, N., Rebaubier, H., Bartoli, G., Bohaty, S., Cacho, I., Clarke, L., Cooper, M., Daunt, C., Delaney, M., deMenocal, P., Dutton, A., Eggins, S., Elderfield, H., Garbe-Schoenberg, D., Goddard, E., Green, D., Groeneveld, J., Hastings, D., Hathorne, E., Kimoto, K., Klinkhammer, G., Labeyrie, L., Lea, D. W., Marchitto, T., Martínez-Botí, M. A., Mortyn, P. G., Ni, Y., Nuernberg, D., Paradis, G., Pena, L., Quinn, T., Rosenthal, Y., Russell, A., Sagawa, T., Sosdian, S., Stott, L., Tachikawa, K., Tappa, E., Thunell, R., Wilson, P. A., 2008. Interlaboratory comparison study of calibration standards for foraminiferal Mg/Ca thermometry. Geochemistry, Geophysics, Geosystems. 9, Q08010.

Herbert, T. D., Schuffert, J. D., Andreasen, D., Heusser, L., Lyle, M., Mix, A., Ravelo, A. C., Stott, L. D., Herguera, J. C., 2001. Collapse of the California Current During Glacial Maxima Linked to Climate Change on Land. Science. 293, 71-76.

K. A. Hughen, M.G.L. Baillie, E. Bard et al., 2004. *Radiocarbon* **46** (3), 1030.

Leduc, G., Vidal, L., Tachikawa, K., Rostek, F., Sonzogni, C., Beaufort, L., Bard, E., 2007. Moisture transport across Central America as a positive feedback on abrupt climatic changes. Nature 445, 908–911.

LeGrande, A. N. and Schmidt, G. A., 2006. Global gridded data set of the oxygen isotopic composition in seawater. Geophysical Research Letters. 33, L12604.

Linacre, L., Durazo, R., Hernández-Ayón, J. M., Delgadillo-Hinojosa, F., Cervantes-Díaz, G., Lara-Lara, J. R., Camacho-Ibar, V., Siqueiros-Valencia, A., Bazán-Guzmán, C., 2010. Temporal variability of the physical and chemical water characteristics at a coastal monitoring observatory: Station ENSENADA. Continental Shelf Research. 30, 1730-1742.

Marchitto, T. M., Lehman, S. J., Ortiz, J. D., Flückiger, J., van Geen, A., 2007. Marine Radiocarbon Evidence for the Mechanism of Deglacial Atmospheric CO2 Rise. Science. 316, 1456-1459.

Marchitto, T. M., Muscheler, R., Ortiz, J. D., Carriquiry, J. D., van Geen, A., 2010. Dynamical Response of the Tropical Pacific Ocean to Solar Forcing During the Early Holocene. Science. 330, 1378-1381.

McClymont, E. L., Ganeshram, R. S., Pichevin, L. E., Talbot, H. M., van Dongen, B. E., Thunell, R. C., Haywood, A. M., Singarayer, J. S., Valdes, P. J., 2012. Sea-surface temperature records of Termination 1 in the Gulf of California: Challenges for seasonal and interannual analogues of tropical Pacific climate change. Paleoceanography. PA2202.

McManus, J.F., Francois, R., Gherardi, J.-M., Keigwin, L.D., Brown-Leger, S., 2004. Collapse and rapid resumption of Atlantic meridional circulation linked to deglacial climate changes. Nature 428, 834–837.

Mohtadi, M., Steinke, S., Lückge, A., Groeneveld, J., Hathorne, E. C., 2010. Glacial to Holocene surface hydrography of the tropical eastern Indian Ocean. Earth and Planetary Science Letters. 292, 89-97.

Mortyn, P. G., Herguera, J. C., Martínez-Botí, M. A., 2011. Instrumental validation of Globigerinoides ruber Mg/Ca as a proxy for NE Pacific summer SST. Geophys. Res. Lett. L16601.

Okazaki, Y., Takahashi, K., Asahi, H., Katsuki, K., Hori, J., Yasuda, H., Sagawa, Y., Tokuyama, H., 2005. Productivity changes in the Bering Sea during the late Quaternary. Deep-Sea Res. II 52, 2150–2162.

Okazaki, Y., Timmermann, A., Menviel, L., Harada, N., Abe-Ouchi, A., Chikamoto, M. O., Mouchet, A., Asahi, H., 2010. Deepwater Formation in the North Pacific During the Last Glacial Termination. Science. 329, 200-204.

Pak, D. K., Lea, D. W., Kennett, J. P., 2012. Millennial scale changes in sea surface temperature and ocean circulation in the northeast Pacific, 10–60 kyr BP. Paleoceanography. PA1212.

Pena, L. D., Cacho, I., Ferretti, P., Hall, M. A., 2008. El Niño–Southern Oscillation–like variability during glacial terminations and interlatitudinal teleconnections. Paleoceanography. PA3101.

Rintoul, S. R., C. Hughes and D. Olbers, 2001. The Antarctic Circumpolar Current System. In:*Ocean Circulation and Climate*, G. Siedler, J. Church, and J. Gould, (Eds.), Academic Press, 271-302.

Rosenthal, Y., Oppo, D. W., Linsley, B. K., 2003. The amplitude and phasing of climate change during the last deglaciation in the Sulu Sea, western equatorial Pacific. Geophys. Res. Lett. 1428.

Saenko, O. A., A. Schmittner, and A. J. Weaver (2004), The Atlantic-Pacific seesaw, J. Clim., 17, 2033–2038.

Scheneider, N., Di Lorenzo, E., Niiler, P., 2005. Salinity Variations in the Southern California Current*. Journal of Physical Oceanography. 1421.

Skinner, L. C., Fallon, S., Waelbroeck, C., Michel, E., Barker, S., 2010. Ventilation of the Deep Southern Ocean and Deglacial CO2 Rise. Science. 328, 1147-1151.

Speero, H. J. and Lea, D. W., 2002. The Cause of Carbon Isotope Minimum Events on Glacial Terminations. Science. 296, 522-525.

Stanford, J. D., Hemingway, R., Rohling, E. J., Challenor, P. G., Medina-Elizalde, M., Lester, A. J., 2011. Sea-level probability for the last deglaciation: A statistical analysis of far-field records. Global and Planetary Change. 79, 193-203.

Steinke, S., Chiu, H., Yu, P., Shen, C., Löwemark, L., Mii, H., Chen, M., 2005. Mg/Ca ratios of two Globigerinoides ruber (white) morphotypes: Implications for reconstructing past tropical/subtropical surface water conditions. Geochemistry, Geophysics, Geosystems. 6, Q11005.

Stott, L., Southon, J., Timmermann, A., and Koutavas, A.: Radiocarbon age anomaly at intermediate water depth in the Pacific Ocean during the last deglaciation, Paleoceanography, 24, PA2223, doi:10.1029/2008PA001690, 2009.

Thunell, R. C., Curry, W. B., Honjo, S., 1983. Seasonal variation in the flux of planktonic foraminifera: time series sediment trap results from the Panama Basin. Earth and Planetary Science Letters. 64, 44-55.

Toggweiler, J. R. and Russell, J., 2008. Ocean circulation in a warming climate. Nature. 451, 286-288.

Timmermann, A., Krebs, U., Justino, F., Goosse, H., Ivanochko, T., 2005. Mechanisms for millennial-scale global synchronization during the last glacial period. Paleoceanography. PA4008.

Toggweiler, J. R., 2008. Variation of Atmospheric CO_2 by Ventilation of the Ocean's Deepest Water. Paleoceanography. 571.

van Geen, A., Zheng, Y., Bernhard, J. M., Cannariato, K. G., Carriquiry, J., Dean, W. E., Eakins, B. W., Ortiz, J. D., Pike, J., 2003. On the preservation of laminated sediments along the western margin of North America. Paleoceanography. 1098.

Wang, L., 2000. Isotopic signals in two morphotypes of Globigerinoides ruber (white) from the South China Sea: implications for monsoon climate change during the last glacial cycle. Palaeogeography, Palaeoclimatology, Palaeoecology. 161, 381-394.

Wang, X., Auler, A. S., Edwards, R. L., Cheng, H., Ito, E., Wang, Y., Kong, X., - Solheid, M., 2007. Millennial-scale precipitation changes in southern Brazil over the past 90,000 years. Geophys. Res. Lett. L23701.

Yamamoto, M., Yamamuro, M., Tanaka, Y., 2007. The California current system during the last 136,000 years: response of the North Pacific High to precessional forcing. Quaternary Science Reviews. 26, 405-414.

5.7. Supplementary information

Tabla S1. The ^{14}C AMS measurements used to construct the MD02-2505 age model. We used Calib06 and assumed a reservoir age (ΔR) of 200 yr to calibrate to calendar years before present (cal. yr BP).

Depth (cm)	14C age (yr)	Calibratated calendar age (yr BP)
669	7030	7355±80
778	7415	7677,5±97
879	8495	8863±151
980	9305	9831±181
1182	10100	10826±161
1411	12205	13421±127
1540	13400	15141±191
1720	14619	17045±199
2261	18330	21199±337
2495	19840	22893±400
3600	29430	33411±748
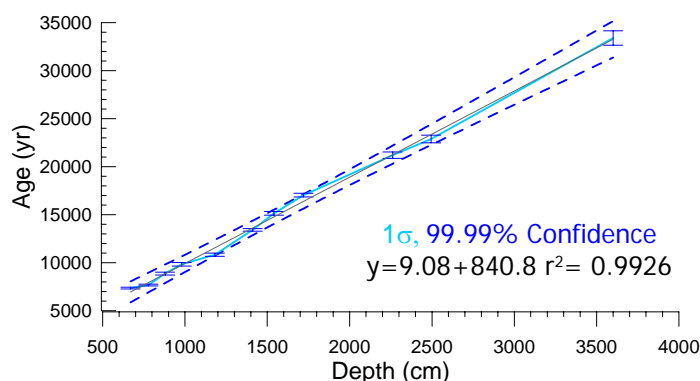
Figure S1. Calibration used to construct the age model for the early part of the record (Holocene) where radiocarbon measurements where not available. It is based on the data reported in table S1.

CHAPTER 6

Conclusions and future work

Paired Mg/Ca-$\delta^{18}O_C$ measurements using multispecies planktonic foraminifera have allowed us to understand past changes in the structure of the upper water column in two different ocean basins across diverse geological timescales. Based on records of Mg/Ca-temperature and ice volume free seawater $\delta^{18}O$ ($\delta^{18}O_{SW-IVC}$; a proxy for past changes in salinity; *LeGrande and Schmidt, 2006*), we have inferred past hydrographical changes in the Southern and Pacific Oceans, and their implications for the global carbon (C) cycle and ocean circulation during the Middle Pleistocene Transition (MPT) and Termination 1 (T1), respectively.

Chapter 3 focused on understanding upper water column temperature and $\delta^{18}O_{SW-IVC}$ changes in the Southern Ocean during the MPT and their effects on the exchange of C between the deep ocean and the atmosphere during the time span. Reconstructions based on *Neogloboquadrina pachyderma* (sinistral) from a core located in the Subantarctic Zone of the Atlantic Ocean (at 42ºS, ODP Site 1090) suggest a change toward fresher and cooler conditions at the onset of the MPT (~1250 ka), which persisted across glacial stages of the transition. These changes occurred virtually in tandem with increases in the glacial type lithologies in a core retrieved from Antarctica *(Naish et al., 2009)* pointing to a strong link between hydrographical changes in the Subantarctic Zone and seaward expansion of the West Antarctic ice sheets. We speculate that the observed cooling and freshening at ODP Site 1090 reflects Southern Ocean hydrographical changes across the MPT. Based on the known ocean density sensitivity to salinity changes under cold conditions *(Adkins et al., 2002; de Boer et al., 2008)*, the freshening suggested by the *N. pachyderma* (s.) $\delta^{18}O_{SW-IVC}$ record likely accounted for increased Southern Ocean upper water column stratification at the onset of the MPT, which persisted during glacial stages of the transition. Southern Ocean upper water column stratification probably helped to more efficiently store C at depth by hindering the release of respired CO_2 from the deep ocean to the atmosphere. This is in line with increases in the Southern Ocean $\delta^{13}C$ gradient with respect to the North

Atlantic and Pacific Oceans at the onset of the MPT, which points to enhancing C storage in the deep ocean at that time *(Hodell and Venz-Curtis, 2006)*. Similarities between pCO$_2$ measurements in the Antarctic Ice Cores *(Luthi et al., 2008)* and hydrographical changes in the Southern Ocean in two glacial-interglacial cycles after the transition points to a close coupling of these features on these timescales. We propose that Southern Ocean stratification, probably in combination with increases in productivity due to Fe-Fertilization *(Martinez-Garcia et al., 2011)* accounted for the ~30 ppm decrease in glacial pCO$_2$ proposed by *(Hönisch et al., 2009)*. Implications of hydrographical changes in the Southern Ocean in the C cycle should be further studied by extending δ^{18}O$_{SW-IVC}$ records to multiple glacial-interglacial cycles after the MPT, where pCO$_2$ measurements in the Antarctic ice cores allow more direct comparisons. Alternatively, increasing the temporal resolution of pCO$_2$ *(Hönisch et al., 2009; Tripati et al., 2009)* using the boron planktonic foraminiferal proxy would also provide excellent new insights. In this sense, the extension of both δ^{18}O$_{SW-IVC}$ and pCO$_2$ reconstructions back in time would also help to understand the role of Southern Ocean stratification during other climatic transitions, such as the Plio-Pleistocene transition and/or its response to the onset of the Northern Hemisphere glaciations.

Chapter 4 further explored the role of the Southern Ocean (ODP Site 1090) physical water column conditions in modulating pCO$_2$ across the MPT. We tracked past changes in the structure of the upper water column of the Subantarctic Zone by taking advantage of the different depth habitats of *Globigerina bulloides* (surface), *N. pachyderma* (s.) and *Glogorotaliid crassaformis* (subthermocline). Mg/Ca-based temperature and δ^{18}O$_{SW-IVC}$ reconstructions from the relatively deeper planktonic foraminifera species suggest a sustained warming and saltier conditions from 1500 to 1300 ka, which was absent in *G. bulloides* reconstructions. After this period, all records feature similar amplitude temperature and δ^{18}O$_{SW-IVC}$ changes and the gradient among them was reduced. Modern observations suggest that the thermocline and halocline shoals from the subtropics toward the Subantarctic Zone *(Rintoul et al., 2001)*. Based on this, we interpreted the observed changes in the planktonic foraminifera records as the shoaling of the thermocline and halocline at 1500-1300 ka as a consequence of the expansion of the Antarctic polar fronts. We speculate that the new position of these oceanographic features in the Subantarctic Zone across the MPT improved glacial upper water column

conditions for increasing primary productivity in the region, then enhancing the uptake of pCO_2, and hence the sensitivity of the climate to glacial Fe-fertilization over the last 1200 ky *(Lamber et al., 2004; Martinez-Garcia et al., 2011)*. Using modern ocean observations as an analog *(Rintoul et al., 2001)*, the revised water column structure during the MPT would have shifted ODP Site 1090 from Subtropical to Subantarctic conditions at the onset of the MPT. The modern Subantarctic Zone is characterized by higher nutrient concentration than the subtropical region, implying that the availability of macro-nutrients in the area was likely increased with changing physical structure of the water column across the MPT. In this sense we propose that synchronous shoaling of the thermocline/ halocline and concomitant increases in macro-nutrient supply, coupled with sharp increases in Fe-supply *(Martinez-Garcia et al., 2011)* to the Subantarctic Zone acted as a plausible mechanism to explain increases in glacial primary productivity at the onset of the MPT and glacial stages after the transition. The influence of the shoaling of the thermocline/halocline in the supply of macro-nutrients to the Subantarctic Zone should be further tested by reconstructions of $\delta^{15}N$ in planktonic foraminifera or Cd/Ca ratios in benthic foraminifera during the time span. Confirmation of macro-nutrient utilization increases in the Subantarctic Zone and enhancement of Southern Ocean stratification during glacial stages only after the MPT would provide a convincing positive feedback mechanism for the transition. This would further imply that only after the onset of the MPT the Southern Ocean reached a threshold where all the conditions to uptake and efficiently store C at depth were achieved and that mechanisms other than pCO_2 fluctuations themselves acted as actual drivers of the transition.

We have also used Mg/Ca-temperature and $\delta^{18}O_{SW-IVC}$ to infer past oceanic and atmospheric changes in the southernmost part of the California Current System (CCS), using a core retrieved from the Northeast Pacific (NEP; MD02-2505, 25ºN) across T1 and the early-Holocene. Sea surface temperature (SST) records from MD02-2505 using separately the two different morphotypes of *Globigerinoides ruber* white, sensu lato and sensu stricto, have shown that the NEP was gradually warmed across T1 by ~2ºC and weakened abruptly in tandem with Northern Hemisphere (NH) cold events, that is, Younger Dryas (YD) and stadial Heinrich 1 (stadial-H1). *G. ruber*-$\delta^{18}O_{SW-IVC}$ increases up to ~0.7‰ (relatively salty conditions) during NH-cold events further support this

notion. Millennial-scale variability changes in the *G.ruber*-$\delta^{18}O_{SW-IVC}$ reconstruction agree well with those from the tropical Pacific *(Rosenthal et al., 2003; Benway et al., 2006; Pena et al., 2008)*. Salinity changes in the tropical Pacific have been mainly associated to the influence of the position of the Intertropical Convergence Zone (ITCZ) in the moisture transport between the Atlantic and Pacific Ocean and the intensity of the Eastern Asian Mosoon (e.g. *Rosenthal, et al., 2003; Leduc et al., 2007*). However, we proposed that the observed millennial-scale $\delta^{18}O_{SW-IVC}$ changes in the tropical/subtropical Pacific Ocean should not only be explained by local variations in the freshwater input but also by regional hydrographical changes of the ocean basin. We speculate that the ocean basin was relatively salty during NH-cold events than for the rest of T1, and that the position of the ITCZ and decreases in the influence of the CC reduced the freshening of the tropical Pacific and CCS, respectively, hence amplifying the salinity signal. Synchronous upper water mass $\delta^{18}O_{SW-IVC}$ changes in the Pacific Ocean and variations in the characteristics of intermediate water masses of the ocean basin (*Marchitto et al., 2007; Stott et al., 2009*) suggest major changes in the features of the water masses advected from the Southern Ocean. Overall saltier conditions in the ocean basin, and concomitant activation of the Pacific Meridional Overturning Circulation (PMOC), have been proposed to occur as a result of weakening the Atlantic Meridional Overturning Circulation (AMOC) during YD and stadial-H1 *(Saenko et al., 2004; Timmermann et al., 2005)*. We cannot assess whether the salinity changes observed accounted for the strengthening of the PMOC, however we demonstrated that the salinity anomaly is observed beyond the tropical region. In this sense new ε_{Nd} and radiocarbon reconstructions, in combination with those already available *(Okazaki, et al. 2010)*, would provide valuable information on the response of the Pacific Ocean circulation to those hydrographical changes during periods of AMOC weakening. New insights in this regard would demonstrate whether an Atlantic-Pacific seesaw mechanism is indeed activated to maintain the heat and salt transport to the NH when this process is reduced in the Atlantic Ocean *(Saenko et al., 2004)*.

References

Adkins, J. F., McIntyre, K., Schrag, D. P., 2002. The Salinity, Temperature, and δ18O of the Glacial Deep Ocean. Science. 298, 1769-1773.

Benway, H. M., Mix, A. C., Haley, B. A., Klinkhammer, G. P., 2006. Eastern Pacific Warm Pool paleosalinity and climate variability: 0–30 kyr. Paleoceanography. PA3008.

de Boer, A. M., Toggweiler, J. R., Sigman, D. M., 2008. Atlantic Dominance of the Meridional Overturning Circulation. - Journal of Physical Oceanography. 435.

Hodell, D. A. and Venz-Curtis, K. A., 2006. Late Neogene history of deepwater ventilation in the Southern Ocean. Geochemistry, Geophysics, Geosystems. 7, Q09001.

Hönisch, B., Hemming, N. G., Archer, D., Siddall, M., McManus, J. F., 2009. Atmospheric Carbon Dioxide Concentration Across the Mid-Pleistocene Transition. Science. 324, 1551-1554.

Lambert, F., B. Delmonte, J. R. Petit, M. Bigler, P. R. Kaufmann, M. A. Hutterli, T. F. Stocker, U. Ruth, J. P. Steffensen, and V. Maggi, (2008). Dust-climate couplings over the past 800,000 years from the EPICA Dome C ice core, Nature, 452(7187), 616 – 619, doi:10.1038/ nature06763.

LeGrande, A. N. and Schmidt, G. A., 2006. Global gridded data set of the oxygen isotopic composition in seawater. Geophysical Research Letters. 33, L12604.

Leduc, G., Vidal, L., Tachikawa, K., Rostek, F., Sonzogni, C., Beaufort, L., Bard, E., 2007. Moisture transport across Central America as a positive feedback on abrupt climatic changes. Nature 445, 908–911.

Luthi, D., Le Floch, M., Bereiter, B., Blunier, T., Barnola, J., Siegenthaler, U.,

Raynaud, D., Jouzel, J., Fischer, H., Kawamura, K., Stocker, T. F., 2008. High-resolution carbon dioxide concentration record 650,000-800,000[thinsp]years before present. Nature. 453, 379-382.

Marchitto, T. M., Lehman, S. J., Ortiz, J. D., Flückiger, J., van Geen, A., 2007. Marine Radiocarbon Evidence for the Mechanism of Deglacial Atmospheric CO2 Rise. Science. 316, 1456-1459.

Martinez-Garcia, A., Rosell-Mele, A., Jaccard, S. L., Geibert, W., Sigman, D. M., Haug, G. H., 2011. Southern Ocean dust-climate coupling over the past four million years. Nature. advance online publication, .

Naish, T., Powell, R., Levy, R., Wilson, G., Scherer, R., Talarico, F., Krissek, L., Niessen, F., Pompilio, M., Wilson, T., Carter, L., DeConto, R., Huybers, P., McKay, R., Pollard, D., Ross, J., Winter, D., Barrett, P., Browne, G., Cody, R., Cowan, E., Crampton, J., Dunbar, G., Dunbar, N., Florindo, F., Gebhardt, C., Graham, I., Hannah, M., Hansaraj, D., Harwood, D., Helling, D., Henrys, S., Hinnov, L., Kuhn, G., Kyle, P., Laufer, A., Maffioli, P., Magens, D., Mandernack, K., McIntosh, W., Millan, C., Morin, R., Ohneiser, C., Paulsen, T., Persico, D., Raine, I., Reed, J., Riesselman, C., Sagnotti, L., Schmitt, D., Sjunneskog, C., Strong, P., Taviani, M., Vogel, S., Wilch, T., Williams, T., 2009. Obliquity-paced Pliocene West Antarctic ice sheet oscillations. Nature. 458, 322-328.

Okazaki, Y., Timmermann, A., Menviel, L., Harada, N., Abe-Ouchi, A., Chikamoto, M. O., Mouchet, A., Asahi, H., 2010. Deepwater Formation in the North Pacific During the Last Glacial Termination. Science. 329, 200-204.

Pena, L. D., Cacho, I., Ferretti, P., Hall, M. A., 2008. El Niño–Southern Oscillation–like variability during glacial terminations and interlatitudinal teleconnections. Paleoceanography. PA3101.

Rintoul, S. R., C. Hughes and D. Olbers, 2001. The Antarctic Circumpolar Current System. In:*Ocean Circulation and Climate*, G. Siedler, J. Church, and J. Gould, (Eds.), Academic Press, 271-302.

Rosenthal, Y., Oppo, D. W., Linsley, B. K., 2003. The amplitude and phasing of climate change during the last deglaciation in the Sulu Sea, western equatorial Pacific. Geophys. Res. Lett. 1428.

Saenko, O. A., A. Schmittner, and A. J. Weaver (2004), The Atlantic-Pacific seesaw, J. Clim., 17, 2033–2038

Stott, L., Southon, J., Timmermann, A., Koutavas, A., 2009. Radiocarbon age anomaly at intermediate water depth in the Pacific Ocean during the last deglaciation. - Paleoceanography. PA2223.

Timmermann, A., Krebs, U., Justino, F., Goosse, H., Ivanochko, T., 2005. Mechanisms for millennial-scale global synchronization during the last glacial period. - Paleoceanography. PA4008.

Tripati, A. K., Roberts, C. D., Eagle, R. A., 2009. Coupling of CO2 and Ice Sheet Stability Over Major Climate Transitions of the Last 20 Million Years. Science. 326, 1394-1397.